Content based retrieval of PET neurological images

A Doctoral Thesis
submitted in partial fulfilment of the
requirement for the award of
Doctor of Philosophy
from Middlesex University

Author:
Stephen Batty - Middlesex University.

October 2004

Acknowledgements

This research has been primarily supervised by Dr. Xiaohong Gao, and would not have been possible without her advice, direction and knowledge.

External supervisor Dr. John Clark and Dr. Tim Fryer have also provided invaluable information and without their input this thesis could not have been produced.

Thanks and acknowledgement goes to all staff at both Middlesex University and the Wolfson Brain Imaging Centre.

Special thanks to Mr. Michael Batty, Mrs. Patricia Batty and Miss Denise Sourris for proof reading this document and supplying significant advice and encouragement.

This project is funded by the Engineering Physics Sciences Research Council (EPSRC) of Britain. Their support is gratefully acknowledged.

Images obtained, pre-processed and analyzed at the Wolfson Brain Imaging Centre, Addenbrookes Hospital, Cambridge (UK). Algorithm and system development performed at Middlesex University, London (UK), as part of the computer science research group.

Content

Included CD contains all images and lesion results.
PNG and TIF image formats both supported.
Folder titled "Lesions" contains all the detected lesions shown as red pixels. Folder titled "Originals" shows all the original image files.
The "Readme" file provides a brief summary of results.

Index of Figures

Index of Equations

Index of Tables

Abbreviations

AD	=	Alzheimer's disease.
API	=	Application Programmer Interface.
CT	=	Computed Tomography.
CIE	=	Commision Internationale de L'Eclairage
CBIR	=	Content based image retrieval
CBIRS	=	Content Based Image Retrieval System.
HI-PACS	=	Hospital Integrated Picture Archiving and Communications.
iMSP	=	Ideal Mid Sagittal Plane.
MCI	=	Mild Cognitive Impairment.
MRI	=	Magnetic Resonance Imaging.
PACS	=	Picture Archiving and Communications
PCA	=	Posterior Cortical Atrophy.
PET	=	Positron Emission Tomography.
keV	=	Kilo electron volt.
SPECT	=	single-photon emission tomography

Abstract

Medical image management has posed challenges to many researchers, especially when the images have to be indexed and retrieved using their visual content that is meaningful to clinicians. In this study, an image retrieval system has been developed for 3D brain PET (Position emission tomography) images. It has been found that PET neurological images can be retrieved based upon their diagnostic status using only data pertaining to their content, and predominantly the visual content.

During the study PET scans are spatially normalized, using existing techniques, and their visual data is quantified. The mid-sagittal-plane of each individual 3D PET scan is found and then utilized in the detection of abnormal asymmetries, such as tumours or physical injuries. All the asymmetries detected are referenced to the Talairarch and Tournoux anatomical atlas. The Cartesian co-ordinates in Talairarch space, of detected lesion, are employed along with the associated anatomical structure(s) as the indices within the content based image retrieval system. The anatomical atlas is then also utilized to isolate distinct anatomical areas that are related to a number of neurodegenerative disorders. After segmentation of the anatomical regions of interest algorithms are applied to characterize the texture of brain intensity using Gabor filters and to elucidate the mean index ratio of activation levels. These measurements are combined to produce a single feature vector that is incorporated into the content based image retrieval system.

Experimental results on images with known diagnoses show that physical lesions such as head injuries and tumours can be, to a certain extent, detected correctly. Images with correctly detected and measured lesion are then retrieved from the database of images when a query pertains to the measured locale. Images with neurodegenerative disorder patterns have been indexed and retrieved via texture-based features. Retrieval accuracy is increased, for images from patients diagnosed with dementia, by combining the texture feature and mean index ratio value.

1 Introduction

Position emission tomography (PET) is an imaging technique that can examine quantitatively and *in vivo*, the physiology and biochemistry of an organ. PET was initially used almost exclusively as a research tool for studying the brain. More recently it has been applied to the diagnosis and assessment of the major forms of cancer, cardiac viability, as well as neurological disorders such as Parkinson's disease. Due to this expansion in use of PET scanners there are now hundreds of PET centres around the world [1], producing large volumes of data. The systematic management of this data, and its corresponding utilization in an effective and efficient manner, is therefore of great importance to both clinicians and researchers. Patients therefore also benefit from any improvements in data management. One strategic approach, to achieve improved data management efficiency, is to archive the PET images within a data store that allows for content-based image retrieval.

Research and development of content-based medical image retrieval systems has been made by a number of groups [2,3]. Each retrieval system has its own characteristics and is domain dependent. This is due to the fact that each medical imaging technique is designed to reveal a specific ilk of visual content, from human organs. For example, Magnetic Resonance Imaging (MRI) displays the anatomic structure of the human body, while PET imaging reveals functional information. The method applied to each modality of image to extract visual features, is therefore different. This is because each category of information, such as anatomical or functional, posses different visual properties and require a different category of feature extraction algorithms. The extraction algorithms themselves are consequently based upon varied image processing techniques.

Although there has been some work carried out on retrieving PET images by their medically salient content [2], the content extracted is itself not visible. Non-visible content is difficult to interpret by clinicians and associated non-expert personnel. In this study, visual features are extracted to represent three-dimensional PET neurological images. Mapping to anatomical structure using the Talairarch and Tournoux atlas [4] is also performed. Anatomical mapping coupled with PET feature

extraction algorithms, enables the development of a system that can be used by people with a variety of backgrounds including: researchers, clinicians, students, and administrators.

The structure of the thesis is organised as follows. Literature review is given in Chapter two, a review of content-based systems together with the development of medical image systems. The third chapter is the Methodology that is applied in this study. Experimental results are given in Chapter 4. The thesis concludes with a description of the developed, web-based, system that includes anatomical mapping, indexing, and evaluation of the performance.

2 Literature Review

Due to the rapid development of computer technology, large amount of images are acquired and stored in computers. Management of this image data systematically is therefore very important for future applications, such as research and patient treatment. This section provides a comprehensive review of research carried out into Content-Based image retrieval and other related areas of image analysis, such as image segmentation and feature representation. Research related to medicine, and specifically PET imaging, is emphasized although other areas are included in the review.

2.1 The importance of image retrieval systems

Images are a convenient medium for describing and storing spatial, temporal, spectral and physical components of information contained in a variety of domains, such as satellite images and medical images. Images are also a rapid method for conveying and communicating information, e.g. those used in commercial logos.

Due to the low cost of scanners and storage devices, digitised images are now playing an important role in depicting and disseminating pictorial information. As a result, large image databases are being developed and applied in a number of applications. These applications include: criminal identification, multimedia encyclopaedias, geographic information systems, on-line applications for art and art history, computer vision for robotics, computer-aided design, trademark databases and medical image archiving. These databases typically consist of thousands of images and can take up terabytes of computer memory. Although advances in image compression algorithms have alleviated storage requirements it is still difficult for a user to browse through an entire database, simply because the databases are so large. An efficient and automatic procedure is therefore required for indexing and retrieving images from these types of databases.

Over the last ten years image indexing and retrieval has been well studied by scientists from a variety of disciplines. Mathematicians attempting to develop

mathematical models which represent image features so that they can then be applied to the indexing and retrieval of images. Psychologists are studying the way human perception organises image patterns with the aim of producing cognitive models of human vision. Computer scientists on the other hand are working to find optimised algorithms to develop a retrieval system that is not only fast but also accurate.

2.2 Text–Based Image Retrieval

Conventionally, textual features, such as filenames and keywords have been used to annotate and retrieve images. Traditional image databases therefore do not differ significantly from databases that contain non-image data. A user of a conventional image retrieval system manually inputs the image file into the database and at the same time enters any relevant textual details that describe image content. However, this technique of describing and representing an image is limited. The main problems identified with such text-based image systems are: Subjectivity and Time efficiency.

- Subjectivity. Two individuals may describe the same image in a different manner. The textual descriptions of visual attributes such as colour, shape, texture and layout vary greatly among people. Even if an image is always described in exactly the same manner it is possible that important information is systematically missed. It is conceivable that numerous visual features are, mistakenly, ignored.

- Time efficiency. The process of detecting visual data and then describing it using language descriptors is time consuming. A typical approach requires human input to describe and tag the contents of images in terms of a selected set of captions and key words. As image databases increase in size the use of keywords becomes not only complex but also inadequate to represent the content of stored images. The description of visual characteristics requires many man-hours of work.

Examples of text-based retrieval are almost ubiquitous in everyday life. One such system would be Library book searches [5], which are based upon matching a user specified text string to an index of authors and/or titles. Author and title information in a conventional Library system is manually inputted; this is both time consuming and subjective. A second commonly used example of text based retrieval is that contained within the *Microsoft Windows* operating system [6]. To locate a file or folder a user again enters a text string, the retrieval algorithm then attempts to match file names stored on the hard disk to the string entered as the query. File extension can also be specified to limit results to a specific type, images for example. A search for images on the *Windows* [6] operating system is based upon language descriptors that are present in file name. However, as is always the case with text based image retrieval system, there is no way to ensure that the actual visual information is related in an objective manner. The *Google Image* search [7] employs a similar technique for image retrieval. A user is required to input a word or phrase and this is then matched to the pre-defined index of image filenames. The actual visual information, or content, contained within the set of returned images that match the specified text string, can vary greatly. Text-based retrieval of images can be found in the *Getty Image* library [8], also available on the Internet. The *Getty Image* library [8] is a huge online archive of images obtained from a wide range of domains. To search the image collection a user enters a word or phrase, that word or phrase is then matched to an index of image captions; the captions are textual descriptions of the image content that have been entered into the image archive by qualified personnel.

Examples of medical image storage are less widespread and not readily available on the Internet. The storage of medical images at the *Wolfson Brain Imaging Centre*, a department within *Cambridge University*, has however been examined [9]. The strategy implemented requires image files to be saved directly on to *UNIX* file servers; the file format itself can vary but is commonly compatible with *Analyze* [10], which is itself a commercial software package designed specifically for medical image analysis. Searching for images is limited to filename matching; no specialized retrieval system exists. Indexing of images is therefore limited to the location, in file system, of the saved image and its filename. It is not possible to retrieve medical images using anything other than the standard *UNIX* file information such as size and name.

Text based data management systems, although successfully utilized in some applications as described previously, present fundamental limitations when image storage and retrieval is considered. Images contain visual data that can be subjectively interpreted by users, or qualified experts and meaningful data can sometimes be ignored. Traditional text based systems also require the labour intensive process of manually indexing each image with keywords or caption. For these reasons, content-based image retrieval systems are being developed in a wide range of fields, including medicine.

2.3 Content Based Image Retrieval (CBIR)

In attempting to overcome the previously discussed limitations of text-based image retrieval systems it has become popular to index and retrieve an image using its inherent visual features. Visual features, also referred to as visual data, include colour, shape, and texture. Retrieval of images based upon their visual data is referred to as content-based image indexing and retrieval.

The field of content-based image retrieval had its beginnings in the late seventies [11], however it is widely accepted [12] that the subject did not become significant, i.e. - the number of published scientific articles remained minimal, until the mid nineteen nineties. The reason for this, as befits Moore's law [13], is until that time the availability of computer processor resources was restricted. CBIR relies on image analysis which is itself a relatively resource intensive procedure, this is due to the large file sizes and complex measurement routines that are involved. During the nineties the microchip speed to price ratio reached a level that made it possible for many research groups to actively study content-based image retrieval. This coupled with increased network bandwidths, the birth of the *Worldwide Web,* and the availability of high quality digital image scanners led to an exponential increase in CBIR research.

When using content-based retrieval image systems, a user will normally be required to give an example image or to manually (digitally) sketch a picture, for use as the database query. The system then extracts pre-defined visual features of the query image and compares these with the features stored in the image database. The image with the smallest distance between its own features and the query features will be retrieved first. The distance formula, or similarity metric, is pre-defined in the system. A query to a CBIR system can also be carried out in the more familiar manner of supplying a textual keyword.

There are a number of different approaches that can be taken when designing a CBIR system, which to a large extent depends on the image domain being studied. In addition to the image domain a wide range of different visual analysis techniques

have to be considered and employed. The following section shows techniques that are employed in the different CBIR systems.

2.3.1 CBIR Systems and Products

A Content-based image retrieval system or CBIRS is a group of devices, or virtual objects, communicating with each other for the express purpose of enabling a human user to store and retrieve visual information files based on their actual optical data [14]. Advantages of CBIRS's over traditional text based retrieval systems include:

- Improved time efficiency.
- Less labour intensive
- New data/files are inserted or added to system autonomously.
- A search can be carried out using an example image.
- Indexing method is objective and consistent.
- All visual data present can be considered.

The advantages of CBIRS, outlined above, have led to a proliferation of products [15,16,17,18,19,20] and research groups in the field. There are now numerous commercial products available and a large number of universities [15] around the world dedicated to the advancement of CBIR technology.

A comprehensive survey conducted in 2000 of thirty-nine separate CBIR systems showed that the majority of the systems are concerned with domain independent image searching across the Internet [15]. The systems reviewed utilized a wide variety of visual features as their indices. Of the thirty-nine systems surveyed thirty-one utilize colour, twenty-five texture and twenty-three shape. The following chart, shown in figure 2.1, summarizes those systems.

Figure 2.1 illustrates each system and the features it utilizes for indexing. These features are firstly extracted by the system based on some pre-defined algorithms that are image domain dependent. The quantified features are then applied to index images.

Some of the most well developed systems that are currently in use and two development toolkits are briefly described below:

- Informix database [16], produced by IBM, with technology from Convera [17]. A plug-in module for the database, called Visual

RetrievalWare, is a software development toolkit for image processing, feature extraction and indexing. Searches are performed with reference to the binary patterns contained within an image.

- Ultimedia Manager and QBIC [18], also produced by IBM. This system asks the user to select one of the three features: colour, shape, and texture. Then the retrieval process is based on a feature selected by the user.

- ImageFinder [19]. The matching engine employed has the capability of learning and drawing conclusions; it functions by applying pattern-matching technology.

- IMatch [20]. IMatch allows you to search for images using many criteria: attributes, properties, colour, texture, and shape. You can combine any number of criteria into one single selection and let IMatch display all matching images.

- NEC's system called Amore [22]. Amore segments the query image into regions of homogenous colour. The shape and colour of the regions are then used as feature vectors for querying the database. The user can decide which of the two features is of most significance.

- Informix [16] databases with the Virage plug-in [20] VIR Image Engine. Similar to the Visual RetrievalWare software, VIR Image Engine is an extendable framework designed to aid the development of Content-Based Image Retrieval systems.

- One of the more developed CBIR systems that has been built is NeTra[19]. The Alexandria Digital Library project [23,24] has in fact implemented a prototype version of the system. NeTra itself uses colour, texture and shape to index images; the database consists of 2,500 colour images organized into 25 different categories (100 images per category). The query image is split into regions and the user can

choose which region is utilized; queries can be performed based on colour, location, shape or texture of the chosen region. Results show that their technique "enhances the perceptual quality of the retrieved result". They also highlight the importance of user feedback in improving the relevance of retrieved results.

- BLOBworld [25], focuses on the retrieval differences between querying based on global features as opposed to those using region of interest techniques. The BLOBworld study, as the name suggests, segments images into separate "Blobs" that exist in the real world as objects or "Things", as opposed to low-level features such as colour or shape, which have been referred to as "Stuff". Colour, texture and positional features are again extracted from the image so that segmentation into regions can occur. The visual characteristics of each region are then used to index the database.

Colour is the visual feature that has been utilized most often as a database indexing method within CBIR systems [15]. A query image is supplied to the retrieval system and the dominant colour is elucidated, which is the colour that covers the largest spatial area. The database can then be searched until images that have a matching or similar dominant colour are found. The majority of surveyed systems retrieve images using this colour-based approach. The visual feature of colour refers to the wavelength of light associated to a pixel, this is represented by the three values for red, green and blue (detailed in section 2.3.1.1.2.3, *Colour or Greyscale*). Alternative visual features, such as texture and shape are also extracted and utilized in the systems surveyed. The processes of texture and shape measurement are however more complex than that of colour. Texture, the repetition of sub-image colours and edges, can be characterized using a variety of image processing tools (described in section 2.3.1.1.2.1, *Texture*). Shape refers to objects within an image and the relative geometric co-ordinates of those objects; the *Hough Transform* is perhaps the best-known method of shape quantification (detailed in section 2.3.1.1.2.2 *Shape Size and Position*).

The three visual features introduced above, colour, texture and shape are low-level primitive visual features as they contain no semantic information. However, they are the most important and commonly used of the visual features. There are a number of different image processing techniques that can be utilized to analyze these visual features, and they are detailed in the next section.

2.3.1.1 Visual Feature Representation

The development of a content-based image retrieval system requires the measurement of visual features using computer algorithms. The visual features are quantified and then utilized as indices within a database system so that retrieval can be carried out. The visual features can be classified into two main areas:

- Low-level primitives
- High-level semantic objects

Low level or *primitive* features refer to representations of colour, texture, and shape in an image. Higher level, *semantic* features include *tumours* (in medical images) and everyday objects like animals, people and houses (in less domain specific image sets). Semantic objects themselves are composed of primitives and consequently any form of CBIRS requires the quantification of primitive, low-level visual features. This process of visual feature representation is split into two main stages: detection/segmentation and measurement/quantification.

2.3.1.1.1 Detection/Segmentation

Virtually all image-processing applications have to start from the same point: the division of an image into parts that have a strong correlation with real world objects [26]. This is referred to as segmentation and has been defined previously:

"[The process by which] a computer attempts to separate objects from the image background and each other" [26]

There are three basic approaches used to achieve this: *Thresholding*, *Edge Based* and *Region Growing and Matching*.

2.3.1.1.1.1 THRESHOLDS [26]

The process of thresholding an image is to separate an image into its constituent elements based upon predetermined fixed data, called the threshold. The simplest form of thresholding is that applied to monochromatic images. Intensity or brightness thresholding creates a binary image based upon each pixel's intensity and the threshold value. Any pixel with a value above the threshold is given a value of 1 while anything below the threshold is given a value of 0, thus background and object features. A more sophisticated approach is to assign two threshold values: one low and one high. Anything below the lower threshold made to equal 0, anything above the higher threshold equal to 1 while anything in the middle stays the same; this is also known as contrast enhancement.

Thresholds can also be applied to certain specified values; any pixels with, for example a grey value of 123 can be given a value of 1 and everything else assigned 0. This is sometimes known as *band-thresholding* [26].

The histogram of an image, a visual representation of the frequency of each pixel value, is also utilized when thresholding. The bimodal histogram, and its subsequent employment, is a simple example of *adaptive thresholding*. The histogram of an image is taken and if shown to be bimodal (having two-peaks), a binary image can created with the threshold value in the middle of the two peaks, at the lowest point, see Figure 2.2; the threshold image is composed of just the background and the one target object.

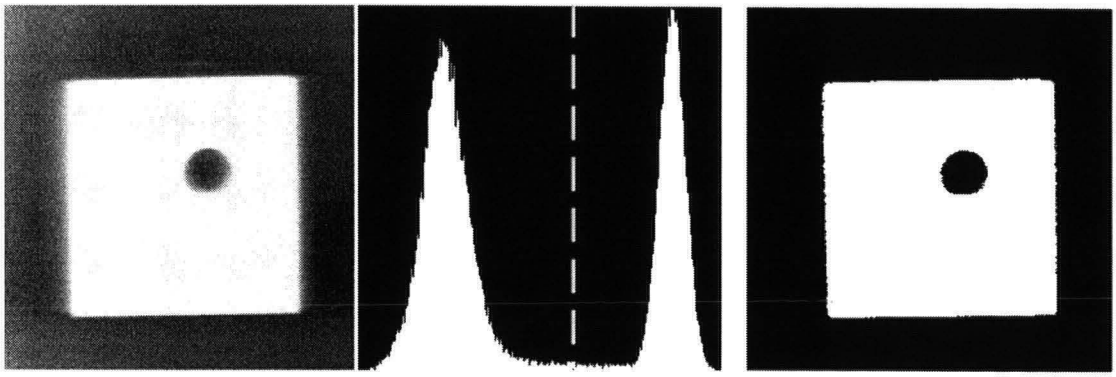

Figure 2.2 Original image (left). Intensity histogram (middle), dashed line represents the threshold value. Binary image (right) created using the bimodal threshold technique [27].

Thresholding, it must be noted, can also be performed on visual properties other than brightness. Characteristics such as texture and chromaticity are also modifiable when thresholding is applied.

2.3.1.1.1.2 EDGES [26]

An edge can be any pixel where there is a discontinuity; the discontinuity can occur in the grey-level, colour, texture, etc. An edge is quantifiable, the subtraction of one pixel from the other results in an absolute value that is the difference across the edge. If an edge pixel neighbours other edge pixels a border is formed. A border consists of pixels belonging to a region *R* that have neighbouring pixels belonging to a region other than *R*. The strength of an edge and/or the strength of its corresponding border are often used as criterion in *region* based image processing (see next section 2.3.1.1.1.3 *Regions*).

Edge detection, although often an important step in the image segmentation process, does not produce a segmented image by itself, post-processing is also required to divide the image into its real world component objects.

2.3.1.1.1.3 REGIONS [26]

Region merging and region splitting are the techniques for segmenting images that rely on differentiating areas with maximum homogeneity; homogeneity of colour, texture, grey level or any other visual characteristics. Region merging begins with each pixel in the image being its own region. A certain point is chosen as the start position and the pixel and its neighbours are compared; if certain criteria are met the

pixel regions are merged into one region. This reduces the number of regions present within an image. The starting point of this process affects the outcome therefore numerous starting points can be combined. Region merging can also be used in conjunction with region splitting.

Region splitting treats an image, to begin with, as one region and subsequently divides the image into smaller sub-regions. It does this by analyzing a pixel and its neighbours and if certain homogeneity criteria are met the pixels remain in the same region otherwise a second region is created. Splitting would appear to be the same process as merging only in the opposite direction, however the results obtained from the two techniques can differ greatly and it is usual to combine the two methods. An example of region splitting is given below:

- Step 1. For every region a random initial intensity value, i_k, is chosen for the region intensity centres.

- Step 2. The difference between every pixel and i_k is evaluated. Each pixel is assigned to a region, which region this is determined by the direction of the difference.

- Step 3. After subdivision i_k is recalculated. If i_k is altered then step 2 is repeated. If however i_k remains the same process stops, region splitting has finished.

Matching of areas and objects is the third region based segmentation process; a known pattern is searched for within the target image. An exact match is not normally possible. Therefore images with regions that reach a certain pre-defined threshold of matching are selected. Matching criteria can be based upon primitive features such as colour and edges or on higher-level features like shape. Region based segmentation, unlike edge detection, is particularly well suited to noisy images.

The above three modes of segmentation all have their own advantages and limitations. The development of each of these modes of segmentation was based on

domain specific image data. For example, using the Hough transform [28] for edge-based segmentation works accurately for line detection only if it is known that there is a line segment in the image. It is however more effective in most situations to use a combination of segmentation methods.

2.3.1.1.2 Measurement

Feature i.e., colour, shape and texture measurement techniques all have the same purpose, the quantification of visual characteristics. After quantification of visual data its use in a database is relatively simple. Values produced, by the image analysis algorithms, are inserted into a database using traditional and widely available database tools such as a Structured Query Language script [29].

There are numerous techniques of visual feature measurement. One of the most important is the *Fourier Transform* [30]. The *Fourier Transform* is shown in Figure 2.3, the transform decomposes a signal into its component sinusoids, which changes the representation of the signal from space-based into frequency-based.

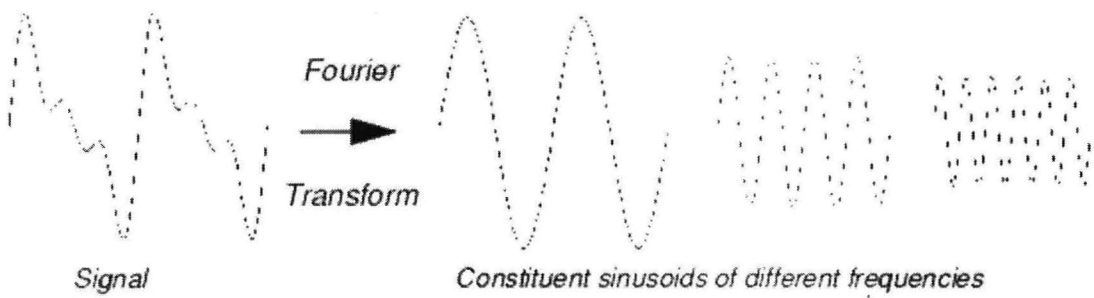

Figure 2.3. Pictorial representation of the *Fourier Transform* [27].

A second major approach to signal decomposition is based upon wavelets. wavelets differ from the *Fourier transform* in the way frequencies are isolated. A wavelet isolates separate occurrences of specific frequencies, whereas the *Fourier Transform* simply isolates a frequency [26]. Wavelets are of finite length while sinusoids, as used in the *Fourier Transform*, extend to infinity. This makes wavelets better suited to measuring localized areas. Both the *Fourier Transform* and a form of *Gabor* [31] based *wavelet* are used in the course of this study to quantify texture.

2.3.1.1.2.1 TEXTURE

Texture is said to consist of component *textons* or *texels* that are its *primitive features.* Texture has been defined as what remains after the consideration of colour and local shape [12]. There are thought to be two visual components of texture: *Tone* and *Structure. Tone* refers to the intensity of pixels while *structure* concerns the spatial relationship between pixels. Textures are visual patterns or spatial arrangements of pixels that cannot be completely described using regional intensity alone. Textures may have statistical properties, structural properties, or both [32]. A popular model for representing texture uses a technique based on Gabor filters of spatial-frequency [33]. Models of the human vision system that use Gabor filters to model the receptive fields have been shown [34] to sufficiently account for psychophysical data obtained in texture discrimination experiments [34].

Texture can be measured as a whole image or via local texture of previously segmented objects. Texture measurement and classification can be realized in a number ways, most of which involve breaking the texture down into its component *primitives*:

- Edge frequency.
- Spatial frequency measured using *Gabor* functions [31], wavelets and filters (scale independent), and also the Fourier transform (Figure 2.3).
- Syntactic description: based on the analogy between the grammar of language and the spatial relationship of texture *primitives.*
- Hybrid methods: a combination of any of the above.

The frequency methods mentioned above can be said to be *Statistical* techniques; it is common to use either a *Statistical* or a *Syntactical* approach. Hybrid methods are less common.

2.3.1.1.2.2 SHAPE, SIZE and POSITION

Segmentation of an image into its component objects enables the subsequent measurement of the objects themselves. Quantification of segmented visual features,

or objects, gives rise to semantic features. Semantic features correspond to actual real world concepts.

The simplest method of characterizing an object is to measure the shape, size and position. The number of pixels belonging to an object equates to its size, and the *X-Y* co-ordinates of those pixels and their geometric relationship refers to the shape and position. These *primitive* visual features can be utilized as comparators, between images, as well as constructing the higher-level semantic features.

After segmenting an image into regions of homogeneity, also known as objects or semantic features, geometric measurements can be taken. Techniques that are commonly used include the decomposition methods outlined previously and also matching strategies such as the *Hough transform* [28]. Size and geometry are not the only properties composing semantic features and visual data. Colour and pixel intensity are also important visual *primitives*.

2.3.1.1.2.3 COLOUR or GREYSCALE

There are three major approaches to quantifying colour. The first method splits the colour of an image, or object into three separate components: hue, intensity and saturation. An image can also be divided into red, green and blue colour elements. The third technique is the CIE standard colour appearance model [35], which breaks colour down to five components: hue, lightness, brightness, colourfulness and chromaticity.

Colour is not always intrinsically available within an image. The vast majority of image modalities within medicine, such as PET, MRI, CT and X-ray, are monochromatic and can therefore only be measured using one dimension, such as the greyscale. They are often referred to as intensity images as it is the concentration, or intensity, of a certain substrate that is quantified. A pixel from an intensity image has only one variable that is not related to its spatial properties and the range of possible values is ultimately dependent on the medical imaging instrument. Medical images, and any other monochromatic image, are however commonly stored in files with a

range of 0–255 (2^8), 0-65535 (2^{16}), or 0-4294967295 (2^{32}) for 8 bit, 16 bit and 32 bit formats respectively.

Analysis of intensity can be carried out using intensity frequency to produce an image histogram. Histogram techniques are commonly applied to whole images but to generate global histograms, they are also however applicable to identified objects that have been segmented Maximal, minimal and derivative measurements can also be taken along with any other statistical values of interest such as mean and standard deviation. Quantification of pixel intensity is fundamental to the previously described segmentation process and it is also utilized by content-based image retrieval systems. The pixel intensity measurements, in the context of content-based image retrieval, are compared between images to perform retrieval based upon visual content. Content-based retrieval however also consists of query formation and a means for a user, of the system, to access the extracted data.

2.3.2 Query styles

The use of image quantification within a content-based retrieval system is dependent on interaction with a user of the system. Within CBIR research there are two main approaches to query formation: query by example and textual query, Figure 2.4 shows a diagram representing the different query by example approaches.

A query by example procedure can be composed of either one image or a group of images. If a group of images is used each image can be assigned a positive or negative value. Figure 2.4 shows a query that requests images most similar to

Audrey Hepburn, and most dissimilar to bank security photo [36,37]. The use of a group query amplifies the common properties of the group. Adding a dissimilar image, or even a group of dissimilar images, increases the magnitude of these properties even further. The query image, as well as being an actual image file, can also be created ad-hoc by the user themselves. This requires a graphical drawing application and is highlighted by the user representation in Figure 2.4. Extending the drawing application so that the definition of regions of interest is possible further enhance functionality. Query by example is not always possible or appropriate. A retrieval system for medical images may, for example, require a query that is composed of semantic information such as patient diagnosis, this would require text based queries.

The textual query is perhaps the more familiar approach; this is due to the fact that the query process is very similar to that used in traditional text based retrieval systems, described previously in section 2.2. A user is required to select keywords, classifiers or language descriptors from a predefined list and consequently build a textual query. The value of the textual query approach increases as the level of semantic interpretation increases; this is graphically represented in Figure 2.5.

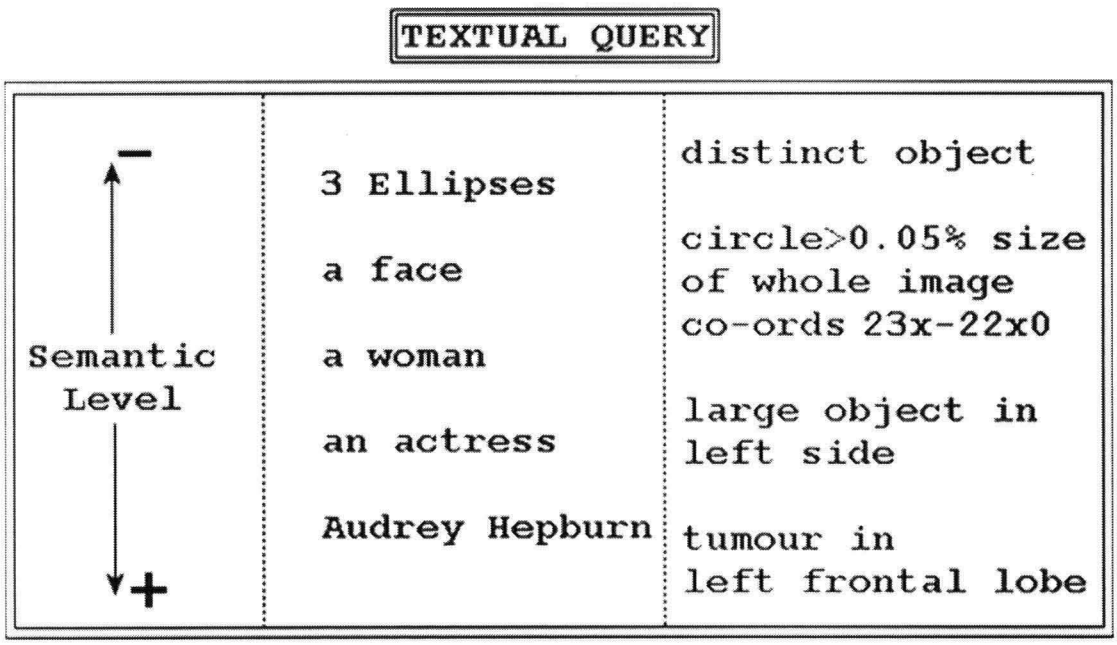

Figure 2.5. Two different queries are shown. One is searching for the actress Audrey Hepburn in a database of domain indistinct images. The second is searching for patients with tumours in database of PET scans. Both use the textual query approach.

Formation of queries and image quantification techniques are not the only prerequisites for a content-based image retrieval system. Retrieval itself is determined by the assessment of similarity between the query data, and the visual data present within each image stored in database.

2.3.3 Similarity Measurement

Similarity measurement plays a fundamental role in image retrieval system. It serves as an organising principle by which the retrieval system classifies objects and makes generalisations. It has been studied extensively by psychologists from analysis of proximity to representation of structure of similar data [38].

The theoretical analysis of similarity relations has been dominated by geometric models, in which similarity is considered to be the complement of distance in an n-dimensional space of one kind or another. Similarity representations can be divided into two classes: spatial models and network models.

The spatial models, called multidimensional scaling, represent each object as a point in a co-ordinate space so that the metric distances between the points reflect the observed proximity between the objects. The database images with the smallest difference in feature vector, when compared to the query image, are returned first. This is referred to as the "nearest *K*-neighbour" approach.

Network models represent each object as a node in a connected graph, typically a tree [39], so that the relations between the nodes in the graph reflect the observed proximity relations among the objects.

For medical images, the similarities are not only based directly on visual data but also on the derived medical saliency. Modelling of the visual data and statistical analysis utilizing predetermined parameters is required to achieve this retrieval based upon medical relevancy. PET image quantification and similarity measurement is detailed in section 2.6.1.

2.4 CBIR and Medical images

So far general computer vision and image retrieval techniques have been outlined. The retrieval procedures and also the feature representation techniques, both previously described in sections 2.3.3 and 2.3.1.1 respectively, give rise to two important issues, which are both dependent on image domain: Visual feature extraction and similarity measurement.

Image domain (i.e. image modality and image subject) relates to what category of images the retrieval systems are going to deal with. Image categories can include:

- Natural images: photographs, video camera stills, and medical images;
- Artificial images: computer graphics, paintings, and drawings;
- Scientific pictures: statistical charts and visualisation patches.

A PET image, for example, is very different to that produced by a commercial closed circuit television camera, and this difference increases if compared to a statistical chart. A medical image, such as a neurological PET scan is typically in the greyscale and has one large circular foreground object and a black background. A typical PET image is shown in Figure 2.6.

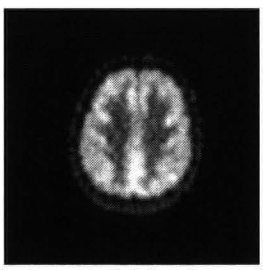

Figure 2.6. Glucose metabolism in transaxial brain section: example of a medical image.

An artificial colour image obtained from the *Microsoft Windows* [6] operating system is shown in Figure 2.7.

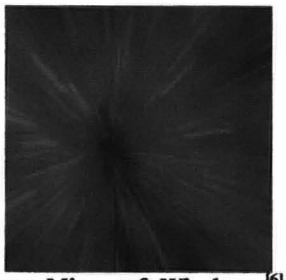

Figure 2.7. Computer graphic from *Microsoft Windows* [6]: Example of an artificial image

A statistical chart, such as a bar graph, contains colour and typically consists of columns, with a high contrast. Figure 2.8 shows a sample scientific visualization.

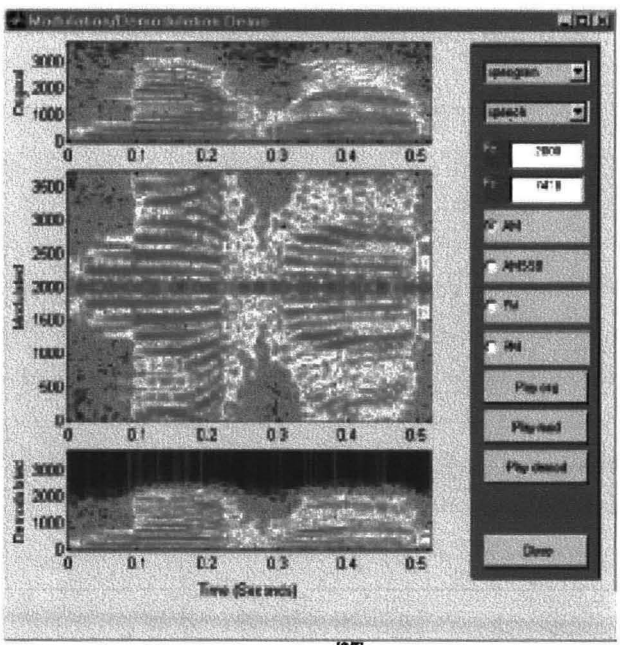

Figure 2.8. Example of a scientific visualization [27], an artificial computer generated image.

Each image domain possesses common visual characteristics, and will therefore require certain visual feature extraction procedures. The importance of each feature such as colour, shape, or texture is entirely dependent on the category of images stored within the database. Extracting colour, for example, would be redundant when utilizing monochromatic PET images. The choice of visual feature extraction technique is therefore dependent on the image domain that is studied. Image domain also therefore determines the similarity metric that is utilized. Similarity metric refers to the method of that is employed to assess the semantic relevance of data.

Image domain is fundamental to the development of a CBIR system; it determines the method of feature extraction and the approach taken to quantify

similarity. This research project is entirely focussed on neurological PET images, which are classed as medical images. It is therefore important to assess progress in this area of CBIR research.

2.4.1 Medical CBIR systems

Retrieval of medical images can be an important part of the patient care process with significance to research, teaching and treatment. There are a few such systems being developed which have been shown to directly improve the accuracy of disease diagnosis [40].

One content-based image retrieval system has been developed by Broderick et al [40,41,42] and utilizes greyscale High Resolution Computed Tomography (HRCT) images of the lungs. The system requires the manual definition of pathology bearing regions (PBR's) and relies on a Custom Query Approach, or CQA. The indexing procedure consists of manually segmenting PBR's from each stored image. PBR's are then characterized using lower level visual features and stored with their associated image and disease type. The CQA is employed to query the database and it does this by splitting the query procedure into two distinct processes. A query image is first analysed for disease type, this disease type is then utilized to retrieve images of the same diagnosis. Images with the same diagnosis are returned, along with the associated set of visual features which optimally describe each image. These returned optimal features are employed to further quantify the query image by characterising visual features of its PBR(s). Visual information that is quantified includes the mean grey level, standard deviation, area histogram and geometric properties such as centre pixel, area and size. Data obtained from this second stage of image characterization is then used to query the database and produce the final set of retrieval results. Retrieval results were shown to increase the accuracy of a physician's diagnosis significantly. Eight doctors were shown a lung image from patients with a range of, previously defined, diagnosis. Each physician was then asked to classify the image from a list of possible diagnosis. The percentage of correct diagnosis increased from 30.2% to 62.4% when the retrieval system could be used as an aid. The results from the Broderick et al study [40] provide a clear indication of the usefulness of content-based medical image retrieval systems and highlight the clinical requirement that is

currently present. The Broderick et al [40,42] study emphasises query formation and the application of retrieval results while relying on expert knowledge input during the feature extraction process. This is not the only strategy that can be taken when researching content-based retrieval of medical images.

An alternate approach to the development of a content-based image retrieval system has been taken to perform content based retrieval on spine X-ray images [43]. Long et al [43] have developed a prototype CBIR system which they split into two distinct areas:

- **Indexing**, the computer assisted reduction of images into mathematical features.
- **Retrieval**, the user interaction to obtain desired images from the database.

Indexing in the Long et al study [43] is composed of the segmentation of images into regions of interest, and the subsequent quantification of these regions using shape characterization. Data from these procedures is then utilized as indices within a *MySQL* [44] database containing the studied spine x-ray images. The retrieval process consists of query formation, feature vector extraction and similarity matching. Long et al [43] rely on the characterization of four separate features: invariant moments, scale space filtering, polygon approximation by curve evolution and *Fourier* descriptors. These features are extracted after an expert has manually segmented the images. Images are classified as normal or abnormal using the previously extracted features. A one layer artificial neural network that has been trained using back propagation performs the analysis and classification. Results show that the artificial neural network method agrees with the diagnosis of a qualified radiologist 85% of the time for images of the cervical spine and 75% for the lumbar spine. This percentage score is achieved after training and validating with two separate sets of images, in total three image sets were used, training, validation and test for each anatomical region.

A third approach to content-based retrieval of medical images is concerned with the classification of images based upon tissue type [45]. Felipe et al [45] utilize texture quantification [46] and also specify a new content feature characterization, the "Gradient Descriptor". The extracted feature ("Gradient Descriptor") is derived from co-occurrence intensity matrices obtained from the original tissue image in four different directions. These visual features are used to differentiate between tissues from various organs of the human body: Brain, spine, heart, liver, adiposity, breast, muscle, bone, and lung. Searching of database and similarity matching performed using Euclidean distance, which is the difference in feature values between the query and those in the database. Retrieval results were reported to be above 90% accuracy for all different tissue types [45].

The three recent research publications reviewed so far [40,43,45] exhibit a number of important differences such as image domain, search algorithm employed and choice of extracted features. Extracted features and search algorithm are to a large extent determined by the image domain...

"...domain knowledge needs to be integrated into specialized query engines" [47].

The following section specifically examines content-based image retrieval in relation to neuro-radiology and PET. This area is significant since PET neurological data forms the basis of the research outlined here.

2.4.2 PET, Neuro-radiology and CBIR

Content-based retrieval of medical neuro-images has not undergone extensive research. There are two predominant research initiatives, Cai *et al* [2] who study PET images, and Liu *et al* [3] who utilize CT (Computed Tomography) and MR (Magnetic Resonance) images.

PET images are represented, by Cai et [2], using physiological data. Physiological information is extracted by applying tracer kinetic modelling techniques that employ blood tracer concentration levels as well as the image data itself. The

data, that Cai *et al* [2] utilize, is not directly visible. Kinetic models require, as parameters the localized intensity levels of radiotracer, obtained from PET images and also the associated blood sample tracer concentration level. This data can then be represented graphically using a simple two axes line graph, with activity and time as the respective axes. It is these two-dimensional graphical representations that Cai et al [2] use to retrieve PET images via their content. The work of Cai et al [2] demonstrates that retrieval of PET images, based on their physiological features, is possible using time-activity curve data as the database index. Tissue time-activity curves, TTAC's, are obtained from dynamic PET images, which are produced by acquiring several contiguous frames over a period of time, typically 60 - 90 minutes. Each scan shows a change in radiotracer activity levels, and it is this change in activity that forms the TTAC. The corresponding plasma time activity curves, or PTAC's, are also obtained at the same time by taking serial blood samples. Dynamic imagery is employed to assess, for example, the binding of drugs to brain receptors. Static imaging is utilized in diagnosing patients with neuro-degenerative disorders, tumours or other physical injuries. There is however some contention over whether the research carried can be classified as content-based image retrieval. This is due to the fact that TTAC's do not pertain directly to visual content, as remarked by [47] ...

" ... [TTAC 's] are not really image features but rather one dimensional temporal signals " [47].

The method implemented does however require a substantial amount of expert knowledge and interaction. It relies on PET scans that have been manually segmented and radiotracer levels in blood supply that are manually derived, which are both not always available. Alternative methods of image quantification must therefore be developed and implemented.

The second major academic group, researching CBIR of neurological images, is that of Liu et al [3]. A technique for extracting features from CT and MR images has been developed, by Liu et al [3], in which the derived visual information is used to perform content-based image retrieval. First, lesions are detected. Then based on the measurements of lesions images are indexed within database. The strategy employed revolves around the detection of a symmetry plane, the ideal Mid-Sagittal Plane or

iMSP, and the subsequent subtraction of the two hemispheres from one another. The iMSP, a virtual geometry plane about which the brain has maximum bi-lateral symmetry, is used to create a mirror image of the original. These two images are then subtracted from one another and any asymmetrical lesions are consequently revealed. Feature measurements include location, size and shape of lesion. Following the quantification of these features they can then be utilized in a database. Retrieval from the database is performed using *Kernel Regression* and *Bayes* decision theory. An offline search of available classifiers is performed, and the associated similarity metric is used to query the database; in other words each of the features is given a weighting based on previous classifications, these features are then compared with those stored in the database. Retrieval results from the preliminary study demonstrate accuracy of "approximately 80%" when tested with images from patients diagnosed as normal, with a stroke or an acute bleed. No attempt is made to classify images from patients diagnosed with neuro-degenerative diseases such as Alzheimer's.

A third research group investigating neuro-radiological images and retrieval have targeted the retrieval of scientific articles based upon neuro-anatomical visual information [48]. The system that has been developed is queried using Talairarch and Tournoux [4] spatial co-ordinates, retrieval results consist of scientific articles, available from BrainMap [49], that are related to the neuro-anatomical structure that has been specified by the user formulated query [48]. The system is not a content-based image retrieval system due to the fact that images are not retrieved. It is however relevant due to the fact that a visual query is carried out that uses the standardized Talairarch and Tournoux [4] spatial co-ordinate system.

A significant amount of research has been carried out in the area of content-based retrieval of neurological images [47]. The PET modality, and neuro-radiology in general, has however been somewhat neglected. At present only one other academic research group [2] is working towards PET image retrieval, and three in total are researching the content-based retrieval of neuro-radiological images.

Classification and retrieval of PET images based upon their actual diagnosis has not been broached, and neither has PET image retrieval based directly upon visual

features. CT and MRI image retrieval based upon visual features and concurrent with clinical diagnosis has however been successfully researched [3].

The mechanisms and theories that are used to achieve content-based image retrieval have been shown to be entirely dependent on the image domain being studied [2,3,40,43,45,47,48]. A detailed understanding of the applications and characteristics of the images being studied is thus fundamental to the development of a content-based image retrieval system. Comprehensive knowledge of PET imaging and quantification is therefore required before content-based PET image retrieval can be developed.

2.5 Positron Emission Tomography

To understand PET image retrieval it is necessary to have some insight into the history of medical imaging, the technology and physics that it is based upon and the role it plays within medicine.

The first medical images produced using ionising radiation were the x-ray radiographs taken at the turn of the last century (1895) by, the winner of the first Nobel Prize in physics, William Conrad Roentgen [50]. In order to produce three-dimensional images, rather than two-dimensional ones such as radiographs, tomographic reconstruction algorithms and scanners that could acquire the data necessary for tomography were needed. The major breakthrough in tomographic medical imaging was the development of computed tomography (CT) and the first commercial medical instrument capable of obtaining digital axial images with high-contrast resolution. This occurred in 1972, and was carried out by Sir Godfrey Hounsfield who together with Alan Cormack was awarded the Nobel Prize in Medicine in 1979 [50]. In 2003, Prof. Peter Mansfield from Nottingham University together with Professor Paul Lauterbur from the USA also won the Nobel Prize in Medicine, for their discoveries concerning Magnetic Resonance Imaging (MRI) [50]. These discoveries, during the 1970's, have led to the development of modern MRI, which represents a major breakthrough in the fields of medical diagnostics and research [50]. The enormous diagnostic impact of CT inspired those already working in non-tomographic imaging using positron-emitting tracers to develop a tomographic version of the technique, which came to be known as positron emission tomography (PET).

The first PET scanners were operational in 1975. In 1997 there were approximately 150 health centres with PET scanning facilities, the vast majority of which are in North America and Western Europe [1], as distributed in Figure 2.9. There have been no studies into the volume of PET images that have been produced, it can however be assumed that each PET centre has many gigabytes of stored data.

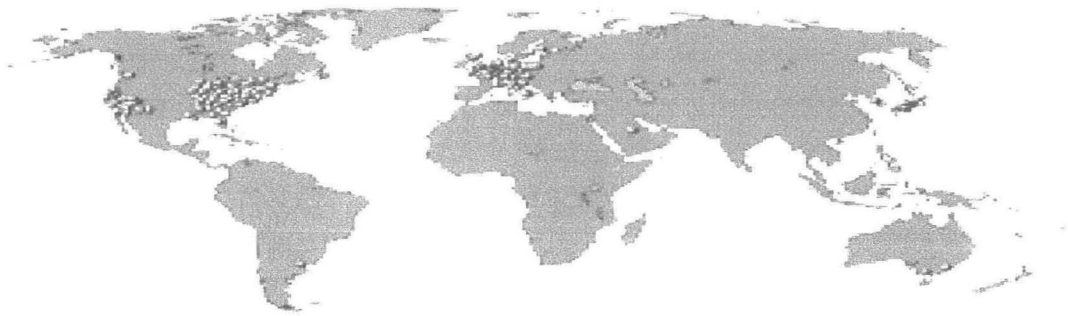

Figure 2.9. Distribution of PET scanners around the world [1].

A neurological PET scan measures the localized intensity of a radio-labelled tracer within the brain. This information is refereed to as functional or physiological data, a PET image contains very limited anatomical information which is tracer dependent. Intensity levels revealed by the PET scan correspond to the concentration of tracer substance, which itself equates to neuronal activity. When an analogue of glucose is used as the tracer its uptake and rate of metabolism are derived. Different tracers can be used to quantify alternate activation pathways within the brain and PET scanning is therefore particularly useful in the drug discovery process. Although PET images have a poor spatial resolution (~5mm), when compared to MRI (~1mm) and CT (~1mm), they are still very much at the forefront of scientific research and play a significant role within medicine. This is due to the fact that a PET scan can reveal physiological, or functional, information that is complimentary to the anatomical information provided by MR and CT. In many disorders a change in physiology both precedes a change in anatomy and provides more specific information. The most recent high-resolution brain PET scanners have a resolution ~3.5mm [51].

Functional information can also be obtained from MR using the non-quantitative blood flow imaging technique known as *functional*-MRI, or *f*MRI [52,53]. This approach has become widely used in the field of brain mapping. Compared to PET imaging it has superior resolution (temporal and spatial), high signal-to-noise ratio, more affordable cost, and it eliminates the requirement of ionising radiation. The sensitivity for tracers labelled with MR tags is much lower than PET.

Functional forms of MR will not replace PET as many kinds of molecules can be tagged with positron-emitters, such as carbon-11. PET imaging allows specific ligands to be labelled using radioactive tracers this makes receptor-ligand studies possible whereas they are not with *f*MRI. This ability, to quantify and localize a variety of substances within the living brain, is the primary advantage of PET over *f*MRI.

Radiotracer research continues with the most recent development that of an amyloid tracer, Pittsburgh-compound B, which can quantify amyloid deposits in the living brain [54]. Recent developments have also introduced the prospect of much cheaper PET scanners [55]. The prohibitive cost of producing radioactive neurotransmitters can theoretically, be reduced by using lasers [55]. Consequently, PET will remain a widely used method for assessing the different physiological pathways in the brain.

2.5.1 Characteristics of PET imaging

PET provides the means for imaging the rates of biological processes *in vivo*. It requires the administration of radio-labelled tracers into subjects in order to generate PET images. Depending on the information clinicians would like to see from the images, different tracers might be applied. For example, when detecting tumours the most commonly used tracer is FDG. The most common nuclides used are Oxygen-15 that has a half-life of 2.1 minutes, Nitrogen-13 with half-life of 10.0 minutes, Carbon-11 with half-life of 20.4 minutes, and Fluorine-18 with half-life of 109.7 minutes [56]. The half-life is the time period within which half the nuclei will, on average, decay.

A typical 3D PET scam of a human brain is given in Figure 2.10. It utilizes fluorodeoxyglucose, or FDG, an analogue of glucose as the radiotracer.

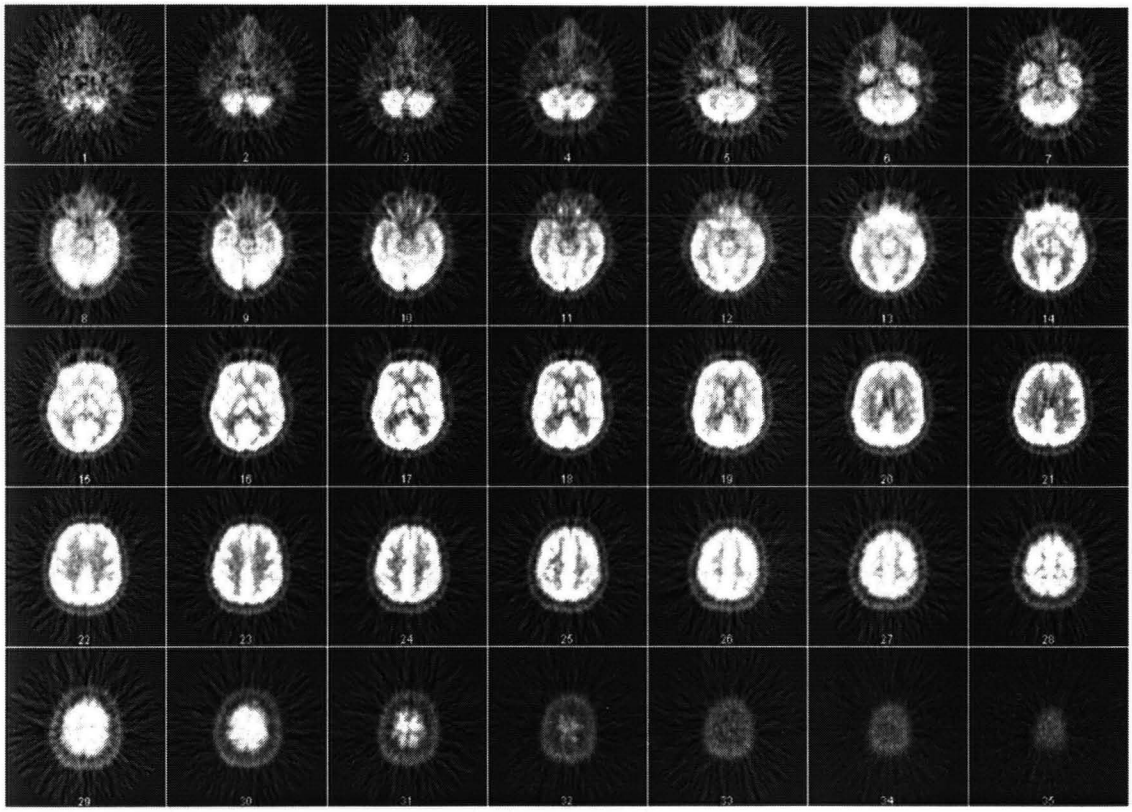

Figure 2.10. A typical, glucose metabolism, brain PET scan of a normal subject.

2.5.2 Clinical Application of PET to Neurology

The examination of PET images, by experienced clinicians and radiologists, can reveal the presence of neurological disorders, such as Alzheimer's disease, Brain tumours, and head injuries, which are the abnormalities that are studied in this PhD project.

2.5.2.1 Alzheimer's disease

Alzheimer's disease (AD) is a degenerative disorder that is the most common neurological cause of dementia. AD has a unique pathology, with a characteristic pattern of hypo-metabolism due to a reduction in synaptic activity and cell loss.

It is possible to diagnose AD early on in its progression, non-invasively, and reliably with PET. The 3D PET image of a patient suffering from AD is given in Figure 2.11 [56].

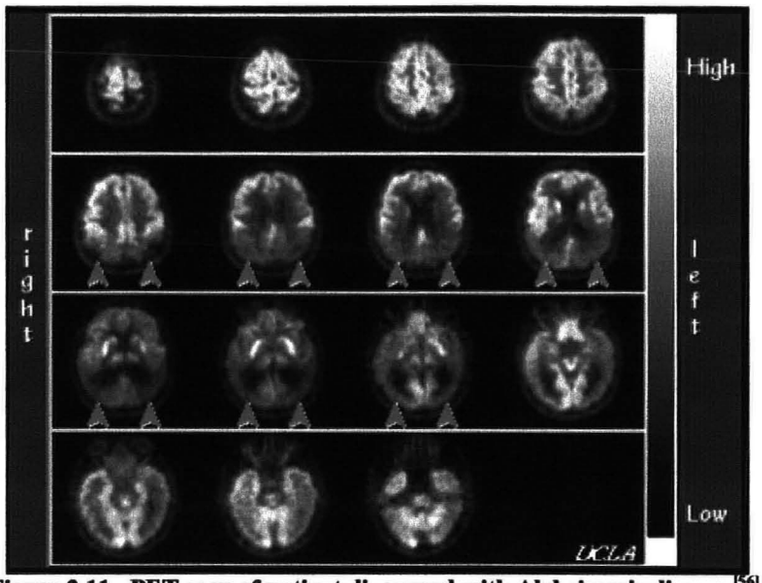

Figure 2.11. PET scan of patient diagnosed with Alzheimer's disease [56].

Figure 2.12 shows the comparison of an AD image with the image from a normal subject [56].

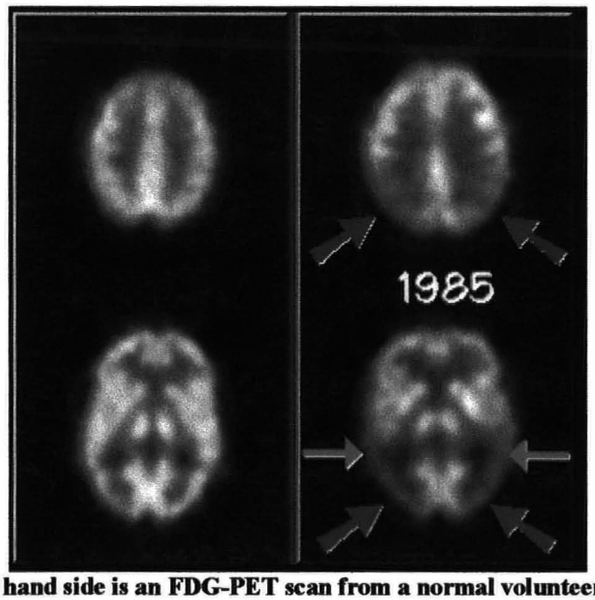

Figure 2.12. The left hand side is an FDG-PET scan from a normal volunteer, whilst the image on the right is from a patient diagnosed with Alzheimer's [56].

Figures 2.11 and 2.12 show that the intensity values around parietal and temporal lobes are much lower for an AD patient as compared to that from a normal subject [56]; which increases the possibility that such diseases can be diagnosed through the appearance of abnormal brain activity in PET images.

2.5.2.2 Brain Tumour

Figure 2.13 shows, on the right hand side, a slice from a PET scan of a patient with a tumour. The arrow indicates the tumours' position. On the left hand side is the corresponding CT image from the same subject [56]. To interpret a brain tumour using FDG-PET, identification of a region or focus of abnormal intensity tissue in relation to the surrounding white or grey matter is the first step.

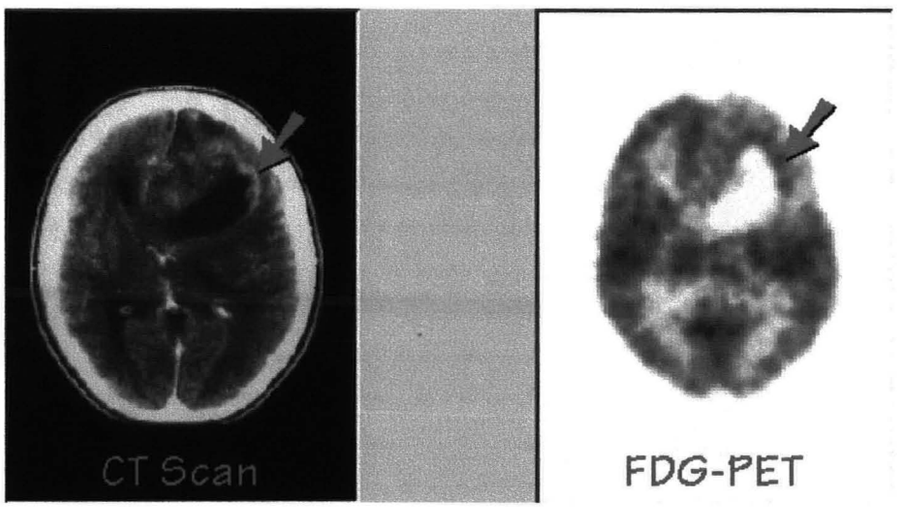

Figure 2.13. CT and PET scan of subject with a brain tumour [56].

Careful visual examination of images by experts enables diseases, and injuries to be diagnosed. Co-registration of a PET image to a CT, or MRI scan reveals the anatomical structure of the brain, the effected area can therefore be determined. CT and MRI scans of patients are however not always available.

2.6 PET Analysis Methods

Complex methods of analysis, involving the modelling of radio-tracers and the localization of anatomical structures have been developed to assess PET images, with their accompanying anatomical scans, and also without. There are a number of different techniques and algorithms that can be utilized to perform quantitative analysis of PET neurological images. This section will focus on examining the different modes of analysis used in the fields of medical imaging and computer science.

2.6.1 Spatial Normalization and Co-Registration

The processes of spatial normalization and co-registration are important to a wide range of medical imaging fields. Spatial normalization, of an image set, tries to make all images have the same size and shape; the images are warped to fit a standard space. Co-registration is the closely related procedure in which images are translated and rotated so that they best match an image from a different modality.

PET studies, and also studies that use alternate brain imaging technologies such as MRI and CT, rely to a large degree on inter-brain or inter-subject comparisons. A typical study involves obtaining PET scans groups of subjects and controls and then performing statistical analysis on the group(s) to elucidate any significant differences. Before statistical analysis can commence on a group of images the anatomical variability and movement artefacts must first be removed. If anatomical variability is not removed voxel *a* in subject one may belong to a different anatomical structure than voxel *a* in subject two. A voxel is the equivalent of a two dimensional image pixel in three dimensional space.

To obtain valuable medical information from PET images voxel by voxel analysis can be performed, a voxel is equivalent to an image pixel in three-dimensional space. Specifically the voxel intensity property, which represents metabolic activity, is associated with an anatomical brain structure. There are two standard approaches that are used to create this association. The first method requires a Magnetic Resonance Image of

the same subject to be taken and co-registered with the PET image, the co-registered image can then be warped to fit a standard pre-defined space. Regions of interest can then be manually defined, using software such as *Analyze* [10].

The alternate method, used to associate voxels with the correct anatomical structures, is to warp the original PET image to a template from the same modality. The PET image will then fit into a standard space, such as that defined by Talairarch and Tournoux [4] or the Montreal Neurological Institute [57]. The difference is that the warping is performed without first co-registering the PET image to an anatomical image from the same subject.

To perform spatial normalization a template image is required that conforms to a standard known space. In this research all the PET images are spatially normalized to the MNI template [57] as supplied with the software package *SPM* [58] and recommended by the International Consortium for Brain Mapping [60]. The MNI template was originally produced by the McConnell Brain Imaging Centre part of the Montreal Neurological Institute (McGill University) [61]. The Talairarch and Tournoux brain was approximately matched to the MNI template using a two-stage procedure. Various landmarks were manually defined on 241 normal MRI scans. Each brain scan was scaled so that the defined landmarks fitted with equivalent positions in the Talairarch and Tournoux atlas. 305 normal MRI scans were then taken, and an automated 9 parameter linear algorithm was applied to match the 305 brains to the average of the 241 brains that had been previously matched to the Talairarch atlas. The 305 transformed brain images were averaged to produce the MNI template [57]. It must be noted that the MNI brain and Talairarch and Tournoux space are not exact matches. Equation 2.1 [62] represents the process for calculating the transformation that must be applied, to co-ordinates from the Talairarch and Tournoux atlas so that they are concurrent with the MNI brain, where P is transformation parameter determined by V_{xyz}.

$$T^S = V_{XYZ} \bullet \begin{bmatrix} 1.0000 & 0 & 0 & 0 \\ 0 & 0.9988 & -0.0500 & 0 \\ 0 & 0.0500 & 0.9988 & 0 \\ 0 & 0 & 0 & 1.0000 \end{bmatrix} \bullet \begin{bmatrix} 1.0101 & 0 & 0 & 0 \\ 0 & 1.0309 & 0 & 0 \\ 0 & 0 & P & 0 \\ 0 & 0 & 0 & 1.0000 \end{bmatrix} \quad \textbf{(2.1)}$$

The two procedures of *spatial normalization* and *co-registration* are in fact based upon exactly the same theories and can use identical algorithms. There are a number of different approaches that have successfully been applied to the problems of inherent within *spatial normalization* and *co-registration*; all approaches however are based upon the same principal, maximizing similarity between the two different images.

Comprehensive reviews and surveys of these image manipulation techniques have been published [63,64] and each of the different techniques has been shown to have advantages and disadvantages. No significant performance increase for any particular technique has been found [63] and the different approaches "produce satisfactory results most of the time" [63]. Techniques utilized in co-registration and spatial normalization can be classed into a number of different categories [64]:

- ***Non-image based***: scanners are calibrated together.
- ***Dimensionality***: designed for 2D, 3D, or 4D (time series) image sets.
- ***Extrinsic***: Subject has had foreign objects introduced, such as Fiducials, moulds and stereotactic frames, to aid analysis.
- ***Intrinsic***: Based on image information generated from subject alone. Utilizing anatomical/geometrical landmarks or segmentation methods. The final intrinsic method is based upon voxel properties.

Perhaps the most widely used implementation, of *co-registration* and *spatial normalization* algorithms, is *Statistical Parametric Mapping* or *SPM,* which is distributed by University College London [58]. *SPM* is a set of routines within *Matlab* [27] that was designed for the express purpose of registering and spatially normalizing radiological

images (PET, SPECT, CT and MRI) of the brain and performing statistical analysis of these images. The approach taken by *SPM* is detailed in the next section.

2.6.2 SPM Methodology

The image analysis and manipulation algorithms, employed as part of *SPM*, are based upon affine image registration techniques [65,66]. They can be classed as *intrinsic* due to the fact that they use the full image content of the voxel intensity property. Affine transformation conserves the ratios of distances along lines; this means that parallel lines remain parallel, as shown in Figure 2.14.

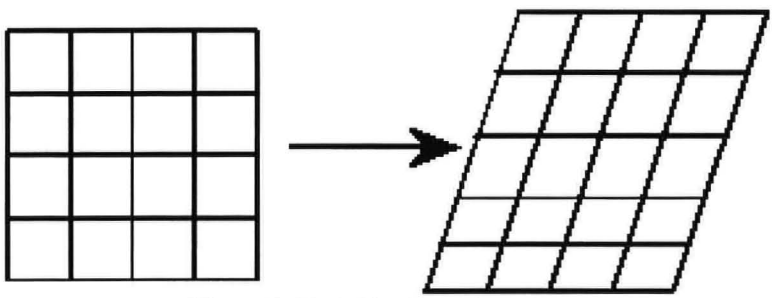

Figure 2.14. Affine transformation.

To achieve spatial normalization two images, one called a source and the other called template, are first registered together to produce a set of transformation parameters. The source image is that which is warped to fit the template. For the least squares registration to produce an unbiased estimate of the spatial transformation, the image contrast in the templates (or linear combination of templates) should be similar to that of the image from which the spatial normalization is derived. The registration searches for an optimum solution. The registration process itself is based upon utilizing the maximum *a 'priori* posterior estimate within a Bayesian framework, to generate a best fit for the transformation parameters.

SPM is used to perform *spatial normalization*. The approach that *SPM* employs relies on minimizing a basis function representing the difference between the template and test images. The difference, X^2, between the template image and subject image is minimized by iteratively altering the twelve transformation parameters, and the one additional intensity scaling parameter. Iteration is stopped when X^2 no longer decreases.

This is a gradient descent approach with the probability of halting at a local minima reduced by first smoothing the subject image. The spatial transformation, referred to as tp=Mp, contains the 12 spatial parameters and is shown below in Equation 2.2. Where p refers to a voxel at a certain position in the original image and tp is the transformed position of voxel in new image.

$$\begin{pmatrix} tp_1 \\ tp_2 \\ tp_3 \\ 1 \end{pmatrix} = \begin{pmatrix} M_1 & M_4 & M_7 & M_{10} \\ M_2 & M_5 & M_8 & M_{11} \\ M_3 & M_6 & M_9 & M_{12} \\ 0 & 0 & 0 & 1 \end{pmatrix} \cdot \begin{pmatrix} p_1 \\ p_2 \\ p_3 \\ 1 \end{pmatrix} \qquad \textbf{(2.2)}$$

Spatial parameters $M_1 - M_6$ relate to the position of the patient head in scanner and the spatial transformations of rotation and translation. $M_7 - M_9$ refer to warping along the Z-axis to fit into the templates' standard space. $M_{10} - M_{12}$ are the parameters for scaling and shearing the subject brain. The function that is minimized, X^2, is therefore represented as the sum, of spatial mapping minus the intensity scaling in relation to the subject image, at each position in the template image. This is represented in Equation 2.3; where S is subject image, T is template image and M_{13} is the intensity scaling parameter.

$$X^2 = \sum_i \left(S(Mp_i) - M_{13}T(p_i)\right)^2 \qquad \textbf{(2.3)}$$

Equation 2.3 shows the function X^2 which is minimized during the spatial normalization procedure. The approach taken by *SPM* [66], and consequently used in this study, incorporates *Bayes* probability using 51 MRI images transformed using the basic operation. These 51 transformations supply a multi-normal *a priori* distribution of parameter estimates. Implementation of *Bayes* probability theory alters the spatial normalization so that the transformation parameters are not solely dependent on the minimization of X^2; they are also determined by their difference to that which is expected by the predetermined estimates.

The registration procedure can be summarized as finding the minimum sum of squared voxel intensity differences between the target and template images. The

registration process is sensitive to a small number of voxels that have large intensity variations, and is, consequently, most suitable to intra-modality (i.e. the same modality) registration [67].

The parameters, obtained from the registration procedure, are then applied, using a transformation function, to the target image so that it fits into the standard space and shape of the template image, which itself fits a pre-defined anatomical atlas such as Talairarch and Tournoux [4].

When spatial normalization is carried out on a group of images it allows comparison between subjects as each brain image fits the standard space and is, to a certain (significantly valid) degree, the same size and shape. During the course of this research the spatial normalization algorithms from *SPM* have been used and are detailed in section 2.6.2. Spatial normalization is not the topic of this research and is merely used as tool. The *SPM* software is applied in this project as it is arguably the most widely used and the *Matlab* source code is freely available and can be easily altered and implemented. It is often considered the most sophisticated software available for the spatial normalization and co-registration of brain images.

Spatial normalization is however only the first step in carrying out a PET study. To obtain meaningful data from a set of PET scans further processing and quantification is required.

2.6.1 Techniques of PET analysis and measurement

To produce experimental data post normalization the PET images are further analysed. All analysis, of PET images, requires the measurement of the Cartesian co-ordinates of a voxel and also its intensity value. Voxel intensity property itself is an extrapolation of, and directly correlated to, metabolic activity. Slice 33 from a normal brain, which has been spatially normalized, is shown in Figure 2.15. Figure 2.16 shows

two typical examples of pixel intensity histograms for a slice 33 of normal brain in Talairarch and Tournoux space [4].

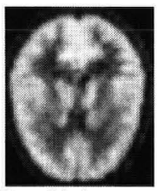

Figure 2.15. Slice 33 from a normal brain.

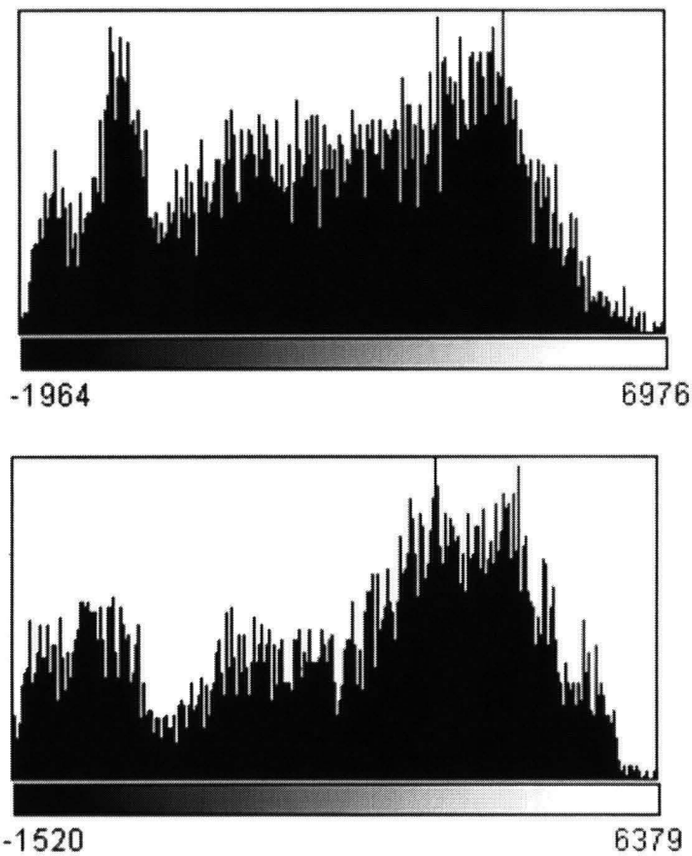

Figure 2.16. Histogram of pixel intensity from the same number slice of two spatially normalized normal brains.

Figure 2.16 shows the histograms from two subjects with the same normal diagnosis, the histograms themselves differ greatly as do the corresponding global properties such as mean and standard deviation. Figure 2.17 shows two further

histograms again taken from slice number 33, but this time the PET images are from patients diagnosed with Alzheimer's.

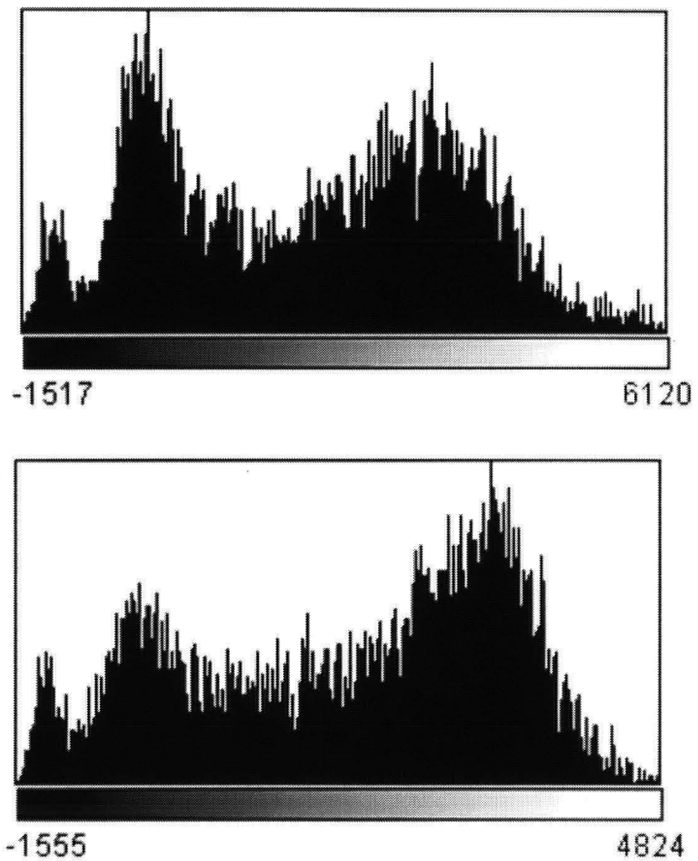

Figure 2.17. Histogram of pixel intensity from the same number slice of two spatially normalized brains diagnosed with Alzheimer's.

Global intensity histograms do not reveal medically semantic information as demonstrated by the histograms presented in Figures 2.16 and 2.17. Due to the fact that global measurements are medically irrelevant the first stage taken in PET studies, after spatial normalization, is to define and segment a specific anatomical region for investigation. Segmentation is carried out using prior knowledge of neuro-anatomical structures, combined with the visual intensity patterns. Analysis of the region of interest can then be carried out by measuring the intensity of pixels; The Crump Institute [56], outline five approaches to the quantitative analysis of PET images:

- ***Radioactivity image***: PET scan presented as a series of 2D slices, colour/intensity of pixel represents activity.
- ***Mean value of ROI***: Region of interest manually drawn on to radioactivity image, mean of pixel values calculated for the region.
- ***Time activity curve for roi***: Mean activity of a region plotted against time. Requires a time series PET scan.
- ***Normalized ROI curve***: The ratio of mean ROI to whole brain mean.
- ***Tracer modelling of roi curve***: Mathematical model fitted to time-activity ROI plot, results in values for binding potential, blood flow and receptor density.

The techniques outlined above are however not all suitable for making comparisons between studies and their respective image sets. Consequently they would not be applicable to image indexing within a content based retrieval system, which is the focus of this research. For the purposes of content-based PET image retrieval new techniques were developed for quantifying PET neurological images and existing methods have been significantly extended.

2.6.2.1 KINETIC MODELLING

Physiological and biochemical data from PET can be obtained by comparing voxel property values of one area of the brain to another over a known time scale; this is called kinetic or tracer modelling. Kinetic modelling can be used to elucidate the binding potential of a certain transmitter within regions. Using the *simplified reference tissue model* [68] it is possible to measure binding potential without the need for arterial cannulation and only utilizing data contained within the image. Binding potential, which is directly proportional to receptor density, can be used to index PET images within a database when receptor density is significant.

2.6.2.2 STATISTICAL MEASUREMENT

Metabolic activation homogeneity/heterogeneity can be used to characterize PET images [70] and is dosage and scanner independent. By calculating the co-efficient of variance, or CV, of voxel intensity within localized structures and also the whole brain, a reliable estimate of functional homogeneity/heterogeneity can be produced. Functional homogeneity/heterogeneity refers to the metabolic activation pattern, which is the distribution of intensity values across the brain and localized structures. Measurement of CV concerns the pattern and distribution of activity rather than the absolute magnitudes of variations in activity.

The CV is a relative value calculated by measuring the standard deviation (SD) and mean of voxel intensity values, and is shown in Equation 2.4.

$$CV = \left(\frac{SD}{MEAN} \right) * 100 \qquad \textbf{(2.4)}$$

The higher the CV value the larger the heterogeneity, and vice versa. A PET image with a low CV has a more constant/uniform distribution of activity values. PET images from patients diagnosed with Alzheimer's have a larger CV than normal patients [70]; the distribution of voxel intensity values is less uniform, there is a greater variation in activity. Homogeneity/Heterogeneity can be used to compare images from different sources, and therefore index images within a database or a content-based image retrieval system. This is due to the fact that dosage and scanner differences are redundant. It is relative intensity distribution patterns are measured and not absolute levels of metabolic activity.

A second statistical technique that quantifies and characterizes PET images utilizes the mean index ratio. Mean index ratio is based on the normalized ROI curve process [56] previously shown. The mean intensity value of an anatomical structure is compared to the mean value for the rest of the brain producing a single ratio. A range of

ratios is derived the normalized ROI curve can is used and can only be used to quantify time series scans. Mean index ratio can however be applied to individual non-time series PET scans and it can therefore be used to characterize PET scans. This is due to the fact that certain diagnosis type's exhibit significantly increased or decreased metabolic activity within specific anatomical structures. Alzheimer's disease exhibits significant hypo-metabolism in the *Posterior Cingulate* [71], the *Parietal Lobes* and the *Temporal Lobes* [72]. To compare the absolute mean values from two different PET scans would not be suitable for image indexing as scanner and dosages differences would be apparent. Mean index ratio is therefore measured; the mean index value is calculated by comparing mean value of the specified ROI to the rest of the brain. It quantifies the anatomical areas with abnormal transmitter uptake by comparing to other anatomical structures with normal metabolism. Any dosage and scanner discrepancies are made redundant as the abnormal area is compared to the rest of brain; the mean index ratio can therefore be applied to the problem of image indexing within a content based retrieval system.

2.6.2.3 ASYMMETRIC ABNORMALITIES

Hemispheric differences in the brain such as those caused by tumours, strokes, and head injuries can also be used to classify images and diagnose patients. A sample slice from a patient diagnosed with a tumour, which is apparent as a bright asymmetric region, is shown in Figure 2.18.

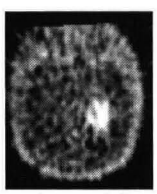

Figure 2.18. PET image from patient with a tumour taken from this study.

Previous research has shown that asymmetrical discrepancies in MRI images can be used to classify and index images within a database system [73] by utilizing the mid-sagittal plane method.

A second widely used method for detecting and measuring abnormalities such as tumours, injuries and strokes is implemented by the software package SPM [58]. The SPM method requires a control image for reference, and all the experimental data must have intensity normalization performed. Abnormalities are then labelled at positions where the pixel intensity is three standard deviations away from the control images intensity at the location. Abnormalities can therefore not be characterized unless a control image is present and intensity normalization carried out.

2.6.2.4 TEXTURE

Texture can be defined in a number of complementary ways. It is...

"[an] identifying quality" ... "the disposition or manner of union of the particles of a body or substance" [14] ... "something consisting of mutually related elements" [26]

Statistical measurements of PET images, outlined in section 2.6.2.2 (*Statistical Measurements*), quantify global properties such as the mean. Texture characterizes and measures the differences in pixel/voxel intensity with reference to spatial attributes such as distance and direction. Classification of images using texture measurements is widespread QBIC, IMATCH and NETRA [18,19,21] for example all use texture as an image classifier.

Texture has also been researched as a diagnostic tool for PET images [74]. Work has been carried out that analyses PET sinograms using texture quantifiers based upon the *Radon* transform [75]. Results showed that it is a valid method for diagnosing Alzheimer's in patients [74], classification using the unreconstructed PET data and texture measurements was 90% accurate [74]. PET sinogram refers to the detected data before 3D reconstruction has been completed. Sinograms are not used in this study.

Texture is used in this research as a tool for classifying reconstructed PET images by quantifying the metabolic activity patterns that are present. Texture is quantified by

utilizing *Gabor Functions* as image filters. *Gabor Functions* are based upon the human neural visual system and are a widely used method within image processing of quantifying digital visual representations. The application of *Gabor* filters to PET images for the purpose of texture quantification [76] is a technique that was initially developed to characterize images from alternate domains [77], and has been described previously in section 2.3.1.1 (*Visual Feature Representation*).

2.7 HI-PACS

The term "Digital Radiology" was introduced as early as the beginning of the 1970's [78,79]. However, due to technological limitations of the time, it did not become well known and there was little work carried out. During the early 1980's advances in computer processing power enabled many researchers to become involved in this area. It was at this time that the concept of Picture Archiving and Communication Systems, or PACS, was first proposed [80]. It was also during this period that the very first conference dedicated to PACS took place [81]. By definition PACS consist of image acquisition, storage and display devices; the simplest and most popular form of PACS today could be said to be the home PC and digital camera. Although this is far removed from the "enterprise" or "data-warehouse" scale HI-PACS (Hospital Integrated PACS) the principles remain the same. A HI-PAC system however needs to be able to process images from a number of different modalities, such as ultrasound, X-ray, CT, MRI and of course PET.

A HI-PAC system not only has to function with the vast amounts of image data present within a hospital it is also responsible for the management of associated diagnostic reports and administrative details. There are numerous implementations of HI-PACS around the world and also many commercial vendors of PACS for health care. Retrieval of images from their respective databases is always carried out using keywords and language descriptors. The systems must therefore rely on consistency between individuals when searching and updating the database. PACS rely on traditional image retrieval techniques that are built around traditional database technologies; this means that results of retrieval are, to a degree, unreliable.

The HI-PACS industry is thought to be worth approximately $1billion. The companies selling HI-PAC systems and related products include: *Kodak*, *Agfa*, *Siemens*, *Marconi*, *Philips*, and *Canon*. The minister of health in the UK, John Hutton, has announced the contracts for every UK Hospital to have an installed HI-PACS by 2007 [82]. This growth of the HI-PACS industry coupled with the *Health Insurance Portability*

and Accountability Act of 1996 [83] which defines standards in for electronic patient records in the USA, suggests that Hospital Integrated Picture Archiving and Communication Systems will play an ever more important role in patient care.

As mentioned previously, PET imaging is a technique that is widely used and will undoubtedly continue to be; its presence in HI-PAC systems would seem to be assured. However, to develop a content-based HI-PACS there is a long way to go. This project attempts to develop a content-based image retrieval system for 3D PET images, which is consequently a step towards content-based HI-PACS.

2.8 Summary

Traditional image databases are no different from any other type of data storage solution. An administrator or user inserts data into the database along with a textual description. The description is either created based on the users' experience, or chosen from a pre-defined list of keywords. In a medical system for example, the patient image files are stored inside the database and indexed using *keywords* such as:

- *Diagnosis*, a description of any abnormalities.
- *Administrative details* like age and gender.
- *Patient identification numbers*.

The main deficiency with such a system is the subjectivity of the indexing data; it is possible that two different users would describe the same image in a different manner. This is the primary problem; other shortcomings such as time efficiency are also present.

Content-based image retrieval is defined as the indexing of images using only data pertaining to their perceived visual features, or the content that the images posses. The benefits of content-based image retrieval over traditional systems include: Objectivity, increased time efficiency, greater reliability and validity, and the elimination of redundant data.

During this study a content-based retrieval system for 3D PET neurological images has been developed. Medically salient visual characteristics are extracted from neurological PET images and then utilized within a database system.

3 Materials

The majority of Positron Emission Tomograph, or PET, images are supplied by the Wolfson Brain Imaging Centre [9]. However some are provided by Hammersmith Hospital. Images are studied using a selection of software development tools and hardware.

3.1 Image Acquisition

The PET image data has been obtained from the Wolfson Brain Imaging Centre, or WBIC, located at Addenbrooke's Hospital, Cambridge, UK. It is part of the University of Cambridge [9]. The technical specification [51] of the PET scanner used at the WBIC is given in Figure 3.1

- average resolution *c.*5x5x5mm
- 2D/3D acquisition
- transaxial FOV: 55cm
- axial FOV: 15.2cm
- patient port: 59cm
- axial sampling: 4.25mm
- detector arrangement:
    - ring diameter: 92.7cm
    - number of rings: 18
    - number of crystals per ring: 672
    - total number of crystals: 12096
- 5-node 3D array processor (*c.*16mins 3D frame reconstruction time)

Figure 3.1. Technical specification and photograph of General Electric Medical Systems *Advance* PET scanner [51].

The simplified procedure for acquiring PET images [9] is as follows:

1. A molecule labelled with a positron-emitting nuclide (carbon-11, oxygen-15 and fluorin-18 are the common nuclides) is administered into a patient, either intravenously or through inhalation.

2. The positrons emitted travel about 1mm in tissue before annihilating with an electron naturally present in the body. To conserve energy-mass (as described by Einstein's $E=mc^2$ formula) and momentum, two gamma rays are emitted in opposite directions from the point of annihilation. Each photon has energy equivalent to the rest mass energy of the electron (511 keV). A ring of detectors is used to detect these photon pairs, each of which define a line in space along which the annihilation, and hence the labelled molecule, lies. Acquiring such data over 180 degrees around the patient allows the three-dimensional distribution of the tracer to be reconstructed using tomographic image reconstruction techniques, similar to those developed for CT.

3. The level of tracer concentration at a point in space reflects the delivery of the tracer to the tissue and its uptake and release from various tissue compartments. In order to convert the radioactivity images into physiological maps of, for example, glucose metabolic rate, the delivery of the tracer to the tissue (input function) needs to be determined as well as PET images. For certain studies only a single PET image is required; for example, glucose metabolism and blood flow. Other tracers require a dynamic series.

4. Post-acquisition, image processing procedures take place and are dependent on the purpose of analysis. These may include re-alignment of scans, image format conversion using *Analyze* [10], intensity normalization, etc.

3.2 Algorithm development and implementation

Investigation of the three-dimensional PET images, obtained from the WBIC, is carried out on personal desktop computers (PC's) using the *Microsoft Windows* [6] operating system. A *Red Hat Linux* [84] server is also employed to provide *Matlab* software licence manager and the *Apache* [85] web-server. A number of different software packages and programming languages have been used to develop the feature extraction algorithms and Content based image retrieval system. They are:

- *Matlab* and the Image Processing Toolkit [27]. – Commercially available technical development kit containing a wide range of commonly used mathematical subroutines. *Matlab* is an API (Application Programmer Interface) that facilitates the construction of mathematically complex program structures. The image processing toolkit itself contains a large number of components specifically designed for image processing and analysis. These include amongst others functions for input/output, transformations, statistical measurements, region of interest operations, and filters. *Matlab* is based upon the *C* procedural language, and all functions can be automatically converted using the supplied compiler.

- Statistical Parametric mapping (*SPM*) [58] – A freely available suite of *Matlab* routines used for neurological image analysis and obtained from the University College London. SPM is an extremely popular tool, written using the *Matlab* API, which is used to perform interpolation, realignment, co-registration, spatial normalization and segmentation on PET, SPECT and *f*MRI neurological data.

- *ImageJ* - Image processing and analysis tool [86]. A general purpose image manipulation device written as open source and possessing a number of plug-ins for medical data analysis, such as the ability to open and alter *Analyze* format images. It can replace the widely used commercial

software for a variety of simple tasks such as viewing, enhancing and altering the format of images. *ImageJ* is written in Java and is also available for free.

- *MySQL* [44] – Database management system software. *MySQL* is again open source software that is freely available. *MySQL* is database management software that is widely used with *Apache* [85], Linux [84], and *PHP* [87] to produce dynamic, data driven websites. *MySQL* is not as sophisticated as commercial software as it is not possible to create stored triggers or procedures, and there is no facility for foreign keys.

- *Apache* [85] – Hyper text transfer protocol server used to display and publish web pages written in *HTML* [88] and embedded *PHP* [87]. *Apache* is also freely available.

Programming Languages:

- *PHP* (Personal HomePage) [87] – General purpose scripting language that can be embedded into html used to create database driven web pages. *PHP* is used within *HTML* to access the *MySQL* database and retrieve image data so that appropriate images can then be displayed. *PHP* is also used ,alongside *HTML*, to display images.

- Hyper Text Mark-up Language (*HTML*) [88] – Method of publishing text on the Internet. Tag based formatting language enables text and images to be viewable using a browser. *HTML* can only produce static web-pages.

- *C* [89] – High level programming language, compiled in this project using *Matlab* [27,90], utilized in image processing algorithms. *C* executes much

more rapidly when compared to *Matlab*, especially when certain program structures are considered. Image processing algorithms within this project are therefore written using both *C* and *Matlab* in conjunction with each other.

- Structured Query Language (*SQL*) - Used to define data structures, and perform operations on data stored within structure [29]. *SQL* is the standard method for accessing all databases. *SQL* is used to retrieve data from a database and also perform simple calculations and also define the order of retrieval. The *MySQL* database implemented is compliant with the *ANSI* standard.

The *Matlab* and *C* procedures access the stored 3D PET images and perform a range of processing and analysis routines. Data generated by the *Matlab* and *C* algorithms is inserted into the *MySQL* database, located on the *Linux* server. Access to the database and retrieval from the database is performed using *SQL*. Retrieval results are presented in a set of *HTML* pages that utilize embedded *PHP* and *SQL* to access the database. Results are displayed and published on the Internet/World Wide Web and can consequently be viewed using an *HTML* browser [91,92,93,94,95].

4 Experimental Methodology

This section describes the methodologies and algorithms that have developed, and subsequently applied to PET neurological images so that medically salient visual features can be extracted. Features are extracted in order to index the images within a database and enable content-based image retrieval of the studied PET scans. An overview of the developed methods and relationships utilized to extract medically salient features is shown below in Figure 4.1. Detailed description of the feature extraction and anatomical mapping processes is given in sections 4.1 – 4.7.

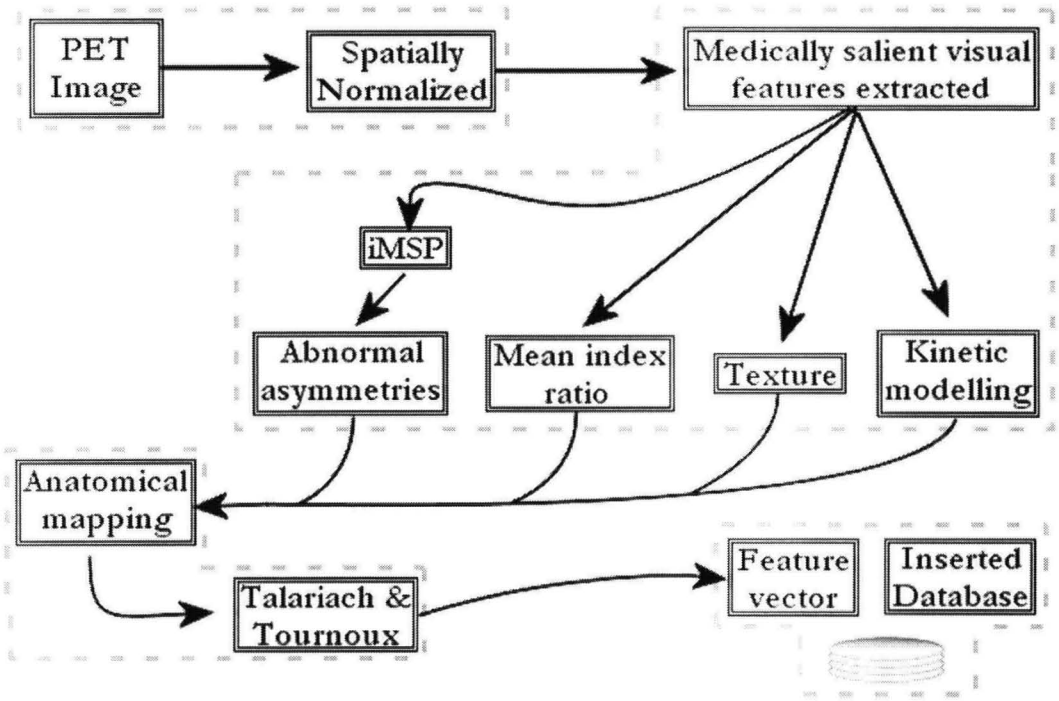

Figure 4.1. Diagram representing the different methodologies implemented.

The initial stage is to perform the spatial normalization of images. Anatomical mapping is then applied to obtain the four separate categories of features, as shown in the Figure 4.1. Each of the four features is independent, and the IMSP is used to obtain the abnormal asymmetries.

4.1 Anatomical Mapping

The process of *spatial normalization* allows different PET scans to be compared by warping each image to the same standard space, a voxel in one image can reliably be said to belong to the same anatomical structure as the comparable voxel in an alternate image. However, the exact nature of the anatomical structure remains unknown. Anatomy is made transparent by referencing the normalized images to a known anatomical atlas using each voxels' Cartesian co-ordinates as the intermediary.

Anatomical labels are applied to the normalized image using the Talairarch and Tournoux atlas. The Cartesian co-ordinates from the atlas must however first be transformed to fit the MNI template, this is due to the fact that MNI space and Talairarch and Tournoux space, although comparable, are not exact matches [62].

The spatially normalized brain images are referenced to a *MySQL* [44] database, containing the Talairarch and Tournoux [4] anatomical labels. Inserted into this database are tuples containing anatomical labels and Cartesian co-ordinate data from the Talairarch and Tournoux atlas [96]. The labels themselves are electronically derived from axial sectional images in the 1988 Talairarch Atlas and are therefore consistent with Talairarch and Tournoux space [96]. The database design of anatomical labels enables very rapid querying of any structure or combination of structures; the anatomical structures are split into five previously defined distinct groups: Hemisphere, Lobe, Gyrus, Tissue type and Cell type [96].

The anatomical mapping procedure and its place within the research as a whole is shown in Figure 4.2

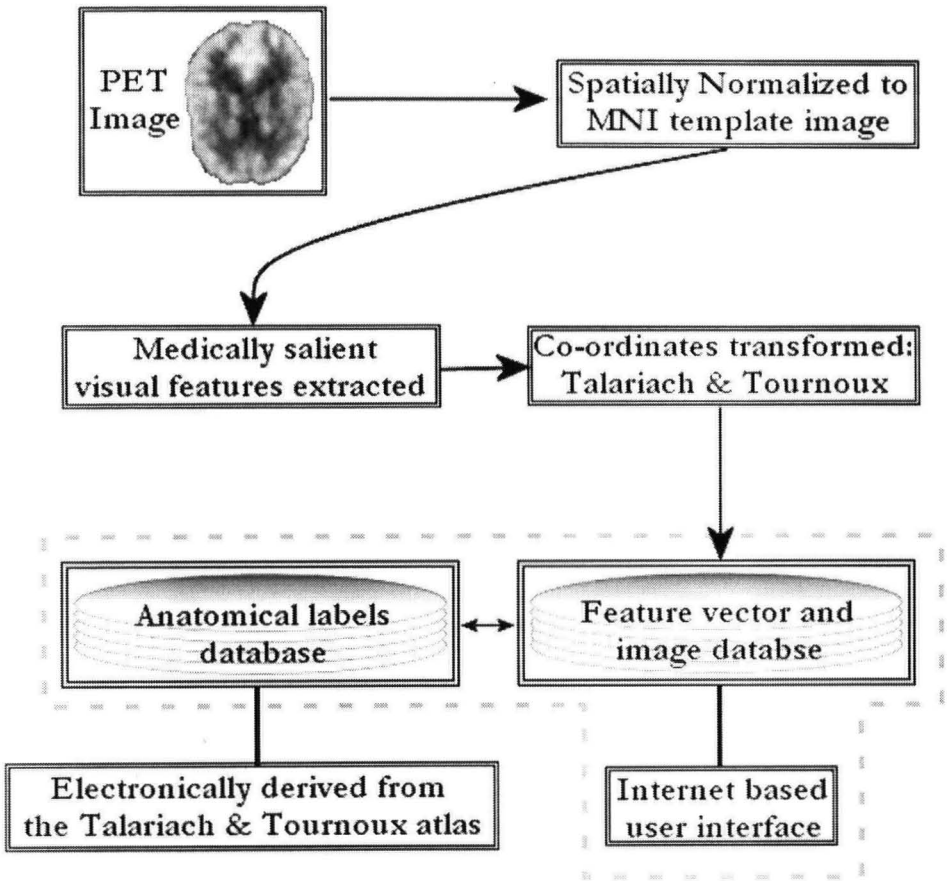

Figure 4.2. Anatomical mapping and feature extraction.

Segmentation of anatomical structures from PET images based solely on their Cartesian co-ordinates is enabled by the database. This method of PET brain image segmentation is utilized when quantifying brain activity and measuring texture of the brain, detailed in sections 2.6.2.2 (*Statistical Measurement*) and 2.6.2.4 (*Texture*) Abnormal asymmetries are also referenced to the anatomical information present within database after their detection. Isolation or detection of asymmetric abnormalities is performed using the extracted ideal-Mid-Sagittal Plane.

4.2 Obtaining ideal Mid-Sagittal Plane

This section outlines a technique used to extract the 3D plane of symmetry called the *ideal* Mid-Sagittal Plane, or *i*MSP which is defined as a plane through the brain where symmetry should be maximal [97]. Co-ordinates for the *i*MSP are extracted using only the visual data present within the image itself. The method extracts the planar co-ordinates for separating the 3D PET brain image into two hemispheres from the top of the head towards the neck passing through the nose. It is based on the assumption that the left and right hemispheres of the brain are symmetrical.

The approach taken, to obtain the co-ordinates for the *i*MSP, is based upon an existing method that measures the cross-correlation of brain sections to identify the position of maximal symmetry. The process was originally designed to function with MR and CT neuro-images [97]. Consequently a number of significant developments have been made to adapt the process to PET images.

Extraction of the *i*MSP is carried out using geometric analysis on the working co-ordinate system and the ideal head co-ordinate system, illustrated in Figure 4.3. The ideal head co-ordinate system centred in the brain with positive X_0, Y_0, Z_0 axes pointing in the right (ears), anterior (nose) and superior (opposite of feet) directions respectively. With respect to this co-ordinate system, the bilateral symmetry plane of the brain is defined as the plane $X_0 = 0$. It is often referred to as the mid-sagittal plane of the brain. Image acquisition produces a set of axial (coronal) slices cut perpendicular to the Z_0 (Y_0) axis. The intersection, of each slice, with the bilateral symmetry plane appears as a vertical line on the slice. In clinical practice, a working co-ordinate system XYZ is applied. X and Y are oriented along the rows and columns of each image slice, and Z is the actual axis of the scan.

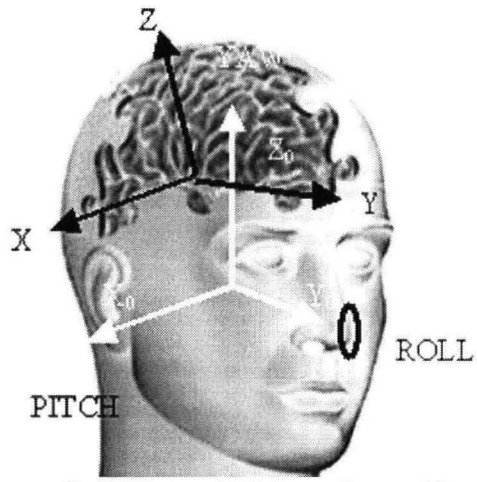

Figure 4.3. Ideal head co-ordinate system $X_0Y_0Z_0$ vs. the working co-ordinate system XYZ.

The orientation of the working co-ordinate system differs from the ideal co-ordinate system by three rotation angles, *pitch*, *roll* and *yaw*, and three translation differences, ΔX_0, ΔY_0, and ΔZ_0, respectively.

Therefore, a transformation from $X_0Y_0Z_0$ to XYZ has to be performed by rotating angle R = yaw (θ) roll (ϕ) pitch (ω) and translating ΔX_0, ΔY_0, and ΔZ_0 using formula shown in Equation 4.4 [97]; where c = cos and s = sin.

$$\begin{bmatrix} X \\ Y \\ Z \end{bmatrix} = \begin{bmatrix} c\phi c\theta & c\theta s\omega s\phi - c\omega s\theta & c\omega c\theta s\phi + s\omega s\theta \\ c\phi s\theta & c\omega c\theta + s\omega s\phi s\theta & c\omega s\phi s\theta - c\theta s\omega \\ -s\phi & c\phi s\omega & c\omega c\phi \end{bmatrix} \begin{bmatrix} X_0 \\ Y_0 \\ Z_0 \end{bmatrix} + \begin{bmatrix} \Delta X_0 \\ \Delta Y_0 \\ \Delta Z_0 \end{bmatrix} \quad \textbf{(4.1)}$$

So that for X_0=0 the *i*MSP can be rewritten in terms of the imaging co-ordinates as Equation 4.5 [97]; where d is the perpendicular distance of the plane from the origin.

$$\cos\phi\cos\theta X + \cos\phi\sin\theta Y - \sin\phi Z + d = 0 \quad \textbf{(4.2)}$$

The cross-correlation between the original image and the reflected (and rotated) one can then be calculated. The biggest cross-correlation (CC) value should be found at the horizontal position with the ideal symmetry when the image is rotated to the correct angle (θ). Therefore the correct rotation angle can be found by locating the biggest CC value when an image is rotated through a range of angles. Figure 4.4 shows the reflected

image rotated by three different angles, top is too far anti-clockwise the middle row is the best match (highest CC value), and the bottom row is too far clockwise.

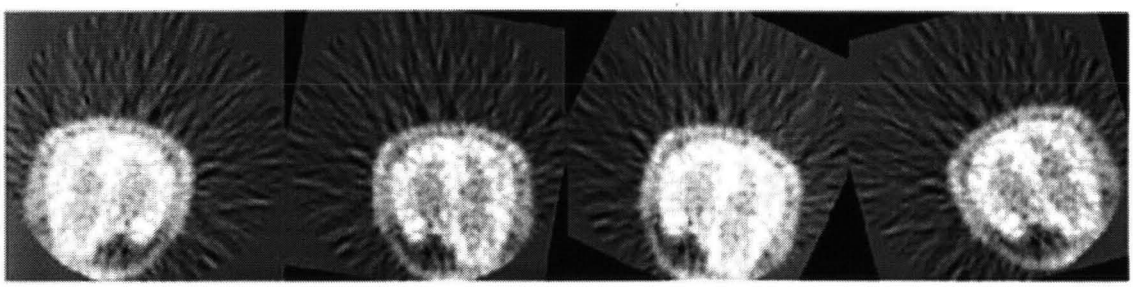

Figure 4.4. Images demonstrating the process of finding the correct angle of rotation. First image is the original, second is the reflected image rotated to the angle of maximum correlation, the third and fourth images show the reflected image rotated by angles with reduced correlation.

The position, horizontally, on the image where correlation is a maximum provides the value for the offset of iMSP. Calculation of correlation value is based upon Equation 4.6; The inverse Fourier transform is represented by F^{-1}, the complex conjugate of the inverse Fourier transform is F^*, F is the Fourier transform, $S_{i\text{-}n}$ is the original section rotated to the tested angles, and the reflected version is ref $(S_{i\text{-}n})$.

$$CC = \max\left\{\max\left\{\int F^{-1}\left(F^*\left(S_{i-n}\right)ref\left(F\left(S_{i-n}\right)\right)\right)\right\}\right\} \qquad (4.3)$$

Correlation is found for every available offset distance at each of the tested rotation angles, the maximum correlation value reveals the ideal rotation angle and its corresponding ideal offset distance.

This process is carried out on all two dimensional slices from a scan and outliers are removed when they are three standard deviations away from the mean. Least squares polynomial regression of the first order is performed on all slices for each of the two sets of parameters. This smoothing produces the final co-ordinates of the *i*MSP, the two sets of results are independently smoothed to reduce errors. The co-ordinates themselves consist of a rotation angle and offset for each 2D slice, therefore if a spatially normalized image is composed of 68 2D slices there will be, in total, 136 separate co-ordinates.

4.3 Feature Detection and characterization

The process of revealing abnormal asymmetries that are medically salient, such as tumours, strokes or physical injuries uses the previously extracted *i*MSP and is described in this section. Two images are created to represent the left and right hemispheres of the brain split along the *i*MSP. Absolute intensity differences between the two hemispheres are revealed by comparing pixel values at each co-ordinate, these differences are represented by an image the same size as the original, two examples of this are shown in Figure 4.5.

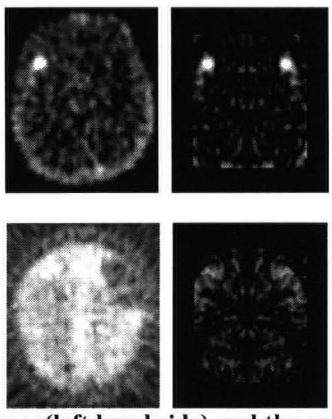

Figure 4.5. The original PET image(left hand side) and the associated image showing absolute differences(on right hand side).

Any asymmetrical differences found are further analyzed using connected component labeling, described in Figure 4.6 (4). The difference image is converted to a binary image, as shown in Figure 4.6 (2 – 3), so that enable connected component labelling can be applied. The binary image is created using a simple thresholding technique in which any pixel with an intensity value above zero is regarded as an object and consequently assigned a value of 1; this ensures that all asymmetries are analyzed. Connected component labeling, represented in Figure 4.6 (4), is used to isolate distinct and separate visual objects within the difference image by labelling neighbouring pixels if they share the same value.

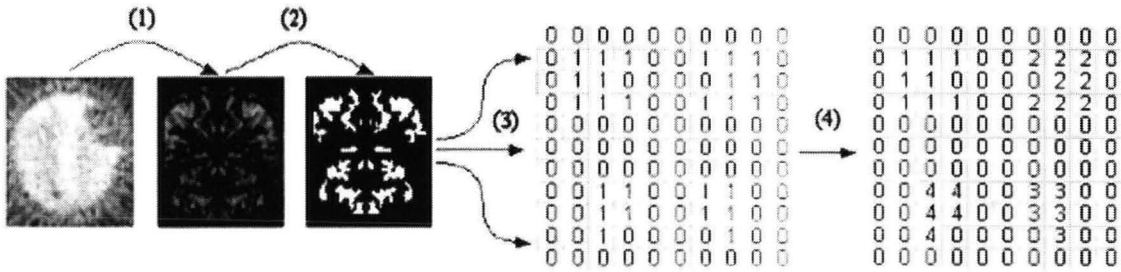

Figure 4.6 Connected component labelling.

Co-ordinates for hypothesised lesions are revealed by the labelling process. These co-ordinates are applied to the original image and used to assess the probability that the pixels belong to an actual abnormal asymmetry or whether they are in fact a false feature. Pixels labelled as a hypothesised lesion are compared to surrounding pixels using a method based on Bayesian probability, represented by equation 4.4 where $P(C_i)$ is the prior estimate that a group of pixels are abnormal, C_i is the normalized probability density function of pixel values from the hypothesised abnormality, X is the group of pixels surrounding the hypothesized lesion and m_i is the mean of X. The result di(x) is the probability that pixels from the hypothesized lesion can be classed as the same as the surrounding pixels.

$$di(x) = \ln P(C_i) - \frac{1}{2}\ln |C_i| - \frac{1}{2}\left[(x - m_i)^T C_i^{-1}(x - m_i)\right] \qquad \textbf{(4.4)}$$

An initial test set of twenty random images provided the threshold for pixels classified as abnormal asymmetries, and a total of 1063 images are tested. The characterization of a lesion is performed by measuring the centre pixel, the area and the mean intensity. Measurement of a lesion's mean intensity reveals whether it possess high or low tracer concentrations, a high level can correspond to a tumour while low activity is typically associated with a physical injury such as a stroke.

4.4 Texture

The middle symmetry plane method (described in section 4.2 (*Obtaining ideal Mid Sagittal-Plane*)) is appropriate only for detecting asymmetric lesions. For images with other pathological patterns, such as Alzheimer's disease, the *i*MSP method is not appropriate. In this section, texture is extracted and quantified for the purpose of characterizing and classifying the images. Gabor filters have previously been utilized to characterize the texture of non-medical images [33]. The two dimensional *Gabor function* g(x, y), and its *Fourier transform* G(u, v), are shown in the following equations, Equations 4.13 and 4.14 [33]:

$$g(x,y)=\left(\frac{1}{2\pi\sigma_x\sigma_y}\right)\exp\left[-\frac{1}{2}\left(\frac{x^2}{\sigma_x^2}+\frac{y^2}{\sigma_y^2}\right)+2\pi jWx\right] \qquad \textbf{(4.5)}$$

$$G(u,v)=\exp\left\{-\frac{1}{2}\left[\frac{(u-W)^2}{\sigma_u^2}+\frac{v^2}{\sigma_v^2}\right]\right\} \qquad \textbf{(4.6)}$$

Where $\sigma_u = 1/2\pi\sigma_x$ and $\sigma_v = 1/2\pi\sigma_y$, W = wavelet transform, σ_x = intensity variance of pixel array, σ_y = intensity variance of pixel array, G(u,v) represents *Fourier* space. A Gabor *Wavelet Transform* of each image is created using a technique where the *fourier transform* of the complex conjugate of the Gabor function, a Gabor filter, is applied to the *Fourier* transform of the PET image. This process is shown in Equation 4.7 where *GF* represents the Gabor Filter previously defined, the Inverse Discrete Fourier Transform is *ift,* the Fourier Transform is *ft*, *GWT* is the resultant Wavelet Transform Magnitude, and PET is the tested image.

$$GWT = real(ift(ft(PET)*GF))^2 + imaginary(ift(ft(PET)*GF))^2 \qquad \textbf{(4.7)}$$

There are twenty four different filters used in total representing the six different orientations and four different scales. Application of these filters to a PET image results in 24 Wavelet Transform Magnitude, from which the texture feature is derived. The

texture feature itself is a 48-element vector that consists of 24 standard deviations (μ) and 24 means (σ). The raw feature vector (fv^I) that is used for indexing can therefore be expressed as equation 4.16:

$$fv^I = [\mu_{00}^I, \mu_{01}^I, ..., \mu_{23}^I, \sigma_{00}^I, \sigma_{01}^I, ..., \sigma_{23}^I] \quad \textbf{(4.8)}$$

This mechanism of texture quantification is utilized with anatomical regions of interest and the whole brain. Raw data from the texture characterization algorithms are inserted into database and combined with the results obtained from Statistical Analysis procedures, detailed in section 4.5.

4.5 Statistical Analysis of Brain physiology

Statistical measurements of voxel intensity within localized anatomical structures and the whole brain reveals the presence of physiological patterns that are associated with neuro-disorders, and also those that are normal. Analysis of these patterns by qualified neuro-specialists is commonly used method of diagnosing patients. The methodology outlined here mirrors a conventional analysis procedure using automated computer algorithms. The exact statistical measurements that are obtained are the co-efficient of variance, the mean pixel intensity property, and the mean index ratio. These measurements relate to the whole brain and also to specific anatomical structures affected by certain disorders.

Anatomical structures are segmented/isolated from the spatially normalized PET scans using the method detailed in section 4.1 (*Anatomical Mapping*). The mean of voxel intensity property is measured for the specified anatomical structure as is the mean value taken from the rest of brain. These measurements provide the mean index ratio result, *MIR*, which is equal to the mean intensity of whole brain divided by the mean intensity of the specified anatomical structure.

The mean values of normal subjects are then tested against Alzheimer's diagnosed patients to find any significant difference using the T-Test. A significantly lower than normal mean value for voxel intensity property is associated with hypo-metabolism while a significantly higher than normal mean is diagnosed as hyper-metabolic. Alzheimer is characterized by hypo-metabolism in certain anatomical structures [71,72].

Co-efficient of variance or CV is also measured. Anatomical structures are again segmented/isolated using the method outlined in section 4.1(*Anatomical Mapping*). Equation 4.8 represents co-efficient of variance of anatomical structure within a PET image, *Vxyz* is the voxel intensity property value.

$$CV = \frac{\sigma(V_{XYZ})}{\overline{V_{XYZ}}} \qquad (4.9)$$

The above calculations and measurements are applied to six different areas that are associated with Alzheimer's disease, Posterior Cortical Atrophy (PCA) and Mild Cognitive Impairment (MCI):

- Parietal Cortex (Alzheimer's)
- Occipital Cortex (Alzheimer's and Posterior Cortical Atrophy)
- Posterior Cingulate (Mild cognitive impairment, very early Alzheimer's)
- Brodmann's Areas 29 and 30
- Hippocampus (Mild cognitive impairment, very early Alzheimer's)

The anatomical structures are represented graphically, on PET images from a patient diagnosed as normal, in figures 4.7 – 4.11

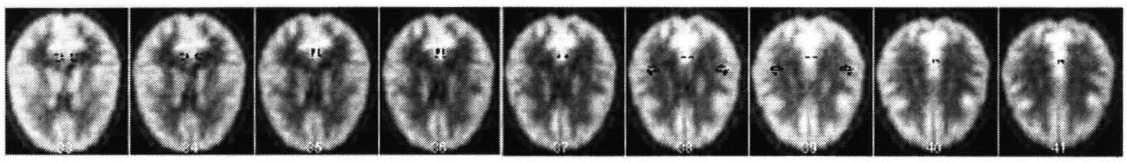

Figure 4.7. Brodmann's Area 29 shown as black pixels.

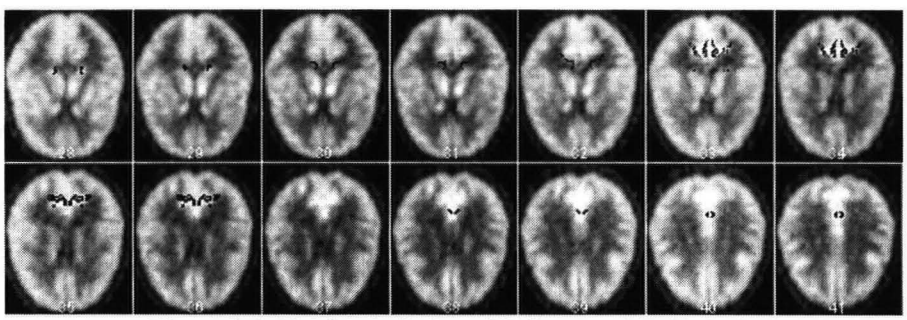

Figure 4.8. Brodmann's Area 30 shown as black pixels.

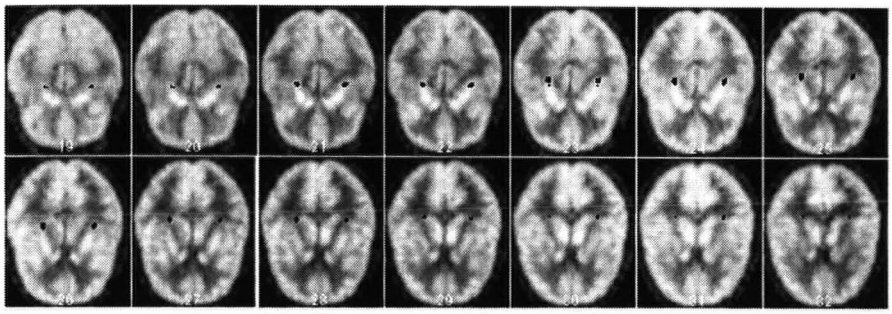

Figure 4.9. Hippocampus shown as black pixels.

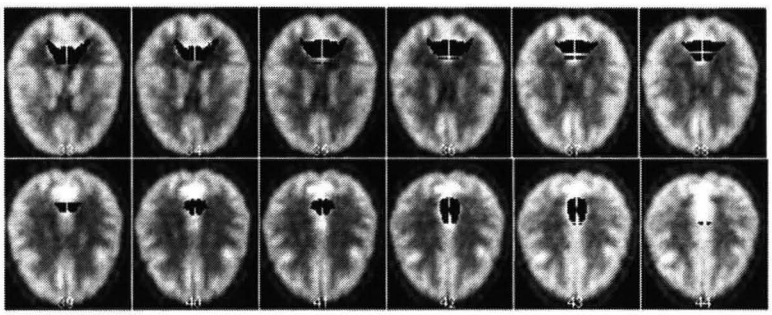

Figure 4.10. Posterior Cingulate (PC) shown as black pixels.

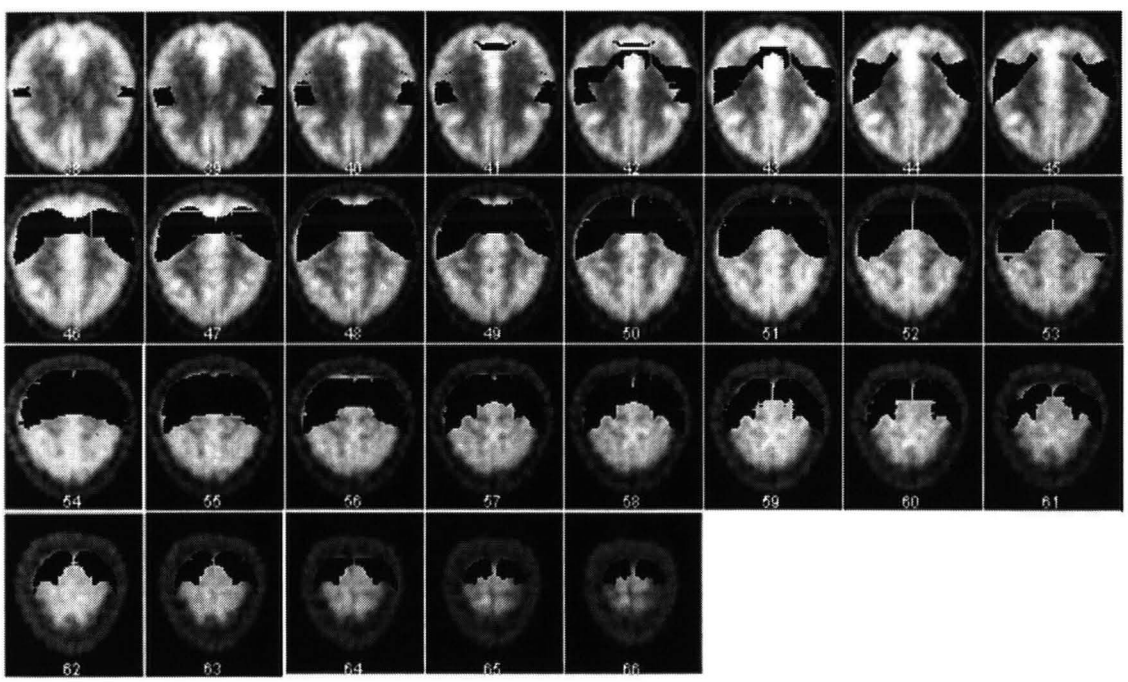

Figure 4.11. Parietal Lobes shown as black pixels.

4.6 Kinetic Modelling

The *simplified reference tissue model* is unlike other mathematical models used to study PET images in that it does not require the direct measurement of blood plasma. Ligand uptake is measured within a reference area that has no specific binding to the studied neuro-transmitter. This uptake level can then be compared to the target tissue, which itself has specific binding with the radioactively labelled ligand. By applying this model the binding potential, which is equal to receptor density divided by the equilibrium dissociation constant, can be calculated to clinical standards of accuracy [98].

Six different sets of images have been used, each containing three regions of interest: A lesion/grafted striatum, its contra-lateral control striatum, and the cerebellum which is the reference region. The regions of interest were manually drawn for each different data set; this was performed using the commercial software package *Analyze* [10]. In total eighteen different regions are analyzed, and correspondingly eighteen time/activity curves produced.

The localized binding potential can be calculated if the tracer concentration over time is measured. Binding potential is an estimate of receptor density, and it is a measure of the affinity between a ligand and a neuro-anatomical structure. A diagram of the *simplified reference tissue* [68] model is shown in Figure 4.12, the full set of equations that represent the model are shown in Equations 4.9 – 4.16 [68] and a table explaining the contents of the diagram is given in Table 4.1.

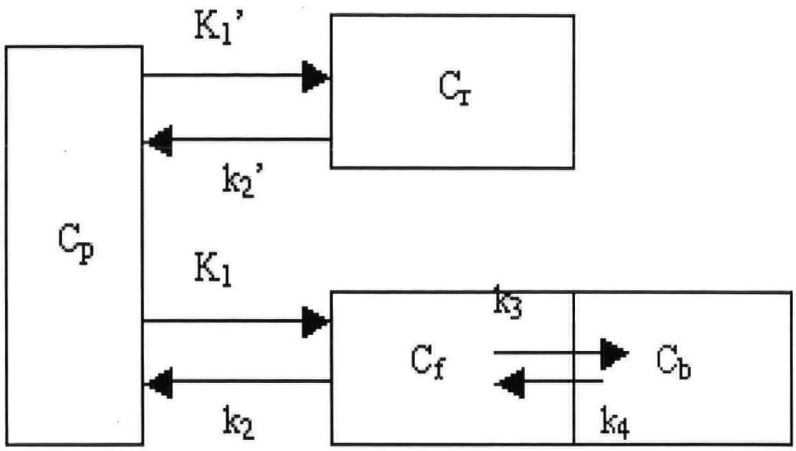

Figure 4.12. Simplified Reference Tissue model [68].

$$\frac{dC_r(t)}{dt} = K'_1 C_p(t) - k'_2 C_r(t) \quad \textbf{(4.10)}$$

$$\frac{dC_f(t)}{dt} = K_1 C_p(t) - k_2 C_f(t) - k_3 C_f(t) + k_4 C_b(t) \quad \textbf{(4.11)}$$

$$\frac{dC_b(t)}{dt} = k_3 C_f(t) - k_4 C_b(t) \quad \textbf{(4.12)}$$

$$\frac{K'_1}{k'_2} = \frac{K_1}{k_2} \quad \textbf{(4.13)}$$

$$\frac{dC_t(t)}{dt} = K_1 C_p(t) - k_{2a} C_t(t) \quad \textbf{(4.14)}$$

$$\frac{K_1}{K_{2a}} = \left(\frac{K_1}{k_2}\right) \cdot (1 + BP) \quad \textbf{(4.15)}$$

$$BP = \frac{k_3}{k_4} \qquad (4.16)$$

Table 4.1 Simplified reference tissue model, explanation of symbols used [68].

C_p	=	metabolite-corrected plasma concentration.
C_r	=	concentration in reference tissue.
C_f	=	concentration of free ligand.
C_b	=	concentration of specifically bound ligand
K_1'	=	rate of transfer from C_p to C_r.
K_1	=	rate of transfer from C_p to C_f
k_2'	=	rate of transfer from C_r to C_p.
k_2	=	rate of transfer from C_f to C_p.
k_3	=	rate of transfer from C_f to C_b.
k_4	=	rate of transfer from C_b to C_f.
k_3/ k_4	=	equal to the binding potential (*BP*).

If C_r is known the following formula, described in Equation 4.17 can be derived from the differential equations shown in Equations 4.10 – 4.16 and then solved iteratively to reveal the value of binding potential [68]. Where BP = Binding Potential, t = time, $R_1 = K_1/K_1'$ and $C_t(t) = C_f(t) + C_b(t)$.

$$C_t(t) = R_1 C_r(t) + (k_2 - \frac{R_1 k_2}{1+BP}) C_t(t) * \exp(\frac{-k_2 t}{1+BP}) \qquad (4.17)$$

The major advantage of this theory is that no direct measurements of blood plasma metabolite concentration need to be taken, which allows the calculation of binding potential non-invasively. All these concentration values are obtained directly from sequential PET images, i.e., PET images from the same subject are repeatedly acquired over a period of 90 minutes. Binding potentials are often used to assess the effectiveness of drugs and to evaluate receptor status in disorders such as Huntington's disease.

Binding potential is represented using a standard decimal number, of the desired accuracy level, and as such can be utilised within a relational-database with no further

manipulation. Binding potential value is therefore suitable as a database index within a content based image retrieval system.

This technique of extracting binding potential, the simplified reference tissue model, coupled with the previously described procedure used to obtain anatomical information provides a novel means to autonomously calculate binding potential for any neuro-anatomical structure referenced within the Talairarch and Tournoux atlas. Anatomical regions of interest can be isolated and the binding potential extraction algorithms applied, to this automatically segmented anatomical region of interest, the resultant decimal value can then be employed within the retrieval system as a database index. A content based image retrieval system for PET images which enables queries based on the binding potential of anatomical regions of interest is made viable.

4.7 Retrieval system

The statistical data, obtained from the separate anatomical regions is inserted into database and the retrieval of images is tested. Retrieval is initially tested using only the statistical data as indices. Retrieval of PET images based on a combination of this statistical data and the texture feature is also performed.

The system possesses a client-server architecture. The server stores the image data and their corresponding features. The client computer has the interface to indices and performs retrieval. Image features include visual and physiological features. Anatomical mapping to the Talairarch and Tournoux space is performed to locate lesion's position anatomically. Figure 4.13 represents the system graphically.

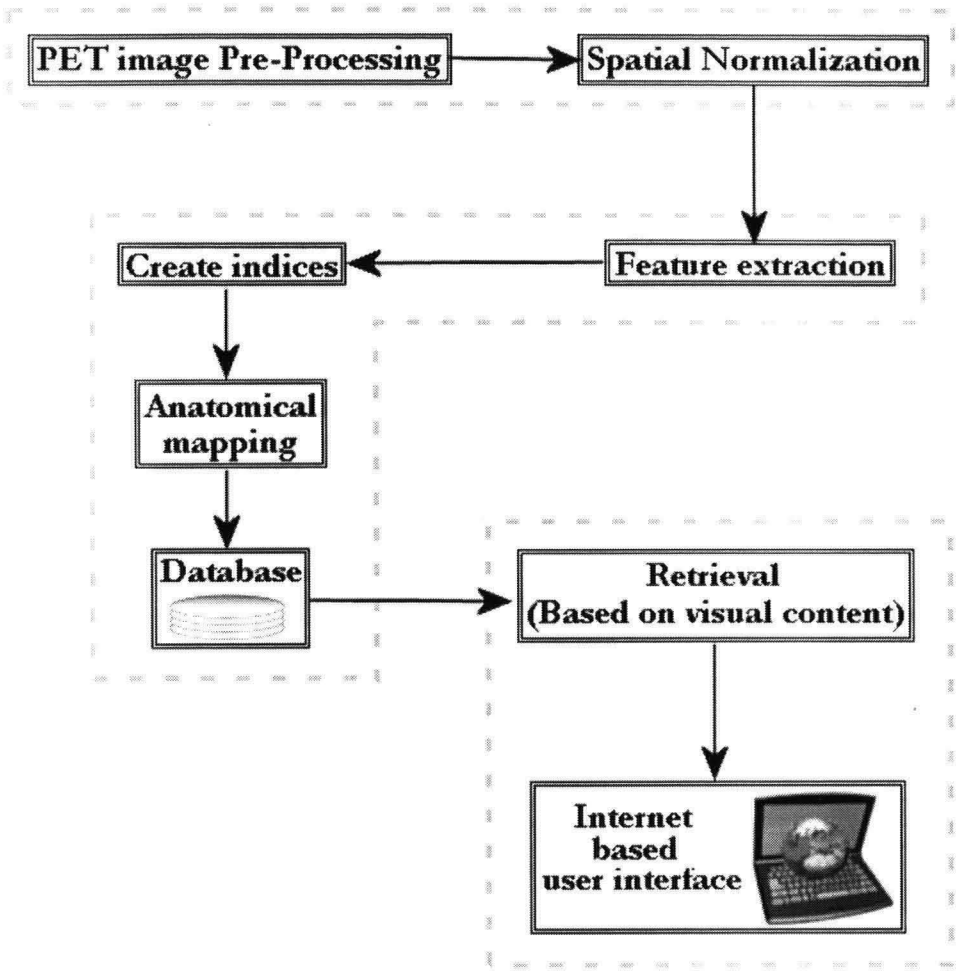

Figure 4.13. Outline of complete PET content based retrieval system.

Localized statistical data, described in section 4.5 (*Statistical Analysis of Brain Activity*), relates to neurodegenerative diseases whereas the asymmetric abnormality data, described in section 4.2 (*Obtaining ideal Mid Sagittal Plane*), relates to tumours, strokes and injuries. Diagnosis of neurodegenerative disorders and lesions are predominant clinical uses of PET imaging.

A final experimental method, employed to show the practicality and validity of the previously documented visual feature extraction methods, is focused on the retrieval process. Previously extracted, medically salient, visual features are used to index a database of the tested PET scans. Experimental indices consist of:

- Cartesian co-ordinates of detected abnormal asymmetric visual features in 3D normalized space.
- Anatomical location of detected abnormal asymmetric visual features.
- Size of detected abnormal asymmetric visual features.
- Global texture feature.
- Mean voxel intensity property values of anatomical locations.
- Co-efficient of variance voxel intensity property values of anatomical locations.

A nearest K-neighbours search algorithm is employed to find the closest matches to the query data. Each of the indices is tested independently and the content-based image retrieval system presented here has two qualitatively different query styles:

- **Textual**, neuro-anatomical structures are chosen from the complete list of available options.
- **Visual**, a spatially normalized PET image from a control subject is displayed and the user then clicks on the structure, or position to be queried.

A third type of query that has not been implemented is **query-by-example**. The query by example approach requires a user supplied image to be analyzed ad-hoc, over the Internet and the extracted visual features are then used to search the database. The implementation of this display method would require a significant amount of development to create the web pages and optimise the execution time of the image analysis algorithms. However Query-by-example would provide no useful scientific data that is not already available by the analysis of the two alternate query approaches previously described. It has therefore not been tested.

Evaluation of query results is achieved by two distinctly separate methods:

- Ensure that retrieved images exhibit an asymmetrical abnormal feature in the expected anatomical location.
- An Alzheimer's query shows that PET scans from patients diagnosed with Alzheimer's are the closest matches; also vice versa that query data from a normal patient returns PET images from normal patients as closest matches.

A preliminary Internet based system has been built to display the above two query methods; the graphical user interface is shown in section 5.7 (*Content Based Image Retrieval*) figures 5.11 and 5.12. The server is located in the Computer Vision Research group area of Middlesex University (Tottenham Campus).

The system is built around a *MySQL* database, containing the experimental indices that utilize the extracted visual feature data. It is accessible from any *HTML* browser. The graphical user interface has been built using *HTML* and the scripting language *PHP* to carry out Structured Query Language searches on the database.

5 Results and Discussion

5.1 Extracted Ideal Mid Sagittal Plane

The ideal mid-sagittal plane extraction methodology was applied to PET images from patients with a variety of diagnosis types to ensure the reliability and validity of the experimental algorithms. Results from each diagnosis type are presented in Figures 5.1 – 5.8. Diagnosis types are normal, head injury, Alzheimer's, tumour and pseudo-lesion. The pseudo-lesions are generated manually for evaluation purposes.

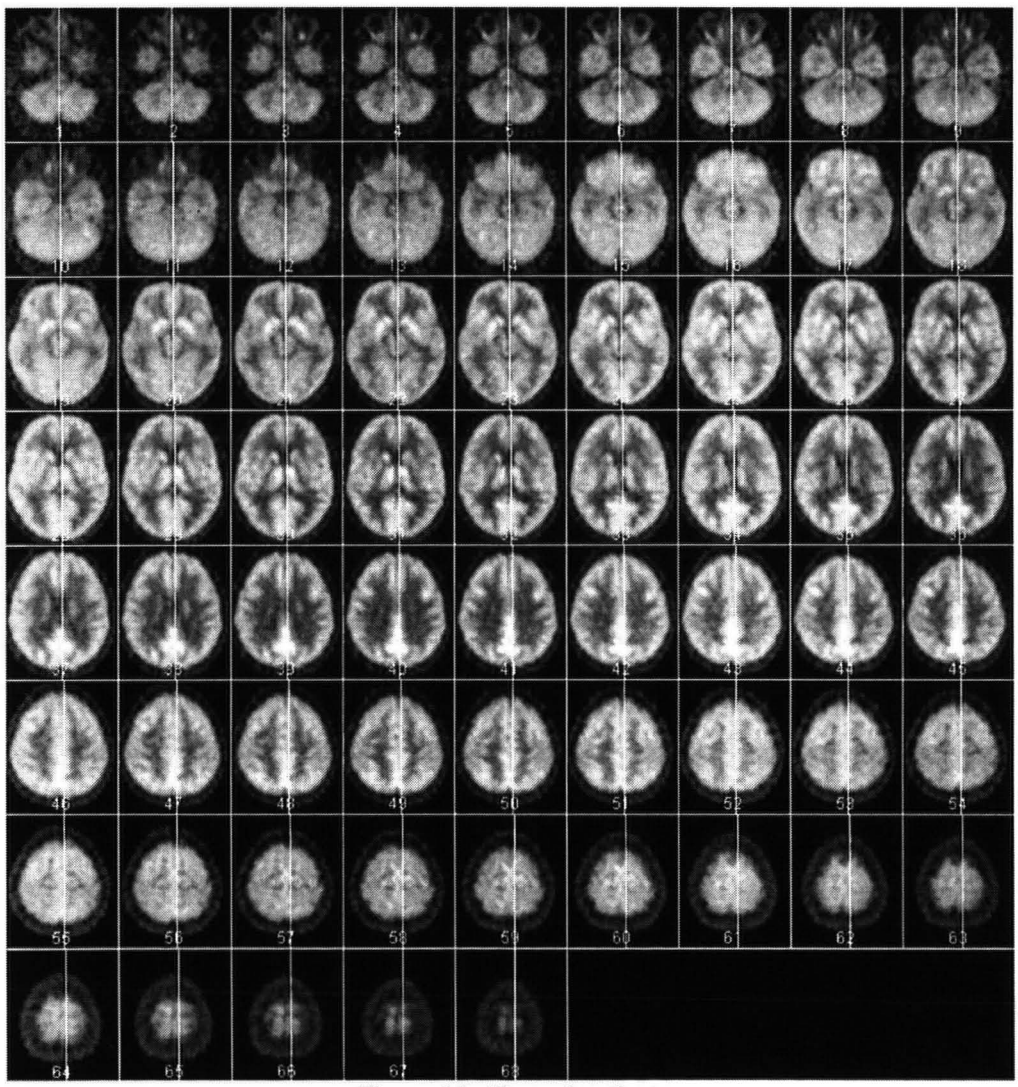

Figure 5.1. Normal patient.

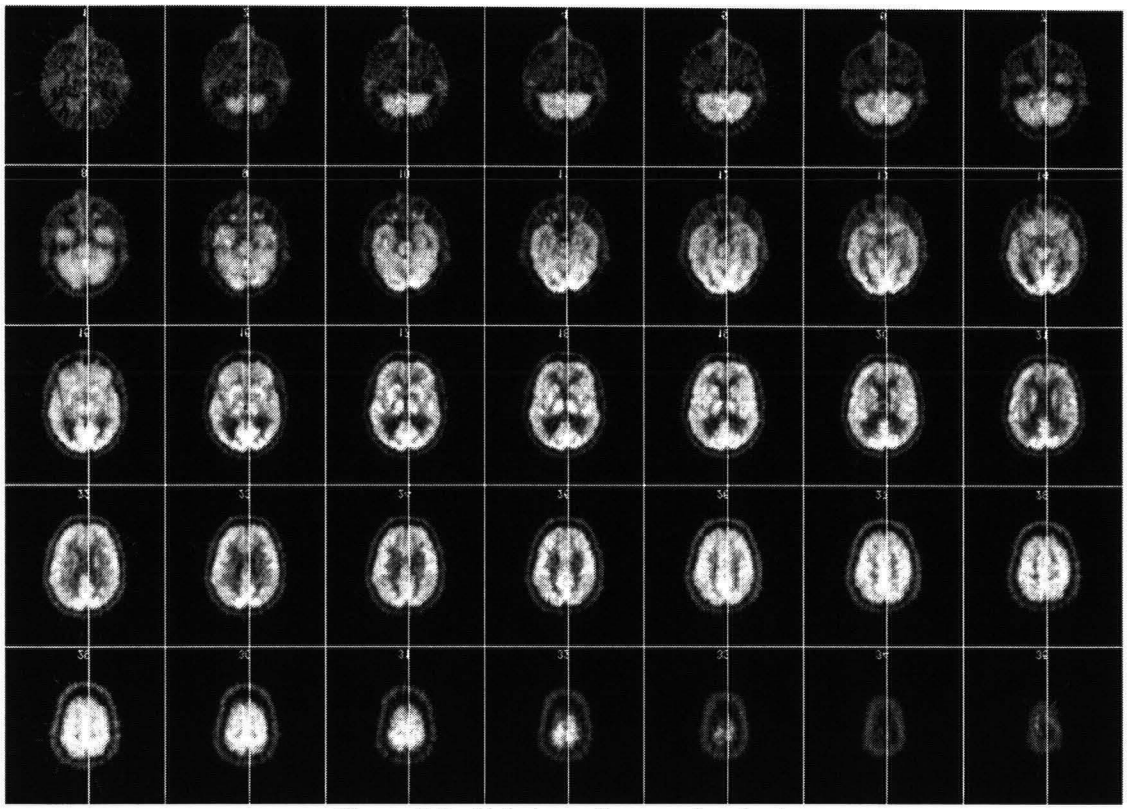

Figure 5.2. Alzheimer diagnosed patient.

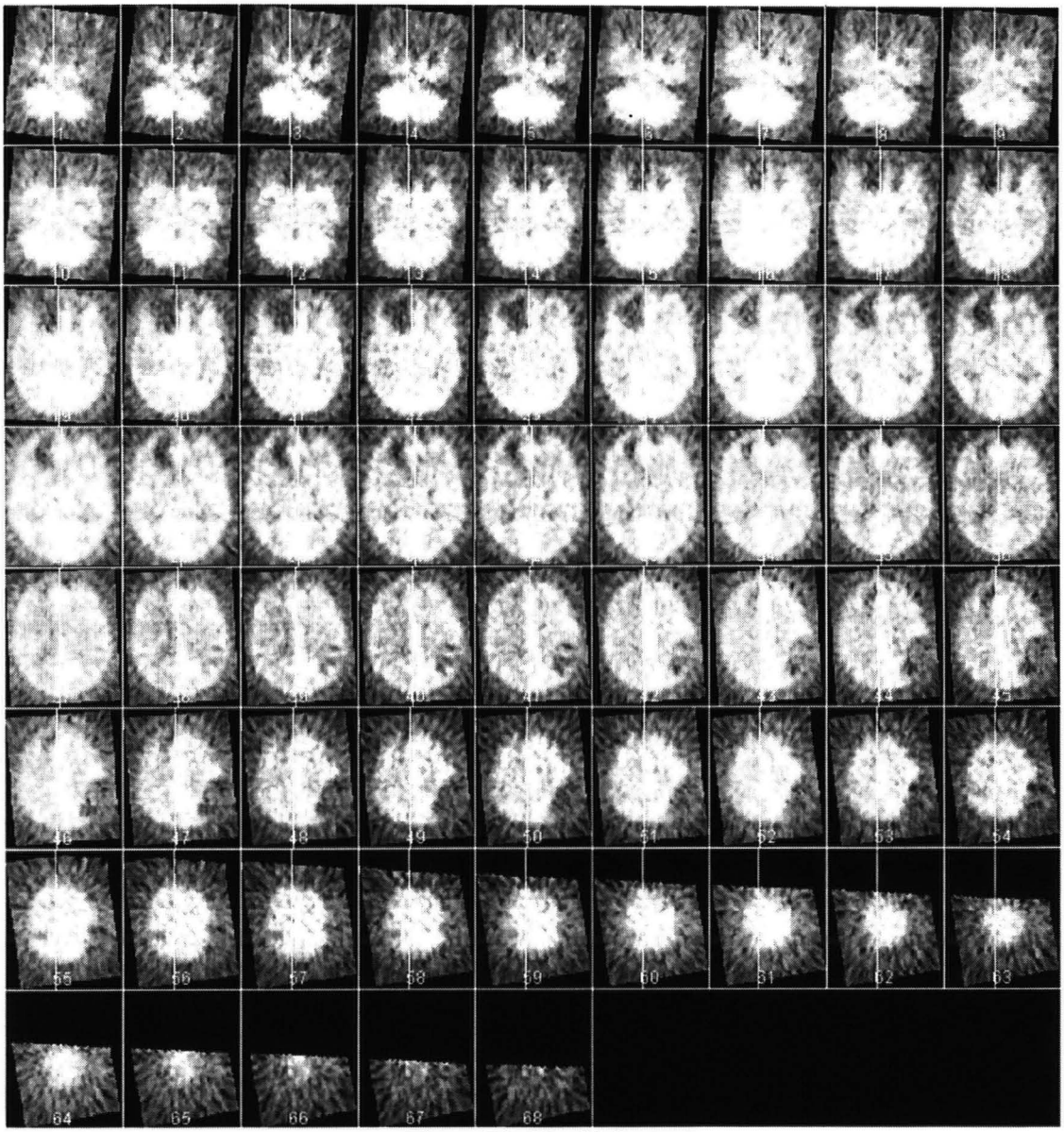

Figure 5.3. Head injury

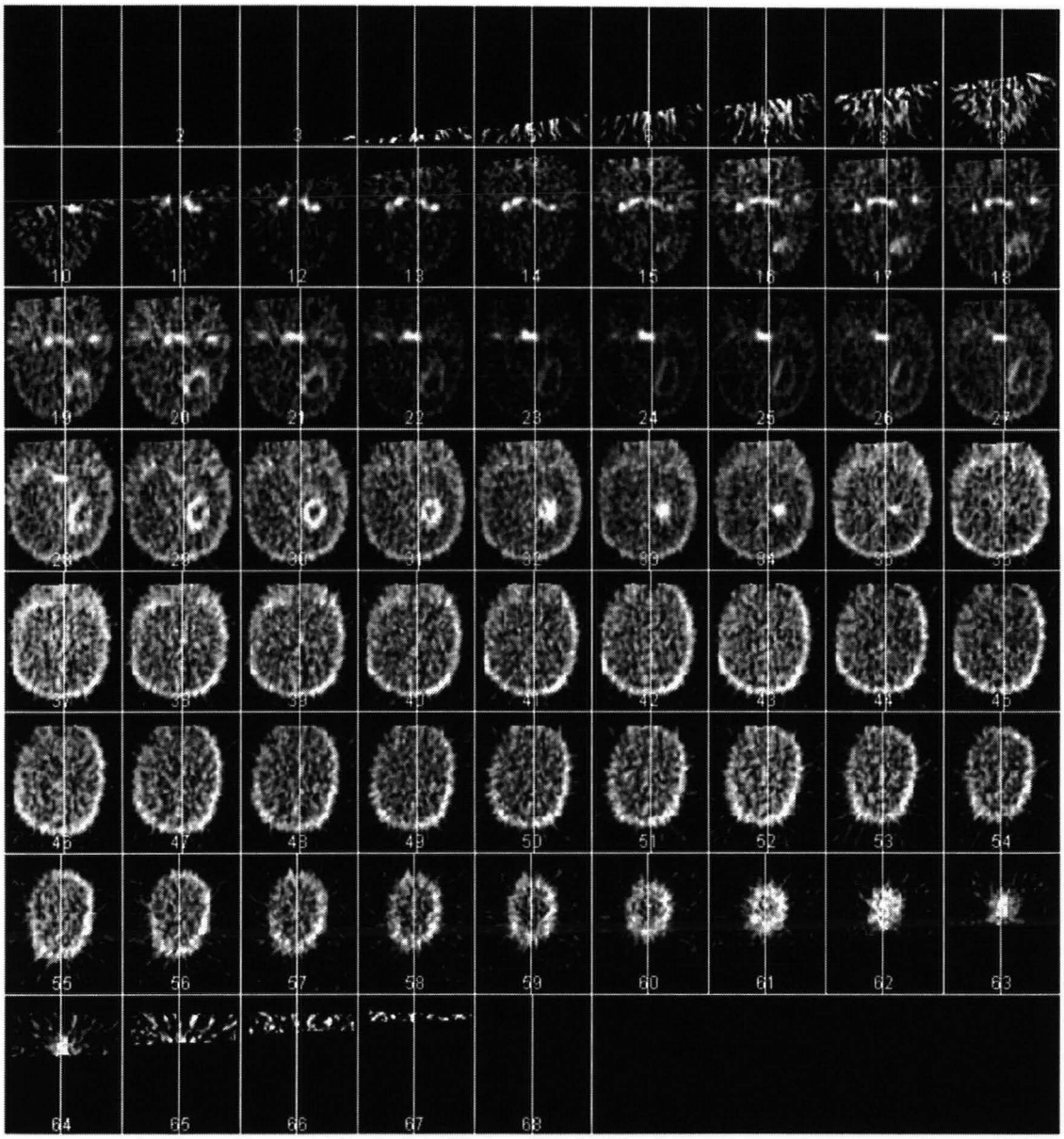

Figure 5.4. Naturally occurring lesion (high activity). Blank frames artefacts caused by spatial normalization and scanning protocol.

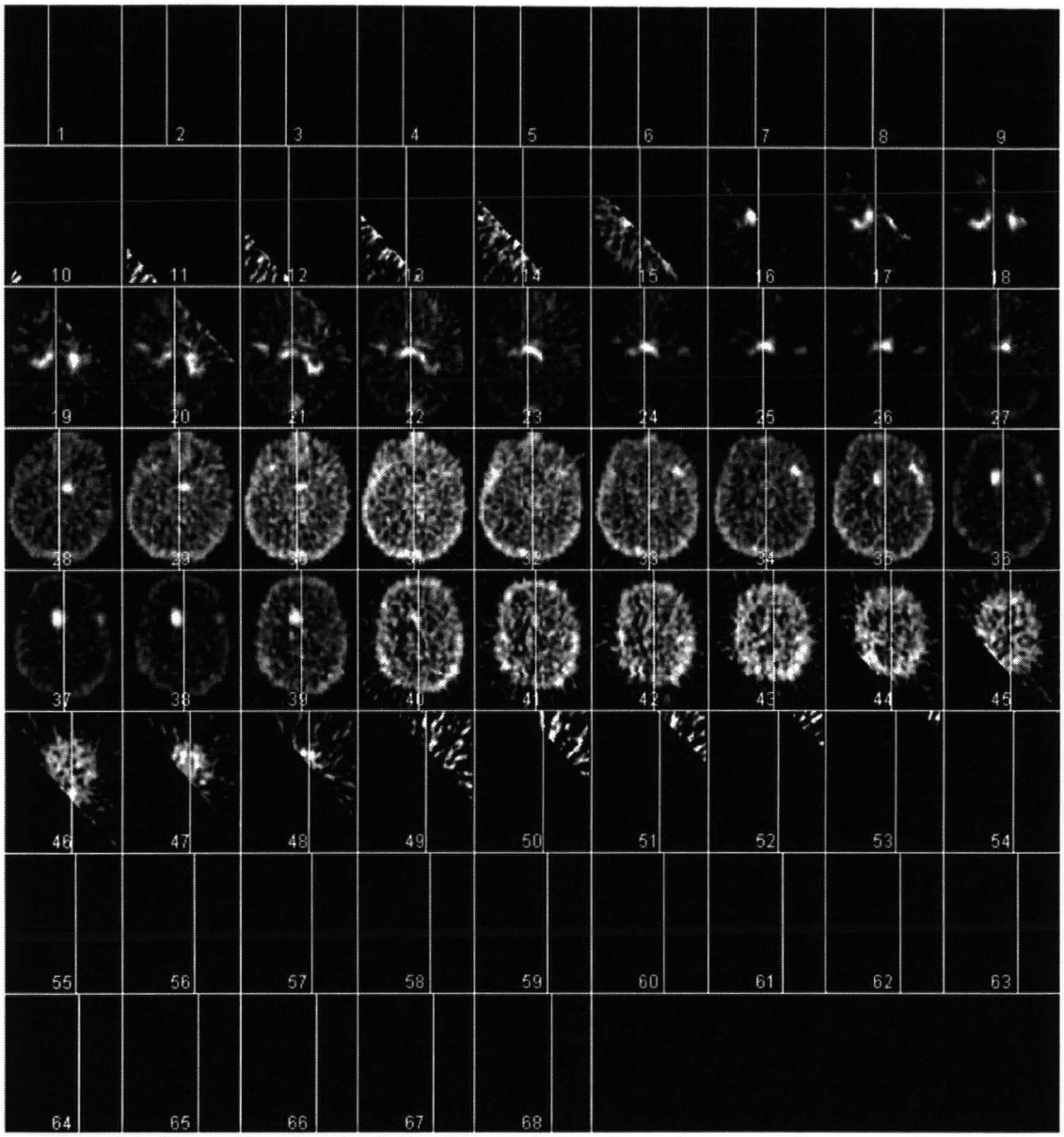

Figure 5.5. Naturally occurring lesion (high activity). Blank frames artefacts caused by spatial normalization and scanning protocol.

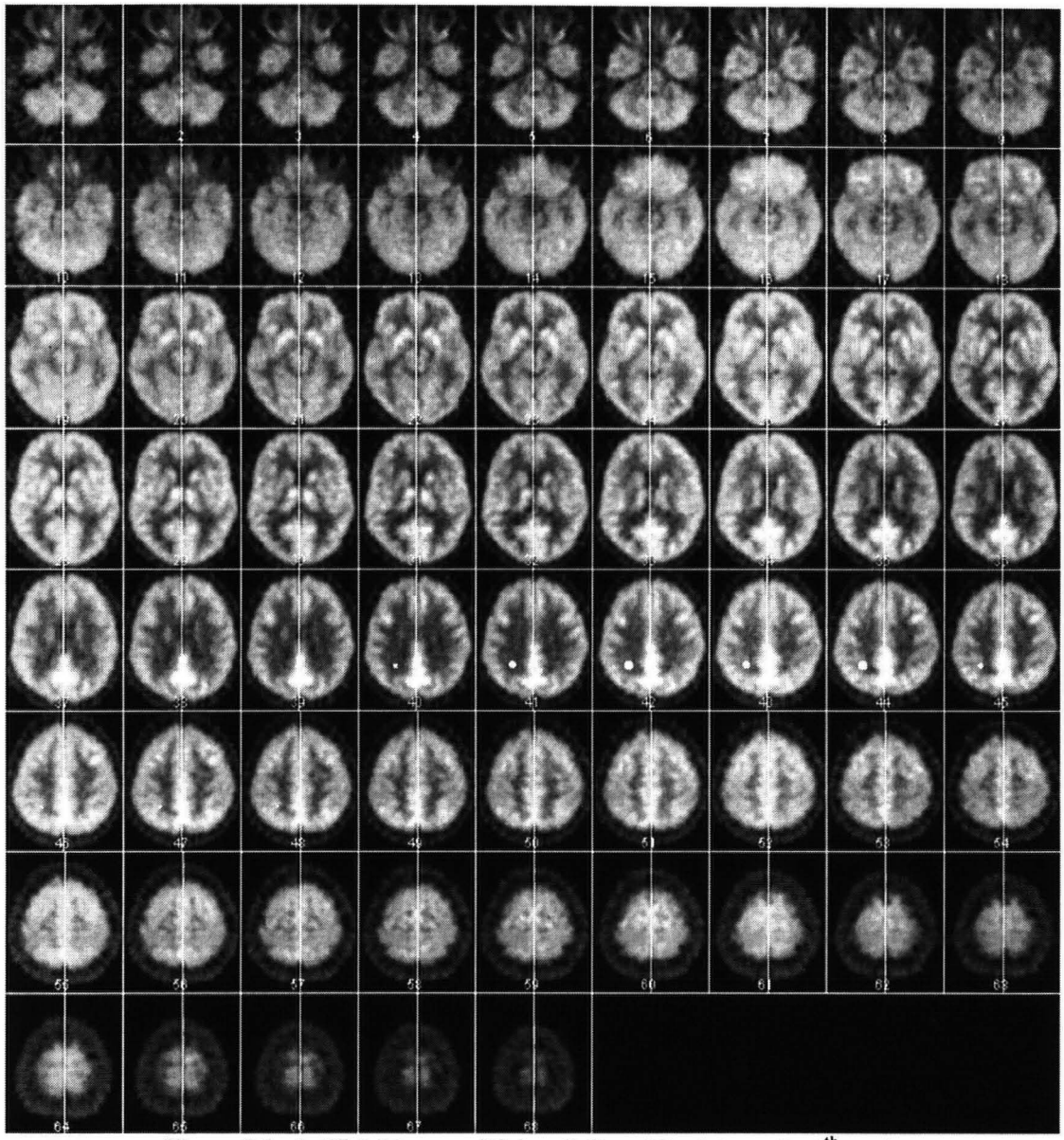

Figure 5.6. Artificial tumour (high activity, white dots on the 5th row).

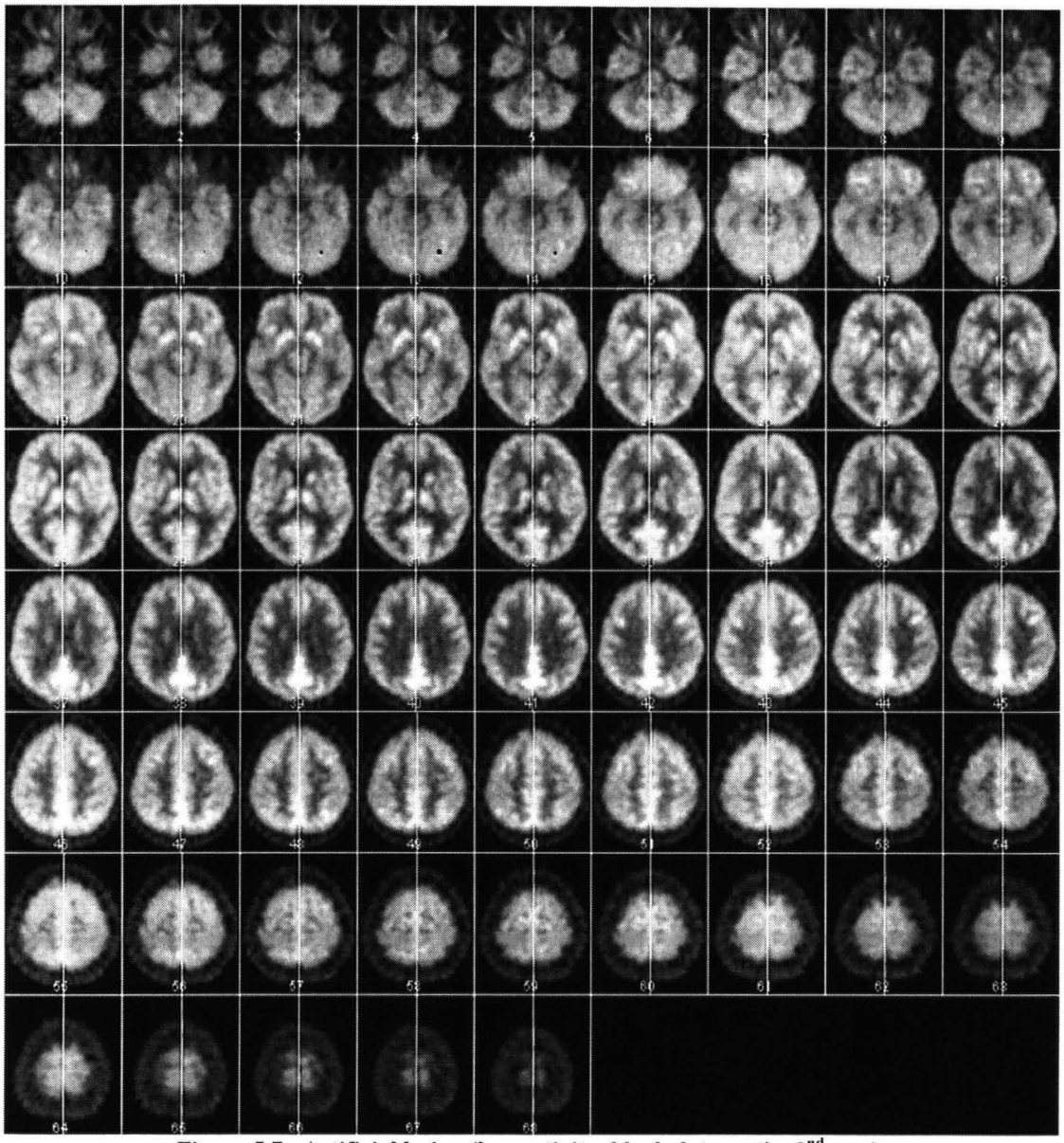

Figure 5.7. Artificial lesion (low activity, black dots on the 2nd row).

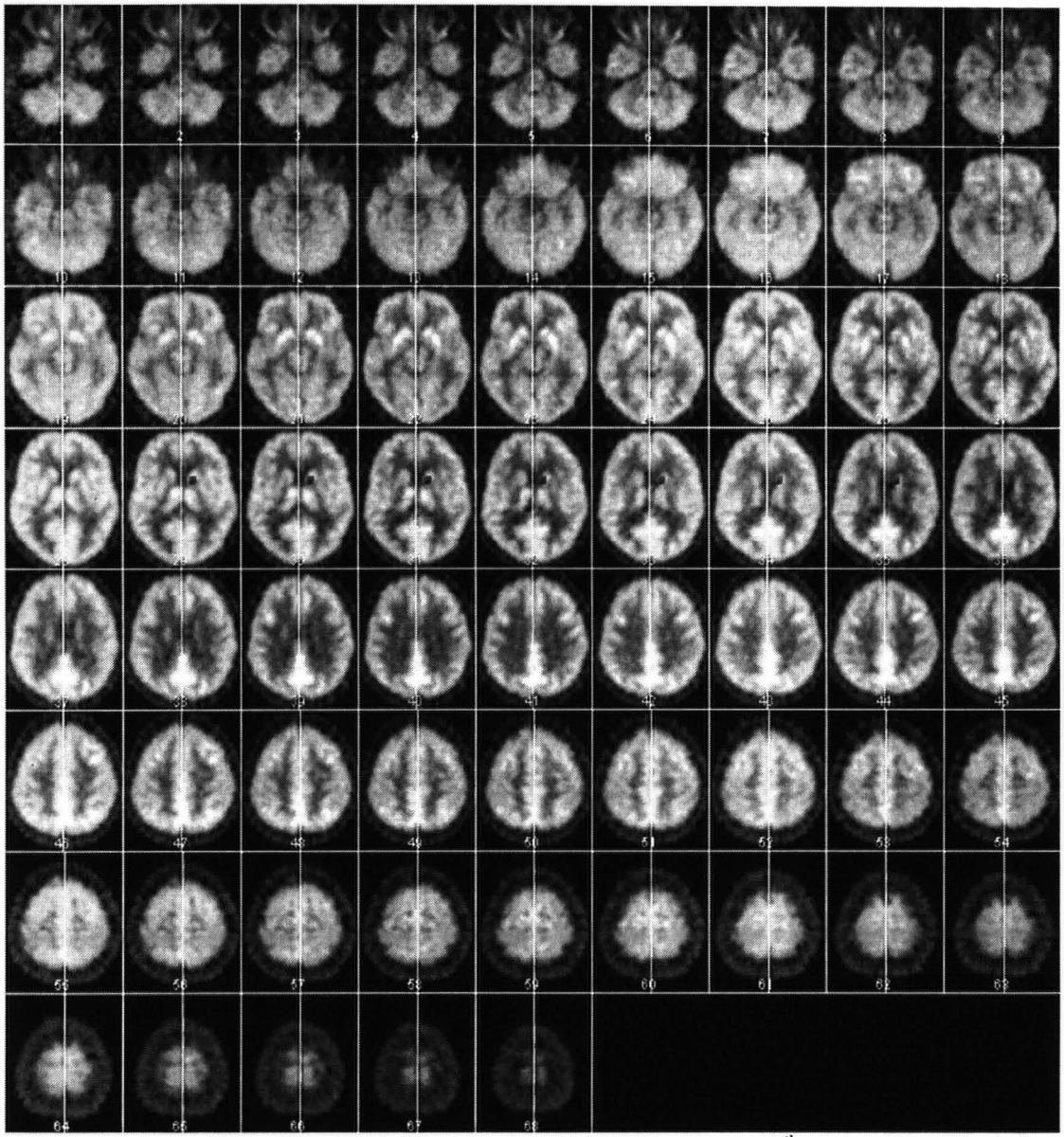

Figure 5.8. Artificial lesion (low activity grey area on 4th row).

Results show that *ideal-Mid-Sagittal Plane* can be reliably extracted using the tested algorithms [99].

5.2 Texture

Texture is quantified using the previously described Gabor filter method. Two examples of the complete texture feature, for the Posterior Cingulate, are given in Equations 5.1 – 5.2 along with the respective diagnosis. The 48-element feature vector is inserted into database to enable content-based image retrieval to be performed.

Normal

| 256.09780 | 92.95680 | 91.84210 | 220.06970| 91.84210
| 92.95680 | 66.85470 | 18.55830 | 18.33030 | 62.27360
| 18.33030 | 18.55830 | 18.33800 | 4.74990 | 4.70130
| 17.71170 | 4.70130 | 4.74990 | 5.89540 | 1.57730
| 1.56600 | 5.79790 | 1.56600 | 1.57730 | 318.90010 **(5.1)**
| 98.60280 | 96.06140 | 288.55120 | 96.06140 | 98.60280
| 144.06870 | 33.48880 | 32.27010 | 129.61540 | 32.27010
| 33.48880 | 58.07810 | 10.72870 | 10.19940 | 52.67680
| 10.19940 | 10.72870 | 26.05130 | 3.83260 | 3.60560
| 23.76080 | 3.60560 | 3.83260 |

Alzheimer's

| 354.90260 | 195.07490 | 195.66550 | 389.91520 | 195.66550
| 195.07490 | 118.38050 | 37.91220 | 37.97560 | 122.92170
| 37.97560 | 37.91220 | 35.54100 | 9.23200 | 9.24110
| 36.16420 | 9.24110 | 9.23200 | 11.78240 | 2.89400
| 2.89560 | 11.88360 | 2.89560 | 2.89400 | 365.40140 **(5.2)**
| 193.97120 | 199.03690 | 469.33990 | 199.03690 | 193.97120
| 192.98220| 63.92190 | 66.04500 | 224.86220 | 66.04500
| 63.92190 | 83.53920 | 19.46420 | 20.37800 | 94.35220
| 20.37800 | 19.46420 | 38.82530 | 6.63680 | 7.03590
| 43.24770 | 7.03590 | 6.63680 |

Retrieval results are presented in Tables 5.1 – 5.6; each anatomical structure is presented in ascending order, with the highest value feature vector at the top of table. Images with the same diagnosis should therefore be grouped together.

Table 5.1 Parietal Lobe

image	diagnosis
990168	Alzheimers
990270	PCA
990189	PCA
990164	PCA
990136	Normal
990121	Alzheimers
990169	Alzheimers
990170	Alzheimers
990276	MCI
000065	Normal

Table 5.2
Posterior Cingulate

image	diagnosis
990270	PCA
990189	PCA
990164	PCA
000065	Normal
990136	Normal
990121	Alzheimers
990276	MCI
990168	Alzheimers
990169	Alzheimers
990170	Alzheimers

Table 5.3
Brodmann's Area 30

image	diagnosis
990270	PCA
990189	PCA
990164	PCA
990121	Alzheimers
990168	Alzheimers
990169	Alzheimers
990170	Alzheimers
000065	Normal
990276	MCI
990136	Normal

Table 5.4
Brodmann's Area 29

image	diagnosis
990270	PCA
990168	Alzheimers
990189	PCA
990121	Alzheimers
990164	PCA
990276	MCI
990169	Alzheimers
990170	Alzheimers
990136	Normal
000065	Normal

Table 5.5 Occipital Lobe

image	diagnosis
990164	PCA
990270	PCA
990168	Alzheimers
990189	PCA
990136	Normal
990276	MCI
000065	Normal
990121	Alzheimers
990169	Alzheimers
990170	Alzheimers

Table 5.6 Hippocampus

image	diagnosis
990270	PCA
990168	Alzheimers
990164	PCA
990169	Alzheimers
990170	Alzheimers
990276	MCI
990121	Alzheimers
990136	Normal
990189	PCA
000065	Normal

The retrieval results obtained using the raw data from the texture quantification procedures exhibit differentiation based upon patient diagnosis, in nine out of ten cases when utilizing BA30 or Posterior Cingulate which produced the best results. Tables have been produced by querying the database of images and ordering results by the value of the texture feature. Each table represent a different and unique anatomical region. Those images with matching diagnosis should therefore be adjacent.

5.3 Feature detection

Abnormal asymmetries are detected and isolated using the previously outlined approach, described in section 4.3. Figures 5.9 – 5.21 show pairs of images, the original PET image is displayed on the left whilst the abnormal feature is highlighted in the right hand side image. The red pixel is the centre pixel of the smallest possible box that would completely contain the detected feature.

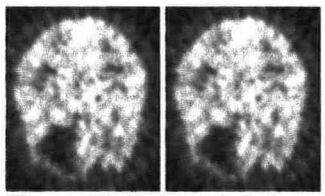

Figure 5.9 Bottom left (low activity)

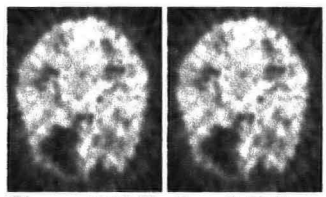

Figure 5.10 Bottom left (low activity)

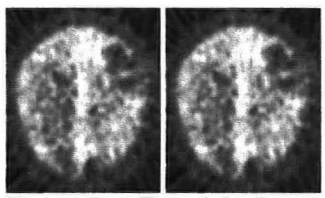

Figure 5.11 Top right (low activity)

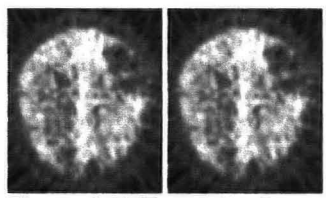

Figure 5.12 Top right (low activity)

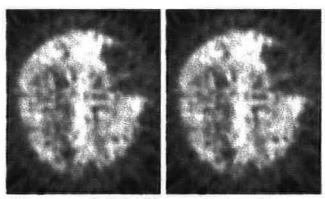

Figure 5.13 Top right (low activity)

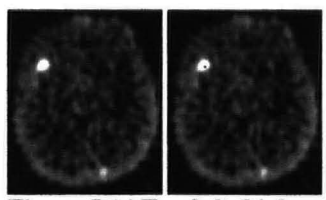

Figure 5.14 Top left (high activity)

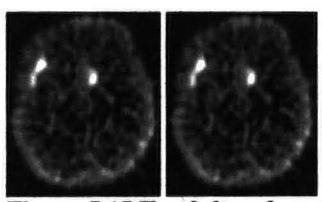

Figure 5.15 Top left and central (high activity)

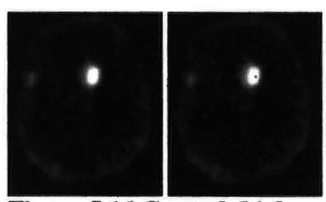

Figure 5.16 Central (high activity)

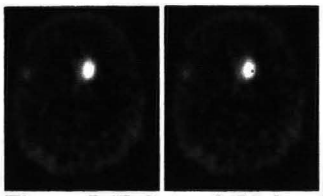

Figure 5.17 Central (high activity).

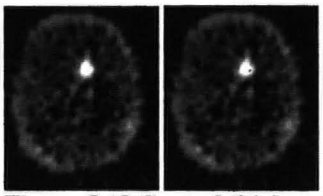

Figure 5.18 Central (high activity).

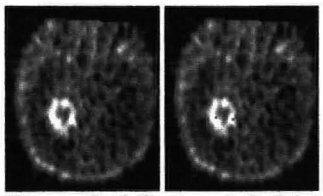

Figure 5.19 Bottom left (high activity).

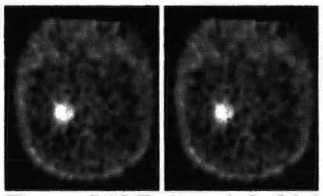

Figure 5.20 Bottom left (high activity).

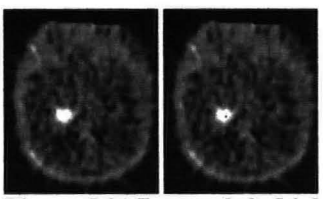

Figure 5.21 Bottom left (high activity).

Centre pixel co-ordinates and area of detected lesion are utilized as indices within a database to perform content based retrieval, of the PET images.

5.4 Activation Homogeneity

Quantification of PET images using the co-efficient of variance, or CV, for voxel intensity has been tested. The anatomical structures measured were the Parietal Lobes, Brodmann's Areas 29 and 30, and the Posterior Cingulate [71], as illustrated in Figures 4.8 to 4.12. The whole brain, with the specified region of interest removed has also been measured for comparison, results shown in Tables 5.7 – 5.12.

Table 5.7 CV values of BA30 compared to rest of whole brain.

Wb-roi	Diff	BA30	Diagnosis
0.44846	0.01370	0.46216	Alzheimer
0.50993	-0.00069	0.50924	Alzheimer
0.50948	-0.00139	0.50809	Alzheimer
0.56589	0.06765	0.63354	Alzheimer
0.50264	0.07253	0.57517	MCI
0.45775	0.01970	0.47745	Normal
0.35959	0.05242	0.41201	Normal
0.49766	-0.04163	0.45603	PCA
0.50216	-0.13215	0.37001	PCA
0.63544	0.44986	1.08530	PCA

Table 5.8 CV values of BA29 compared to rest of whole brain.

Wb-roi	Diff	BA29	Diagnosis
0.56634	-0.16349	0.40285	Alzheimer
0.44856	-0.11988	0.32868	Alzheimer
0.51048	-0.21054	0.29994	Alzheimer
0.51003	-0.21060	0.29943	Alzheimer
0.50282	-0.09396	0.40886	MCI
0.45819	0.18942	0.64761	Normal
0.35996	-0.06967	0.29029	Normal
0.49771	-0.16434	0.33337	PCA
0.50223	-0.20738	0.29485	PCA
0.63627	-0.00013	0.63614	PCA

Table 5.9 CV values of Parietal compared to rest of whole brain.

Wb-roi	Diff	Parietal	Diagnosis
0.57926	-0.16034	0.41892	Alzheimer
0.46517	-0.17186	0.29331	Alzheimer
0.52948	-0.22434	0.30514	Alzheimer
0.52899	-0.22409	0.30490	Alzheimer
0.52157	-0.24205	0.27952	MCI
0.47431	-0.16666	0.30765	Normal
0.37279	-0.14273	0.23006	Normal
0.48872	-0.02395	0.46477	PCA
0.48955	-0.07552	0.41403	PCA
0.65073	-0.20913	0.44160	PCA

Table 5.10. CV values of PC compared to rest of whole brain.

Wb-roi	Diff	PC	Diagnosis
0.56544	-0.01159	0.55385	Alzheimer
0.44892	-0.09295	0.35597	Alzheimer
0.51031	-0.16652	0.34379	Alzheimer
0.50986	-0.16731	0.34255	Alzheimer
0.50266	-0.05049	0.45217	MCI
0.45739	-0.14425	0.31314	Normal
0.35956	-0.08680	0.27276	Normal
0.49891	-0.17830	0.32061	PCA
0.50234	-0.18832	0.31402	PCA
0.63015	0.79295	1.42310	PCA

Table 5.11. CV values of Hippocampus compared to rest of whole brain

Wb-roi	Diff	Hippo	Diagnosis
0.56645	-0.32094	0.24551	Alzheimer
0.44851	-0.24940	0.19911	Alzheimer
0.51035	-0.19582	0.31453	Alzheimer
0.50990	-0.19467	0.31523	Alzheimer
0.50288	-0.22559	0.27729	MCI
0.45820	-0.14687	0.31133	Normal
0.35997	-0.18026	0.17971	Normal
0.49764	-0.26120	0.23644	PCA
0.50238	-0.20823	0.29415	PCA
0.63681	-0.53334	0.10347	PCA

Table 5.12. CV values of Occipital compared to rest of whole brain.

Wb-roi	Diff	Occipital	Diagnosis
0.56570	-0.10485	0.46085	Alzheimer
0.45648	-0.10449	0.35199	Alzheimer
0.51219	-0.14088	0.37131	Alzheimer
0.51172	-0.14091	0.37081	Alzheimer
0.50797	-0.04974	0.45823	MCI
0.45921	-0.07172	0.38749	Normal
0.36054	-0.07467	0.28587	Normal
0.50495	-0.08872	0.41623	PCA
0.50396	-0.11120	0.39276	PCA
0.62855	0.14742	0.77597	PCA

The results show that the co-efficient of variance, or CV, does not differentiate the image sets data based upon their diagnosis. Therefore the retrieval results obtained using the CV value as indices do not perform content based PET image retrieval. There is no apparent classification based upon diagnosis when CV is utilized as the index.

5.5 Hypo - Metabolism

Quantification of PET images using the mean voxel intensity value has been performed. A reduced mean value corresponds to hypo-metabolism. The anatomical structures measured were the Parietal Lobes, Brodmann's Areas 29 and 30, the Hippocampus, the Occipital Lobe and the Posterior Cingulate [71]. Figures 4.8 to 4.12 illustrate these anatomical regions. The whole brain, with the specified region of interest removed has also been measured for comparison. Absolute mean values and mean index ratio have been calculated.

Table 5.13. Mean values of the Parietal Lobes compared to the rest of the Brain(Wb-roi).

Wb-roi	Ratio	Parietal	Diagnosis
2077.12990	0.9031279	2299.92880	Alzheimer
2304.98810	0.9556902	2411.85710	Alzheimer
2711.53230	0.7616675	3559.99470	Alzheimer
2713.42430	0.7619768	3561.03280	Alzheimer
2787.40500	0.7423025	3755.07980	MCI
3261.30010	0.8404196	3880.56180	Normal
3397.70740	0.9719812	3495.65130	Normal
2386.73090	1.3488661	1769.43500	PCA
2296.77070	1.1552350	1988.14150	PCA
1543.70890	0.8949618	1724.88810	PCA

Table 5.14. Mean values of Brodmann's Area 29 compared to the rest of the Brain.

Wb-roi	Ratio	BA29	Diagnosis
2087.53440	0.9018596	2314.70000	Alzheimer
2306.96710	1.0497093	2197.72000	Alzheimer
2793.31340	0.9225098	3027.95000	Alzheimer
2795.15290	0.9219420	3031.81000	Alzheimer
2848.69500	1.1950728	2383.70000	MCI
3316.37920	0.9174904	3614.62000	Normal
3403.28090	0.8169691	4165.74000	Normal
2317.35600	1.0438352	2220.04000	PCA
2224.75930	1.1099378	2004.40000	PCA
1544.40540	1.4559149	1060.78000	PCA

Table 5.15. Mean values of Brodmann's 30 compared to the rest of the Brain

Wb-roi	Ratio	BA30	Diagnosis
2088.73560	1.2324408	1694.79590	Alzheimer
2306.40930	0.9996351	2314.42860	Alzheimer
2794.17310	0.9601862	2910.03270	Alzheimer
2796.00990	0.9588511	2916.00000	Alzheimer
2848.99650	1.1261673	2529.81630	MCI
3314.61430	0.7425496	4463.82860	Normal
3401.93480	0.7984753	4260.53880	Normal
2316.96300	0.9774784	2370.34690	PCA
2224.50190	0.8740774	2544.97140	PCA
1544.97830	1.3895832	1111.82860	PCA

Table 5.16. Mean values of the Posterior Cingulate compared to the rest of the brain.

Wb-roi	Ratio	PC	Diagnosis
2092.10960	1.2862583	1626.50810	Alzheimer
2306.78440	0.9682847	2382.34110	Alzheimer
2794.17280	0.8871118	3149.74130	Alzheimer
2796.00600	0.8860549	3155.56730	Alzheimer
2851.59980	1.0245087	2783.38280	MCI
3304.42560	0.6324842	5224.51900	Normal
3394.92610	0.7450476	4556.65660	Normal
2314.01570	0.8562272	2702.57190	PCA
2223.58360	0.7833148	2838.68450	PCA
1551.57160	1.9368469	801.08120	PCA

Table 5.17. Mean values of the Hippocampus compared to the rest of the brain.

Wb-roi	Ratio	Hippocampus	Diagnosis
2087.03930	1.0287119	2028.78900	Alzheimer
2307.42600	1.2496369	1846.47710	Alzheimer
2794.11360	1.2477759	2239.27520	Alzheimer
2795.94990	1.2479977	2240.34860	Alzheimer
2848.57390	1.0921025	2608.33940	MCI
3317.77440	1.3233994	2507.00920	Normal
3404.54500	1.3627482	2498.29360	Normal
2317.75890	1.2289762	1885.92660	PCA
2224.14330	1.0281937	2163.15600	PCA
1543.71590	0.8271316	1866.34860	PCA

Table 5.18. Mean values of the Occipital compared to the rest of the brain.

Wb-roi	Ratio	Occipital	Diagnosis
2095.56410	0.9230719	2270.20670	Alzheimer
2262.71960	0.8212387	2755.25210	Alzheimer
2726.85320	0.6897022	3953.66780	Alzheimer
2728.74560	0.6896413	3956.76090	Alzheimer
2811.39570	0.8377927	3355.71760	MCI
3250.29270	0.7617111	4267.09380	Normal
3337.33410	0.7850622	4251.04410	Normal
2298.24010	0.9084815	2529.75980	PCA
2231.90100	0.8728679	2556.97450	PCA
1560.84690	1.1448270	1363.39110	PCA

A one tailed T-Test was performed, with a confidence interval of 0.001, on each dataset to elucidate whether there was significant hypo-metabolism in the anatomical regions of interest when compared to the normal.

The Parietal Lobes, Posterior Cingulate, Hippocampus, Brodmann's Area's 29 and 30, of patients diagnosed with Alzheimer's were found to have a significantly reduced metabolism. The Posterior Cingulate, Parietal Lobe, and Brodmann's Areas 29 and 30 of the patient diagnosed with Mild Cognitive Impairment exhibited decreased metabolism when compared to the normal. Patients diagnosed with Posterior Cortical

Atrophy exhibited hypo-metabolism in the Occipital Lobes, Parietal Lobes, Posterior Cingulate, Hippocampus, and Brodmann's Area 29 and 30.

Absolute mean values however are not suitable for use as a database index within a content based image retrieval system as they are dependent on relative dosages. Mean index ratio is therefore calculated, and utilized as the index for retrieval. Results are presented in Tables 5.19 – 5.24, each dataset is in ascending order. Mean index ratio is calculated by dividing the mean of the specified structure by the mean value for the rest of the brain.

Table 5.19. Posterior Cingulate

image	diagnosis
990270	PCA
990121	Alzheimer
990276	MCI
990168	Alzheimer
990169	Alzheimer
990170	Alzheimer
990164	PCA
990189	PCA
990136	Normal
000065	Normal

Table 5.20. Parietal Lobe

image	diagnosis
990164	PCA
990189	PCA
990136	Normal
990168	Alzheimer
990270	PCA
990121	Alzheimer
000065	Normal
990169	Alzheimer
990170	Alzheimer
990276	MCI

Table 5.21. Hippocampus

image	diagnosis
990136	Normal
000065	Normal
990169	Alzheimer
990170	Alzheimer
990168	Alzheimer
990164	PCA
990276	MCI
990189	PCA
990121	Alzheimer
990270	PCA

Table 5.22. Occipital Lobe

image	diagnosis
990270	PCA
990121	Alzheimer
990164	PCA
990189	PCA
990168	Alzheimer
990276	MCI
990136	Normal
000065	Normal
990169	Alzheimer
990170	Alzheimer

Table 5.23. Brodmann's Area 30

image	diagnosis
990270	PCA
990121	Alzheimer
990276	MCI
990168	Alzheimer
990164	PCA
990169	Alzheimer
990170	Alzheimer
990189	PCA
990136	Normal
000065	Normal

Table 5.24. Brodmann's Area 29

image	diagnosis
990270	PCA
990276	MCI
990189	PCA
990168	Alzheimer
990164	PCA
990121	Alzheimer
990169	Alzheimer
990170	Alzheimer
000065	Normal
990136	Normal

Some images with the same diagnosis are grouped together. However there are a number of errors where an image of one diagnosis is grouped with those of different diagnosis. Retrieval using only the mean index ratio cannot be said to be completely reliable with the tested data; Images are not completely differentiated or grouped together in a manner that is concurrent with their respective diagnosis.

5.6 Physiological data (Simplified Reference Tissue Model)

For dynamic images of a ligand tracer, *raclopride*, a kinetic modelling technique, the *simplified reference tissue model* [68], is applied to determine the binding potential. An example of the image data that was utilized in this stage of the study is shown below in Figure 5.22; all the PET scans used in this part of the study originate from animal subjects.

Tracer activity in three separate areas of the brain was measured, the left striatum, the right striatum and also the cerebellum. The tracer used, *raclopride*, has a high affinity for dopamine D_2 receptors, which have a high density in the striatum. There should be no specific binding in the cerebellum (the reference region). By using the Simplified Reference tissue model the binding potential of drug can be calculated for both of the striatum and hence an estimate of the receptor density is obtained. In this experiment the left striatum was lesioned to eliminate D_2 receptors, and consequently reduce the regions binding potential. Two of the lesioned striata were grafted. The purpose of this was to assess D2 receptor status in the striatal grafts in this experimental model of *Huntington's* disease (a neuro-degenerative disorder).

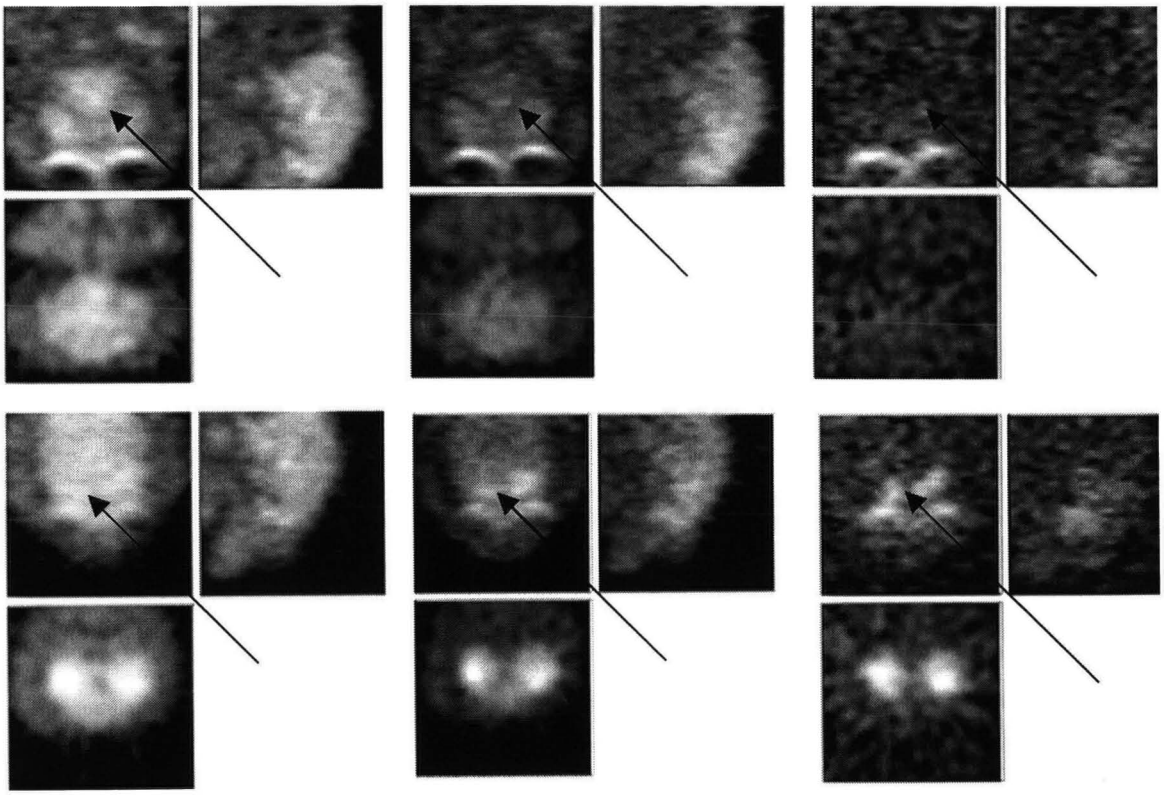

Figure 5.22. Transaxial, coronal, and sagittal projections of brain frames taken in the time periods of 5-10 minutes (left column), 40 minutes (middle column) and 90 minutes (right column) for cerebellum (top row) and striatum (bottom row).

A typical example of the tissue time activity curves obtained from PET images is shown in Figure 5.23. The value of binding potential obtained from this data was 1.4 (for the lesioned left striatum).

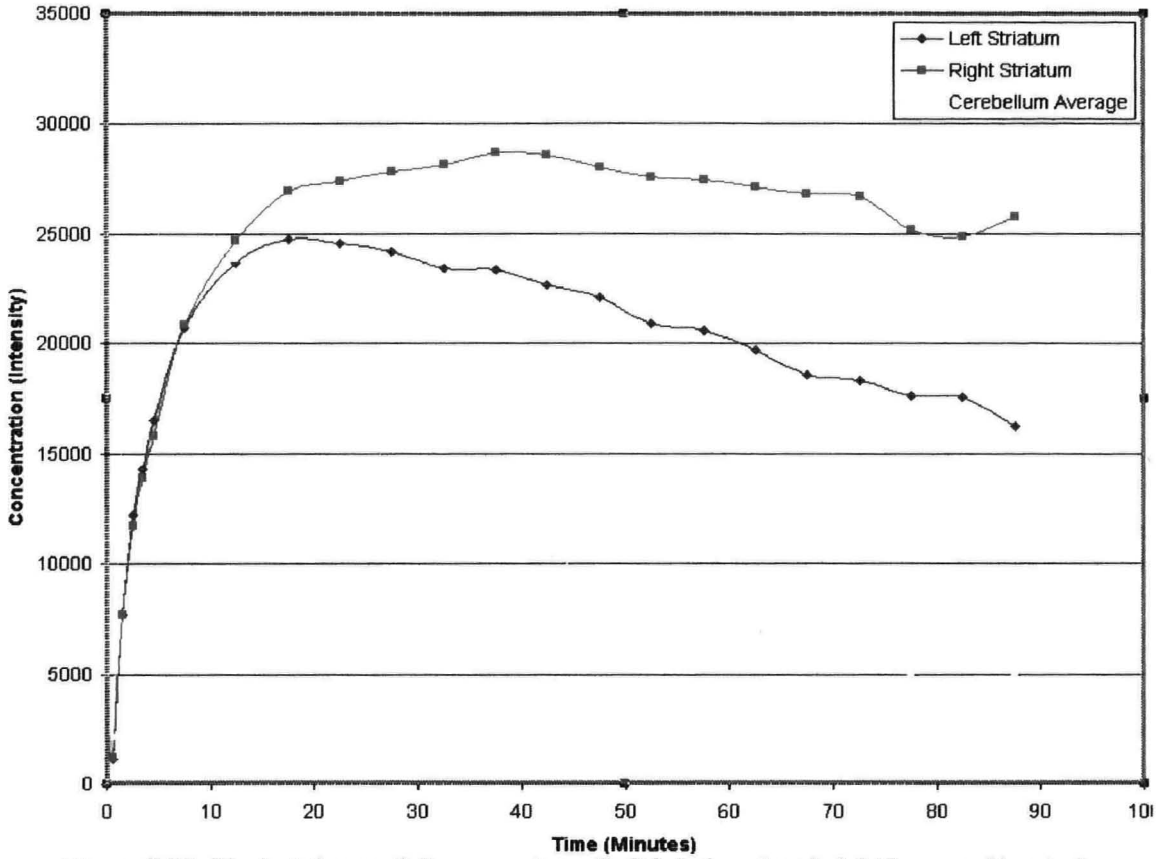

Figure 5.23. Typical time-activity curve data. Left is lesioned and right is normal/control striata and cerebellum is the reference region.

In this study 6 different image sets were analyzed, producing twelve binding potential values, one for each of the two striata. After completing analysis the amount of data available consisted of 18 separate time activity curves, 12 individual binding potentials, and 6 binding potential ratios. Binding potential was found to be 0.7975 for a lesioned striatum and 1.2045 for the normal striatum.

5.7 Content based image retrieval

Image retrieval is carried out in two stages. If an abnormal asymmetry is detected its position is utilized as the database query. The Euclidean distance between the lesions is calculated and employed as the similarity metric. Scans possessing the minimal distance are returned first, shown below is the query image followed by retrieval results in the correct order as returned by the system. All images with detected lesions are retrieved and those that possess a lesion that is closest, in Euclidean distance from the lesion on the query image, are returned first. Results are displayed in Table 5.25.

Table 5.25. Retrieval results using Euclidean distance between lesions.

Voxel co-ordinates of lesion X=51, Y=57, Z=32.

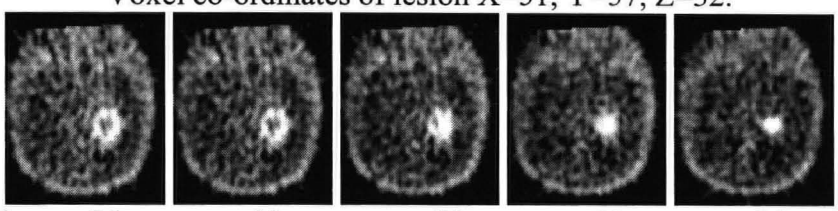

Slice Number 30 31 32 33 34

Query Image

Retrieval Results

Voxel co-ordinates of lesion X=35, Y=32, Z=35.9.

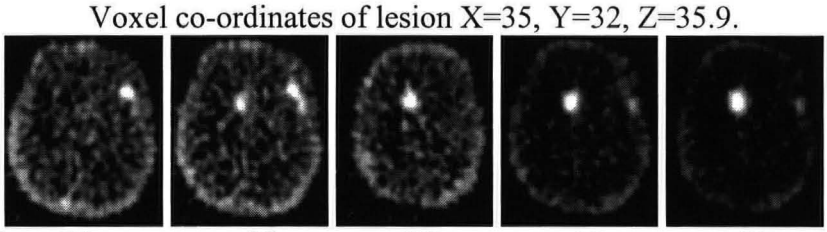

Slice Number 34 35 36 37 38

Voxel co-ordinates of lesion X=22, Y=30, Z=49.

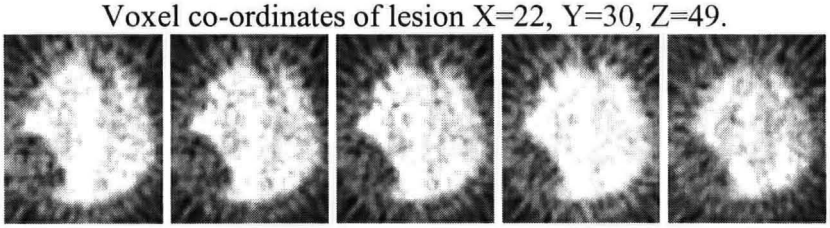

Slice Number 47 48 49 50 51

Voxel co-ordinates of lesion X=52, Y=72, Z=32

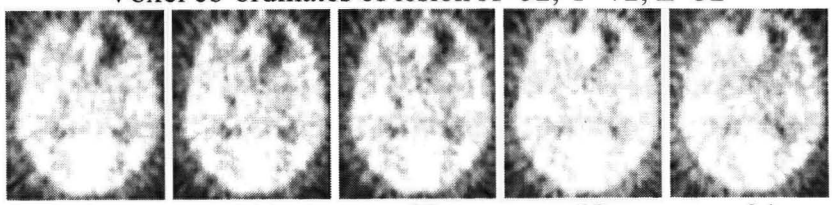

Slice Number 30 31 32 33 34

The Euclidean distance between a lesion and a user specified position is also implemented. Images with an abnormal asymmetry located nearest to the specified position are returned first, a screenshot of this process is shown in Figure 5.11.

Texture and mean index ratio, from the Occipital Lobe, Brodmann's Area's 29 and 30 and the Posterior Cingulate, are also employed to classify and retrieve images. The texture and mean index ratio visual features are combined into one feature. Retrieval results that correspond to the diagnosis are produced. The results of querying using the combined feature are presented in Tables 5.26 - 5.28.

Table 5.26. Ascending order

Image	Diagnosis
990270	PCA
990189	PCA
990164	PCA
990136	Normal
000065	Normal
990121	Alzheimer
990169	Alzheimer
990170	Alzheimer
990168	Alzheimer
990276	MCI

Table 5.27. Normal query data

Image	Diagnosis
990136	Normal
000065	Normal
990270	PCA
990189	PCA
990164	PCA
990121	Alzheimer
990169	Alzheimer
990170	Alzheimer
990168	Alzheimer
990276	MCI

Table 5.28. Alzheimer's query data

Image	Diagnosis
990121	Alzheimer
990169	Alzheimer
990170	Alzheimer
990168	Alzheimer
990276	MCI
90270	PCA
990189	PCA
990164	PCA
990136	Normal
000065	Normal

Texture and mean index ratio of the relevant anatomical structures are combined using the calculation shown in Equation 5.3.

$$TM = \sum_{1}^{A}\left(\left(\sum_{N}^{24} T_N^A\right)\left(\frac{\overline{WB_{XYZ}}}{\overline{A_{XYZ}}}\right)\right) \qquad \textbf{(5.3)}$$

TM represents the texture and mean index ratio combined into one feature vector. The whole brain is *WB* and each anatomical structure is represented by *A*. Raw texture data is shown as *T*, and *N* represents each of the orientations and rotations of the *Gabor filters* used to quantify texture.

A preliminary Internet based system has been built to display the above retrieval methods; the graphical user interface is shown in Figures 5.24 and 5.25. The server is located at Middlesex University (Tottenham Campus).

6 Summary

In summary, the following results have been achieved during this study; they are:

- Extraction of the *ideal – Mid Sagittal Plane* which is applied to PET images to detect lesions.

- Probability of abnormality calculated by comparing pixels belonging to the hypothesised feature to those in surrounding region. Results show 74% accuracy in a test set consisting of 1062 separate 2D slices. Conversely 26% were incorrectly detected, meaning that either a false positive was present or a lesion went undetected.

- Anatomical position has been identified by mapping images to the Talairarch and Tournoux brain atlas. The anatomical position of any detected lesion has been utilized as a database index to enable retrieval based upon medically salient visual characteristics (the anatomical location of abnormality).

- Co-efficient of variance has been shown to be unreliable using the tested data.

- Mean values, measured using the anatomical mapping procedure outlined here, correspond to those previously obtained using traditional manual segmentation techniques.

- Texture quantification of anatomical structures enables retrieval based upon patient diagnosis which has been shown in preliminary tests to be accurate in nine out of ten cases with certain anatomical regions.

- Combining the mean and texture data of relevant anatomical structures into one single feature improves the preliminary results and all ten

cases are correctly ordered, and therefore retrieval is accurate. The local anatomical structures that have been conjoined are the Occipital Lobe to assess Posterior Cortical Atrophy. Brodmann's Area 30, part of the Retrosplinal Cortex is included in relation to Alzheimer's. The Posterior Cingulate is analyzed to ensure Mild Cortical Atrophy (and also Alzheimer's) is accounted for.

- Binding potential has been extracted as part of an animal study using the simplified reference tissue model [68]. Retrieval based upon the binding potential and time activity curve has been shown elsewhere to be a valid and reliable method of indexing PET images within a database. However, in this study, appropriate time sequence data is not available, extensive evaluation is therefore not carried out.

7 Result Analysis

7.1 Anatomical Mapping

Mapping a spatially normalized PET brain image to the Talairarch and Tournoux atlas is a widely used method for reporting which areas of the brain have been studied [58, 96,100]. Anatomical region of interest definition using only Talairarch and Tournoux atlas co-ordinates has not previously been researched with PET images and retrieval.

The segmentation or isolation of anatomical structures using this method has shown to be effective. Measured tracer uptake patterns that correspond to that achieved when manual segmentation methods are employed have been produced using this new method. Results presented in 5.5 (*Hypo-metabolism*) and discussed in section 7.4 (*Statistical Measurement: Mean and CV*)

The accuracy and reliability of both the Talairarch and Tournoux atlas and the Spatial Normalization [58] algorithms are in line with the results of research carried out elsewhere. Implementing this method with other anatomical areas may be more problematic. Warping of the brain during spatial normalization can produce artificial size and shape differences in certain anatomical structures [62]. The probability of a Talairarch and Tournoux atlas label being accurate reduces when alternate anatomical areas are considered [4,96].

Segmentation of anatomical structures is a prerequisite for statistical analysis, Texture quantification and in the majority of cases Kinetic Modelling. Mapping co-ordinates from an image to an anatomical map is essential for indexing PET scans, from patients with any form of lesion. Lesion detection is also dependent on the elucidation of the iMSP co-ordinates.

7.2 Extracted Symmetry Plane

The *ideal*-Mid Sagittal Plane, or *i*MSP has been successfully extracted, as shown in results section 5.1 (*Extracted ideal Mid Sagittal Plane*). The procedures that are implemented to achieve this iMSP extraction provide a number of significant innovations to the existing theory [97].

- The angle of rotation, and the translation distance are calculated simultaneously.
- Polynomial regression, of rotation angle and translation distance, in a least squares sense.
- No weighting given to any slice.

Simultaneous calculation of angle and translation distance is the most fundamental difference. This ensures the cross-correlation value is a maximum for both parameters. The extraction procedure outlined assumes that the *i*MSP is a 3D flat plane through the actual brain but not necessarily flat through the images (due to possible head movements), therefore the rotation angle and translation distance between 2D image slices can differ.

Existing theory relies on an angle which gives the maximum cross correlation value, this is due to the fact that angle is assumed to be constant across all 2D slices. A development of this research is to incorporate polynomial regression in which rotation angle can vary between 2D slices. The final development is the elimination of weighting certain slices. Previous research [97] has utilized MRI images which contain bone data and enable a heavier weighting to be given to those slices with a preponderance of this information. Weighting's based on bone anatomy are impossible with PET images; PET is a functional imaging modality.

These developments show that the symmetry plane can be reliably extracted from PET images. This new approach to extracting iMSP from PET images provides

a reliable mechanism for creating reflection images, which itself enables the detection of asymmetric visual features.

7.3 Localized Texture

Differentiation of PET brain images using the Euclidean distance between studied images, of the 48 dimensional texture feature vector has been attempted. The method is described in section 4.4 (*Texture*) and results shown in section 5.2 (*Texture*).

Nine out of ten images have been successfully differentiated using only the Euclidean distance between texture features. This 90% accuracy is achieved when the texture features of Brodmann's area 30 and the Posterior Cingulate are considered. These two areas also exhibit parallel differences in mean intensity, further examined in section 7.4 (*Statistical Measurement: Mean and CV*).

Accuracy of retrieval results is further enhanced when texture is coupled with mean index ratio, discussed in detail section 7.6 (*Content Based Image Retrieval*) It is important to note that classification based upon texture was more accurate than either absolute mean or mean index ratio.

The use of Gabor filters to differentiate PET images by measuring texture of anatomical areas is a new method, which has been shown to function in this study. Gabor filter have previously not been applied to reconstructed PET images as has been performed in this research. Results presented here show that Gabor filters, and texture quantification of reconstructed PET images is a valid method in the analysis procedure.

7.4 Statistical Measurement: Mean and CV

Absolute mean values of localized anatomical structures show significant hypo-metabolism as expected, see results section 5.5 (*Hypo-metabolism*). Absolute mean values themselves however cannot be viably used within a content-based image retrieval system. This is due to the differences in measured intensity levels caused by variations in tracer concentration and scanner sensitivity.

Mean index ratio, the mean intensity of a certain localized anatomical structure divided by the mean intensity of the whole brain is a valid method for indexing PET images within a database. Mean index ratio, or normalized region of interest curve [56], eliminates the effects of scanner and dosage differences and is a widely used method for analyzing PET scans [56].

Mean index ratio of patients suffering from Alzheimer's or MCI have been shown to be higher than those diagnosed as normal when considering the Posterior Cingulate and Brodmann's Area 30, shown in section 5.5 (*Hypo-metabolism*) tables 5.19 and 5.23 respectively. Patients diagnosed with Posterior Cortical Atrophy show a higher mean index ratio in relation to the Occipital lobe, shown in table 5.22 also section 5.5 (*Hypo-metabolism*). Mean index ratios of other anatomical areas exhibit no reliable differences between diagnosis types.

The three structures, Posterior Cingulate, Brodmann's area 30 and Occipital Lobe, are used in combination with the data from the texture analysis to perform retrieval; this process is described in section 5.7 (*Content Based Image Retrieval*).

Co-efficient of variance does not show any reliable differentiation based upon diagnosis, which contradicts the previous research [70]. This can however be explained by the fact that the PET images come from patients with the Prodormal form of Alzheimer's in which metabolism abnormalities are not as pronounced.

7.5 Kinetic Modelling

Binding potential of *raclopride* in the striata of primates has been calculated using the simplified reference tissue model [68]. Results were as expected with the lesioned subjects demonstrating a lower binding potential. The dynamic PET images were obtained from non-human subjects and therefore anatomical mapping was not possible. The spatial normalization algorithms and Talairarch and Tournoux atlas correspond to human brain anatomy. Utilization of kinetic modelling results as database indices within a content-based PET image retrieval system has not therefore been implemented. The use of this data in has previously been researched with binding potential results obtained from humans [2].

Combining the anatomical mapping process, described in methodology section 4.1 (*Anatomical Mapping*), with the simplified reference tissue model would produce an automated process for extracting the binding potential of the specified drug. This data could then be inserted in the database, and therefore form part of the content-based image retrieval system.

7.6 Content-based image retrieval

All the data that is used in the content-based image retrieval system is extracted independent of scanning protocol and with no prerequisite for a control/normal subject PET from the same study. Pre-processing of images used in the content-based image retrieval system consists of spatially normalizing the reconstructed PET images to the MNI template using the SPM [58] algorithms.

Retrieval of PET scans with lesions has been demonstrated, utilizing Euclidean distance between lesions as the similarity metric. Statistical measurements and texture quantification is applied to localized anatomical structures. Results from these processes classify images as either normal or from a patient suffering from a form of dementia. The developed algorithms are able to classify three forms of dementia: Mild Cognitive Impairment, Alzheimer's and Posterior Cortical Atrophy. This is achieved by combining the mean index ratio and texture features of three anatomical areas, the Posterior Cingulate, Occipital Lobe and Brodmann's Area 30, which when combined produced the most accurate retrieval. To classify PET scans diagnosed with other neurological disorders the correspondingly effected anatomical areas could be measured. Algorithms developed for performing anatomical mapping can be applied to any region of the brain that is listed in the original Talairarch and Tournoux atlas. Statistical measurements and texture quantification can also therefore be applied.

The retrieval system accounts for the two main types of PET images, those from lesioned patients and those diagnosed with dementia. Kinetic modelling data although not utilized in the CBIR system, has been extracted and retrieval of PET images based upon binding potential, the result of kinetic modelling, has been successfully performed elsewhere [2].

8 Conclusion

8.1 Hypothesis and Novel Research

Is it possible to extract medically salient visual features from 3D PET neurological images, using autonomous computer algorithms?

Can the extracted medically salient visual features be practically utilized within a Content-Based Image Retrieval system?

Research carried out as part of this investigation includes the following novel developments:

- Significant development of *i*MSP extraction theories, and creation of new algorithms.
- Statistical measurement of physiological parameters combined with anatomical accuracy provides a novel autonomous approach to PET analysis.
- Application and evaluation of Gabor texture measurements to PET images.
- Disease characterization. Differentiation of images from patients with Dementia and controls/normal.
- Further image differentiation of dementia diagnosed patients. Images classified as Alzheimer's, Posterior Cortical Atrophy or Mild Cognitive Impairment (very early Alzheimer's).

The above processes, which consist of algorithms written in Matlab, C, SQL and PHP are combined with a database of neurological PET images, resulting in the first content-based image retrieval system for PET images. Retrieval is based upon the medically salient information:

- Disease type.
- Anatomical location of any detected asymmetric abnormality.

Research developments produced as part of this project take a significant step towards the goal of content-based medical image retrieval:

"Semantic retrieval based on images that are segmented automatically into objects and where diagnoses can be derived easily from the objects visual features." [47]

8.2 Project Summary

A system for content-based retrieval of PET images has been developed in this study. Medically salient visual features have been extracted from PET neurological images. These extracted features have subsequently been systematically quantified and inserted into a database. Extracted feature data forms the indices within a database; this then enables the content-based retrieval of PET images.

Semantic retrieval has been performed, images are returned from the database based upon their diagnosis. Semantic retrieval is made possible by the newly developed feature extraction algorithms.

The first stage of the feature extraction process is to locate the position of the ideal-Mid-Sagittal Plane, or iMSP. When a PET image is found to possess no abnormal asymmetries further analysis is required. Texture, quantified using Gabor filters, of localized anatomical areas has been shown to correctly classify images when coupled with mean index ratio. Measurement of localized texture is a new approach to PET image quantification, while mean index ratio is a widely used procedure. The extraction of mean index ratio is however carried out by implementing a new approach utilizing the Talairarch and Tournoux atlas as the method for segmenting PET images into anatomical structures. This segmentation process also forms part of the texture quantification procedure.

Content-based retrieval of PET images has been performed. Medically salient visual features have been extracted from PET images. This has been achieved by developing new theories and implementing new algorithms.

Experimental results show that PET images are retrieved in a manner that is in an accord with their diagnosis. Combining the texture feature and the mean index ratio value to provides the bets results.

9 Future work

The developed system is focused on PET images. Inclusion of MR and CT would be beneficial to clinicians and researchers, especially the image data from the same subjects.

Due to the limited amount of time sequence data, physiological information has not been completely utilised. Further collection of this data and evaluation of the kinetic modelling method will be needed in order to make the current system a comprehensive one.

The programming routines developed to extract the symmetry plane from 3D PET images may be applicable to spatial normalization. The process of spatial normalization requires the definition of the anterior commisure – posterior commisure line, which is closely related to the symmetry of the brain. Symmetry of images from alternate modalities could also be investigated.

Texture data could be further analyzed to find those gabor filters which provide the most meaningful results, in this research all 24 combinations of scales and rotations are used. In the future this number could be limited to those which represent the brain and its component anatomical regions optimally.

Anatomically accurate segmentation using the Talairarch and Tournoux atlas [4] is inherently only possible with neurological data. However the incorporation of prior knowledge into segmentation algorithms for modalities such as MRI may not be advantageous. PET images contain a large amount of noise and are therefore difficult to segment. Low noise, high signal image modalities such as MRI may not produce better segmentation with the addition of prior knowledge in the manner outlined in this research.

It would be possible for the content based image retrieval system to be incorporated into a computer aided diagnosis, or CAD software package. Results for the retrieval system could facilitate the decision-making process. Raw data from the feature extraction algorithms could also be utilized directly in patient diagnosis.

10 Publications from this project

Title: Extraction of Physiological Information from 3D PET Brain Images
Authors: Batty, S., Fryer, T., Clark, J., Turkheimer, F., Gao, X.W.
Conference: Visualization, Imaging and Image Processing, Malaga, Spain, 401-405, September 2002.

Title: Towards Archiving 3D PET Brain Images Based on Their Physiological and Visual Content.
Authors: Batty, S., Clark J., Fryer, T., Turkheimer, F., Gao, X.W.
Conference: ICDIA 2002, Diagnostic Imaging and Analysis, Shanghai, China, 188-193, August 2002.
ISBN: 7-5439-2012-3

Title: Extraction of Features from 3D PET Images
Authors: Batty, S., Clark, J., Fryer, T., Gao, X.W.
Conference: Medical Image Understanding and Analysis 2002, 22-23 July 2002, University of Portsmouth, Portsmouth, U.K.

Title: Content- based Retrieval of Lesioned Brain Images from a Database of PET Scans.
Authors: Batty, S., Clark, J., Fryer, T., Blandford, A., Gao, X.W.
Conference: Proceedings of SPIE on Medical Imaging, 4685, 128-136, San Diego, California, USA, February 2002.

Title: Extraction of Sagittal Symmetry Planes from PET Images
Authors: Gao, X.W., Batty, S., Clark, J., Fryer, T., Blandford, A.
Conference: Proceedings of the IASTED International Conference on Visualization, Imaging, and Image Processing (VIIP'2001), pp 428-433, ACTA Press, Marbella, Spain, September 2001.

11 References

[1] R.M.E. Sabbatini, "The PET Scan: A new Window Into the Brain", Brain and Mind Magazine, March 1997, www.epub.org.br/cm/n01/pet/pet_hist.htm

[2] W. Cai, D. Feng, R. Fulton, "Content based retrieval of dynamic PET functional images", IEEE Transactions on Information Technology in Biomedicine, vol 4, No 2, pages 152-158,June 2000.

[3] Y. Liu, W. Rothfus, T. Kanade, "Content based 3D neuroradiologic image retrieval: Preliminary Results", IEEE workshop on Content-based access of Image and Video Databases in conjunction with ICCV'98, January 1998.

[4] Talairarch J, Tournoux P (1988). Co-planar stereotaxic atlas of the human brain. Thieme, New York.

[5] Middlesex University Library, London. http://library.mdx.ac.uk/ipac20/ipac.jsp

[6] Microsoft Corporation. http://www.microsoft.com

[7] Google image search. http://www.google.com/imghp

[8] Getty Image Library. http://www.gettyimages.com

[9] Wolfson Brain Imaging Centre, Cambridge University, Addenbrookes Hospital, Cambridge UK. http://www.cam.wbic.ac.uk

[10] Analyze software, "The Mayo Clinic" http://www.mayo.edu/bir/Software/Analyze/Analyze.html

[11] Albrecht Blaser (ed), "Data Base Techniques for Pictorial Applications", Florence, Italy, June 20-22 (1979), Lecture notes in Computer Science, Vol. 81, Springer, 1980.

[12] A. Smeulders, Marcel Wooring, Simone Santini, Armanath Gupta and Ramesh Jain, "Content-Based Image Retrieval at the End of the Early Years", IEEE Transactions on Pattern Analysis and Machine Intelligence, 22(12):1-32, 2000.

[13] Moore's Law. http://en.wikipedia.org/wiki/Moore's_law

[14] The Merriam Webster online dictionary. http://www.m-w.com

[15] R. C. Veltkamp, M. Tanase, "Content-based Image Retrieval systems: A Survey", Technical report UU-CS-2000-34, Utrect University, The Netherlands, October 2000.

[16] Informix database software. http://www-3.ibm.com/software/data/informix/blades/excaliburimage/

[17] Convera Corporation. Content based Retrieval software. http://www.convera.com

[18] IBM Corporation, Query By Image Content. http://wwwqbic.almaden.ibm.com/

[19] Attrasoft Inc. Universal Image Identification and Retrieval Technology. http://www.attrasoft.com/

[20] Virage Inc. SmartEncode software. http://www.virage.com/products/details.cfm?productID=4&categoryID=1

[21] IMatch software, image management software. http://www.photools.com/imoverview.html

[22] Sougata Mukherjea, Kyoji Hirata, and Yoshinori Hara. Amore: A world wide web image retrieval engine. *The WWW Journal*, 2(3):115-132, 1999.

[23] Digital Library, University of California. http://www.alexandria.ucsb.edu/

[24] T. Smith, "A Digital Library for Geographically Referenced Materials", IEEE Computer Society Press, pages 54-60, 1996.

[25] C.Carson, S.Belongie, H.Greenspan, J.Malik, "Region-based image querying", In Proc, IEEE workshop on Content Based Access of Image and Video Libraries, June 1997. http://elib.cs.berkeley.edu/vision.html

[26] M.Sonka, V. Hlavac, R.Boyle, "Image Processing, Analysis and Machine Vision Second Edition", Brooks/Cole Publishing 1999.

[27] Matlab suite of software. http://www.themathworks.com

[28] P.V.C. Hough. "A method and means for recognizing complex patterns". US Patent 3,069,654. 1962

[29] SQL language definition: ISO/IEC 9075. http://www.iso.ch/iso/en/ISOOnline.frontpage

[30] Cooley, J. W. and J. W. Tukey, "An Algorithm for the Machine Computation of the Complex Fourier Series," Mathematics of Computation, Vol. 19, April 1965, pp. 297-301.

[31] Gabor, D. "Theory of Communication." J. Inst. Electr. Engineering, London 93, 429-457, 1946.

[32] R.M. Haralick, Statistical and Structural Approaches to Texture, Proceedings of the IEEE, 67(5), 1979.

[33] W.Y. Ma and B.S. Manjunath, "Texture Features for Browsing and Retrieval of Image Data", IEEE transactions on Pattern Analysis and Machine Intelligence, vol:18, No:8, August 1996.

[34] J.R. Smith, S. Chang, Automated Image Retrieval Using Color and Texture, Columbia University Technical Report TR# 414-95-20, July, 1995, http://www.ctr.columbia.edu/~jrsmith/html/pubs/PAMI/pami_final.html

[35] International Congress on Illumination . Proceedings, International Congress on Illumination, Cambridge. Cambridge University Press.

[36] Katherine Hepburn resource. http://www.katherinehepburn.com

[37] Auckland University, image processing course, web resources. http://www.ele.auckland.ac.nz/~andrews/ELECTENG709.htm

[38] R.N., Shepard, Representation of Structure in Similarity Data: Problems and Prospects, Psychometrika, 39 (4), 373-420, 1974.

[39] W.S. Torgerson, Multidimensional Scaling of Similarity, Psychometrika, 30(4), 379-393, 1965.

[40] Dy. J, Brodley. C, Kak. A, Broderick. L, Aisen. A, "Unsupervised feature selection applied to content based retrieval of lung images", IEE Transactions on Pattern Analysis and Machine intelligence, vol 25, no 3, March 2003.

[41] Content-Based Image Retrieval (CT Lung, Brodley et al). http://rvl2.ecn.purdue.edu/~cbirdev/WWW/CBIRmain.html

[42] A. Aisen, L. Broderick, C.R. Shyu, C. Brodley, A. Kak, A. Kosaka, " ASSERT: A Physician-in-the-Loop Content-Based Retrieval System for HRCT Image Databases", Computer Vision and Image Understanding, Vol 75, No 1/2, pages 111-132, July August 1999.

[43] 16th IEEE Symposium on Computer-Based Medical Systems (CBMS'03)(p-175) A prototype content-based image retrieval system for spine x-rays Long. R, Anatani K. S, Thoma. G.

[44] MySQL database software. http://www.mysql.com

[45] 16th IEEE Symposium on Computer-Based Medical Systems (CBMS'03)(p-175) Retrieval by Content of Medical Images Using Texture for Tissue Identification. Joaquim Cezar Felipe, Agma J. M. Traina, Caetano Traina Jr

[46] Haralick, R. M., Shanmugam, K., and Dinstein, I., 1973. Textural features for image classification. IEEE Trans. Syst., Man, Cybern., SMC-3, pp. 610-621.

[47] Int J Med Inf. 2004 Feb;73(1):1-23.A review of content-based image retrieval systems in medical applications-clinical benefits and future directions. Muller H, Michoux N, Bandon D, Geissbuhler A. Service of Medical Informatics, University Hospital of Geneva, Rue Micheli-du-Crest 24, 1211 Geneva 14, Switzerland

[48] Artif Intell Med. 2004 Feb;30(2):141-51.Finding related functional neuroimaging volumes. Nielsen FA, Hansen LK. Informatics and Mathematical Modelling, Building 321, Technical University of Denmark, Lyngby, Denmark"

[49] BrainMap. http://ric.uthscsa.edu

[50] Nobel online museum. http://www.nobel.se/

[51] General Electric Corporation. http://www.gehealthcare.com/worldwide.html

[52] J. Belliveau, D. Kennedy, R. McKinstry, B. Buchbinder, R. Weisskoff, M. Cohen, J. Vevea, T. Brady, B. Rosen, "Functional mapping of the human visual cortex by magnetic resonance imaging", Science, 254(17 June), 716-719, 1991.

[53] A.M. Blamire, S. Ogawa, K. Ugurbil, D. Rothman, G. McCarthy, J.M Ellermann, F. Hyder, Z. Rattner, R.G. Shulman, "Dynamic mapping of the human visual cortex by high-speed magnetic resonance imaging", Proc Natl Acad Sci USA, 89, 11069-11073, 1992.

[54] William E. Klunk, Henry Engler,Agneta Nordberg, Yanming Wang, Gunnar Blomqvist, Daniel P. Holt, Mats BergströmIrina Savitcheva, Guo-Feng Huang, Sergio Estrada, Birgitta Ausén, Manik L. Debnath, Julien Barletta, Julie C. Price, Johan Sandell, Brian J. Lopresti, Anders Wall, Pernilla Koivisto, Gunnar Antoni, Chester A. Mathis, Bengt Långström, "Imaging brain amyloid in Alzheimer's disease with Pittsburgh Compound-B." Annals of Neurology Volume 55, Issue 3 , March 2004. Pages 306 – 319.

[55] Fritzler, S. et al. Proton beams generated with high-intensity lasers: applications to medical isotope production. Applied Physics Letters, doi:10.1063/1.1616661 (2003).

[56] The Crump Institute for Molecular Imaging, 700 Westwood Blvd. Los Angeles, CA 90095-1770, Email: crump@mednet.ucla.edu
"Let's Play PET", http://www.crump.ucla.edu/software/lpp/lpphome.html.

[57] A. C. Evans and D. L. Collins and S. R. Mills and E. D. Brown and R. L. Kelly and T. M. Peters, "3D statistical neuroanatomical models from 305 MRI volumes", Proc. IEEE-Nuclear Science Symposium and Medical Imaging Conference, 1813-1817, 1993.

[58] Friston KJ, Ashburner J, Poline JB, Frith CD, Heather JD, Frackowiak RSJ, "Spatial Registration and Normalization of Images", Human Brain Mapping 2:165-189, (1995)

[60] International Community of Brain Mapping. http://www.loni.ucla.edu/ICBM/

[61] Montreal Neurological Institute. http://www.bic.mni.mcgill.ca

[62] Cambridge University, MRC. M. Brett. http://www.mrc-cbu.cam.ac.uk/Imaging/Common/mnispace.shtml

[63] Jay West, J. Michael Fitzpatrick, Matthew Y. Wang, Benoit M.Dawant, Calvin R. Maurer, Jr., Robert M. Kessler, Robert J. Maciunas, Christian Barrillot, Didier Lemoine, Andre Collignon, Fredirk Maes, Paul Suetens, Dirk Vandermeulen, Petra A. van den Elsen, Sandy Napel, Thilaka S. Sumaneweera, Beth Harkness, Paul F. Hemler, Derek L.G. Hill, David J. Hawkes, Colin Studholme, J.B. Antoine Maintz, Max A. Viergever, Gregoire Malandain, Xavier Pennec, Marilyn E.Noz, Gerarld Q. Maguire, Jr., Michael Pollack, Charles A. Pelizzari, Richard A. Robb, Dennis Hanson, and Roger P. Woods. "Comparison and Evaluation of Retrospective Intermodality Brain Image registration techniques". Journal Of Computer Assisted Tomography, 21(4):554-566. Lippincott-Raven Publishers (1997).

[64] Maintz, J. Viergever, M., "A survey of medical image registration", Medical Image Analysis (2:1), 1-36 (1998).

[65] Collins, D. L., Peters, T. M., Evans, A. C., "An automated 3D Non-linear image deformation procedure for determination of gross morphometric variability in human brain", Proceedings from Conference on Visualisation in Biomedical Computing, 180-190, 1994.

[66] Ashburner J, Friston KJ, "Nonlinear Spatial Normalization using Basis Functions", Human Brain Mapping 7(4):254-266, (1999).

[67] Medical Image Registration. Eds. JV Hajnal, DLG Hill, DJ Hawkes. CRC Press, 2001

[68] A.A. Lammertsma, S.P. Hume, "Simplified Reference Tissue Model for PET Receptor Studies", NeuroImage, 4 : 153-158, 1996.

[69] Robert A. Sweet, MD; Ronald L. Hamilton, MD; Matthew T. Healy, MEd; Stephen R. Wisniewski, PhD; Ruth Henteleff, AB; Bruce G. Pollock, MD, PhD; David A. Lewis, MD; Steven T. DeKosky, MD, "Alterations of Striatal Dopamine Receptor Binding in Alzheimer Disease Are Associated With Lewy Body Pathology and Antemortem Psychosis", Arch Neurol. 2001;58:466-472.

[70] Volkow ND, Zhu W, Felder CA, Mueller K, Welsh TF, Wang GJ, de Leon MJ, "Changes in brain functional homogeneity in subjects with Alzheimer's disease", Psychiatry Research: Neuroimaging Volume 114, Issue 1 , 15 Feb 2002, Pages 39-50.

[71] P. J. Nestor, T. D. Fryer, M. Ikeda and J. R. Hodges "Retrosplenial cortex (BA 29/30) hypometabolism in mild cognitive impairment (prodromal Alzheimer's disease)", European Journal of Neuroscience Volume 18 Issue 9 Page 2663 - November 2003 doi:10.1046/j.1460-9568.2003.02999.x

[72] Fukuyama H, Ogawa M, Yamauchi H, Yamaguchi S, Kimura J, Yonekura Y, Konishi J. "Altered cerebral energy metabolism in Alzheimer's disease: a PET study." J Nucl Med. 1994 Jan;35(1):1-6.

[73] Liu. Y, Dellaert. F, "Classification-driven medical image retrieval", Computer Vision and Pattern Recognition Conference (CVPR'98), Santa Babara, CA, June, 1998.

[74] Sayeed A, Petrou M, Spyrou N, Kadyrov A, Spinks T. "Diagnostic features of Alzheimer's disease extracted from PET sinograms", Phys Med Biol. 2002 Jan 7;47(1):137-48.

[75] Eric W. Weisstein. "Radon Transform." From MathWorld--A Wolfram Web Resource. http://mathworld.wolfram.com/RadonTransform.html

[76] S. Batty, J. Clark, T. Fryer, X. Gao, "Content-based retrieval of lesioned brain images from a database of PET scans", SPIE Conference Proceedings: Medical Imaging, PACS and Integrated Medical Information Systems, 4685, 128-136, San Diego, California, USA, February 2002.

[77] W.Y. Ma and B.S. Manjunath, "Texture Features for Browsing and Retrieval of Image Data", IEEE transactions on Pattern Analysis and Machine Intelligence, vol:18, No:8, August 1996.

[78] George C.Sun, H.K. Huang, Guy Scalzi, "Experiences of Healthcare Integrated Picture Archiving and Communications Systems (PACS)", Healthcare Information and System Society, conference proceedings 1999.

[79] H.K. Huang, "PACS: Basic Principles and Applications," Wiley-Liss, 1999.

[80] Heinz U. Lemke, "A network of medical workstations for integrated word and picture communication in clinical medicine," Sixth conference of the Society for Computer Applications in Radiology, March 1979.

[81] "First International Workshop and Conference on Picture Archiving and Communications Systems (PACS) for Medical Applications", Society of Photographic Instrumentation Engineers, Newport Beach, CA, January 1982.

[82] Michael Cross, The Guardian newspaper, Life section, Public Domain, page-15, May 13th 2004.

[83] Centers for Medicare & Medicaid Services (US). http://cms.hhs.gov

[84] Red Hat Linux Distribution. http://www.redhat.com

[85] Apache web-server. http://httpd.apache.org/

[86] ImageJ, imaging tool. http://rsb.info.nih.gov/ij/

[87] PHP scripting language. http://www.php.net/

[88] Hyper Text Mark-up Language. http://www.w3.org/MarkUp/ ISO/IEC 15445

[89] American National Standards Institute, American National Standard for Information Systems—Programming Language C, X3.159-1989.

[90] Matlab C compiler. http://www.mathworks.com/access/helpdesk/help/techdoc/matlab_external/matlab_external.html

[91] Internet Browser. http://www.microsoft.com/windows/ie/default.asp

[92] Internet Browser. http://www.opera.com/

[93] Internet Browser. http://channels.netscape.com/ns/browsers/default.jsp

[94] Internet Browser. http://www.mozilla.org/

[95] Internet Browser. http://www.apple.com/safari/

[96] Lancaster JL, Woldorff MG, Parsons LM, Liotti M, Freitas CS, Rainey L, Kochunov PV, Nickerson D, Mikiten SA, Fox PT, "Automated Talairarch Atlas labels for functional brain mapping". Human Brain Mapping 10:120-131, 2000.

[97] Y. Liu, R.T. Collins, W.E. Rothfus, "Automatic Bilateral Symmetry (Midsagittal) Plane Extraction from Pathological 3D Neuroradiological Images", SPIE International Symposium on Medical Imaging, San Diego, February, 21-27, 1998.

[98] Jan Passchier, Aren van Waarde, Willem Vaalburg and Antoon T.M. Willemsen, "Quantification of [18F]MPPF Binding to 5-HT1A Receptors in the Human Brain". J Nucl Med. 2001; 42: 1025-1031.

[99] X. Gao, S. Batty, J. Clark, T. Fryer, A. Blandford, "Extraction of sagittal symmetry planes from PET images", IASTED Conference Proceedings: Visualization, Imaging and Image Processing (VIIP' 2001), pages 428-433, ACTA Press, 2001.

[100] Desco, M. Pascau, J. Reig, S. Gispert, JD. Santos,A. Benito, C. Molina, V. Garcia-Barreno, P. " MultiModality image quantification using Talairach grid Medical Imaging 2001: Image Processing. Proceeding of SPIE Vol 4332, pp-1385-1390.